University of Nevada Reno

Removing Barriers for Effective Deployment of Intermittent Renewable Generation

A dissertation submitted in partial fulfillment of the
Requirements for the degree of Doctor of Philosophy in
Electrical Engineering

By

Amirsaman Arabali

Dr. Mehdi Etezadi-Amoli/Dissertation Advisor

August, 2014

THE GRADUATE SCHOOL

We recommend that the dissertation
prepared under our supervision by

AMIRSAMAN ARABALI

Entitled

Removing Barriers for Effective Deployment of Intermittent Renewable Generation

be accepted in partial fulfillment of the
requirements for the degree of

DOCTOR OF PHILOSOPHY

Dr. Mehdi Etezadi-Amoli, Advisor

Dr. M. Sami Fadali, Committee Member

Dr. Andrzej M. Trzynadlowski, Committee Member

Dr. Yantao Shen, Committee Member

Dr. Ahmad M. Itani, Graduate School Representative

David W. Zeh, Ph. D., Dean, Graduate School

August, 2014

ABSTRACT

The stochastic nature of intermittent renewable resources is the main barrier to effective integration of renewable generation. This problem can be studied from feeder-scale and grid-scale perspectives. Two new stochastic methods are proposed to meet the feeder-scale controllable load with a hybrid renewable generation (including wind and PV) and energy storage system. For the first method, an optimization problem is developed whose objective function is the cost of the hybrid system including the cost of renewable generation and storage subject to constraints on energy storage and shifted load. A smart-grid strategy is developed to shift the load and match the renewable energy generation and controllable load. Minimizing the cost function guarantees minimum PV and wind generation installation, as well as storage capacity selection for supplying the controllable load. A confidence coefficient is allocated to each stochastic constraint which shows to what degree the constraint is satisfied. In the second method, a stochastic framework is developed for optimal sizing and reliability analysis of a hybrid power system including renewable resources (PV and wind) and energy storage system. The hybrid power system is optimally sized to satisfy the controllable load with a specified reliability level. A load-shifting strategy is added to provide more flexibility for the system and decrease the installation cost. Load shifting strategies and their potential impacts on the hybrid system reliability/cost analysis are evaluated trough different scenarios. Using a compromise-solution method, the best compromise between the reliability and cost will be realized for the hybrid system.

For the second problem, a grid-scale stochastic framework is developed to examine the storage application and its optimal placement for the social cost and transmission congestion relief of wind integration. Storage systems are optimally placed and adequately sized to minimize the sum of operation and congestion costs over a scheduling period. A technical assessment framework is developed to enhance the efficiency of wind integration and evaluate the economics of storage technologies and conventional gas-fired alternatives. The proposed method is used to carry out a cost-benefit analysis for the IEEE 24-bus system and determine the most economical technology. In order to mitigate the financial and technical concerns of renewable energy integration into the power system, a stochastic framework is proposed for transmission grid reinforcement studies in a power system with wind generation. A multi-stage multi-objective transmission network expansion planning (TNEP) methodology is developed which considers the investment cost, absorption of private investment and reliability of the system as the objective functions. A Non-dominated Sorting Genetic Algorithm (NSGA II) optimization approach is used in combination with a probabilistic optimal power flow (POPF) to determine the Pareto optimal solutions considering the power system uncertainties. Using a compromise-solution method, the best final plan is then realized based on the decision maker preferences. The proposed methodology is applied to the IEEE 24-bus Reliability Tests System (RTS) to evaluate the feasibility and practicality of the developed planning strategy.

Acknowledgments

First and foremost, my special thanks go to my advisor, Dr. Mehdi Etezadi-Amoli for his guidance and support throughout my doctoral studies. It was a great honor for me to pursue my PhD degree under his supervision. I would like to express my sincere thanks to Dr. M. Sami Fadali for his significant contributions to my knowledge. I also wish to thank my advisory committee members, Dr. Andrzej M. Trzynadlowski, Dr. Yantao Shen, and Dr. Ahmad M. Itani for their time, interest, and valuable comments. Last but not least, I would like to express my deepest gratitude to my family for their lifetime dedication, support and patience.

This work is supported in part by the Nevada Renewable Energy Center (NVREC), grant No. #656.1769.01.

List of Publications

1. A. Arabali, M. Ghofrani, M. Etezadi-Amoli, and Y. Baghzouz, "Ramping requirements and operation cost in a power system with dispersed wind generation," in *Proc. IEEE PES Transmission and Distribution Conference and Exposition (T&D)*, May 2012.
2. A. Arabali, M. Ghofrani, M. Etezadi-Amoli, M. S. Fadali, Y. Baghzouz, "Genetic Algorithm Based Optimization Approach for Energy Management," *IEEE Transactions on Power Delivery*, Vol. 28, No. 1, Page(s): 162 – 170, Jan. 2013.
3. A. Arabali, M. Ghofrani, M. Etezadi-Amoli, M. S. Fadali, "Stochastic Performance Assessment and Sizing for a Hybrid Power System of Solar/Wind/Energy Storage," *IEEE Transactions on Sustainable Energy*, Vol. 5, No. 2, Page(s): 363-371, April 2014.
4. A. Arabali, M. Ghofrani, M. Etezadi-Amoli, "Cost Analysis of a Power System Using Probabilistic Optimal Power Flow with Energy Storage Integration and Wind Generation," *International Journal of Electrical Power & Energy Systems (IJEPES)*, Elsevier, Vol. 53, No. , Page(s): 832-841, Dec. 2013.
5. A. Arabali, M. Ghofrani, M. Etezadi-Amoli, and M. Sami Fadali, "A Multi-Objective Transmission Expansion Planning Framework in Deregulated Power Systems with Wind Generation," *IEEE Transactions on Power Systems* (Early access is available).

Table of Contents

List of Figures

List of Tables

Nomenclature

a, b	Shape parameters for Beta distribution
A_c	Surface area of the PV array
c	Cluster number
C	Total number of clusters
C_P	Cost of power rating of the storage system
C_{PV}	Installation cost of PV
C_S	Installation cost of the storage system
C_W	Installation cost of Wind
d	Hourly self-discharge rate of the storage system
EE	Excess energy
EE_t	Excess energy at hour t
f_{X_k}	PDF for the k^{th} input random variable
G_{PV}	Net PV output power
G_W	Net output power of the wind generator
$G_{PV,t}$	PV power generation at hour t
$G_{W,t}$	Wind power generation at hour t
G_{W_r}	Wind rated power
G'_{PV}	PV output power
G'_W	Output power of the wind generator
k	Shape parameter for Weibull distribution
L_t	Load demand at hour t
$\acute{L}_t$	Modified HVAC loads at hour t
$L_{S,t}$	Shifted load demand at time t
P	Maximum power rating of the storage system
$P_{k,1}, P_{k,2}$	Probabilities of concentrations
P_t	Power rating of the storage system at time t
S	Maximum capacity of the storage system
S_t	Energy stored in the storage system at time t
t	Time
v	Wind speed
v_i	Cut-in wind speed
v_o	Cut-out wind speed
v_r	Rated wind speed
$x_{k,1}, x_{k,2}$	Concentrations of f_{X_k}
X_k	k^{th} input random variable
α_{PV}	Installed capacity of PV
α_W	Installed capacity of Wind
δ	Percentage of HVAC load to be shifted to next hour
η_{PV}	Efficiency of the PV power interface

η_S	Roundtrip efficiency of the storage system
η_W	Efficiency of the wind power interface
η'_{PV}	Efficiency of the PV array
λ	Scale parameter for Weibull distribution
$\lambda_{k,3}$	Coefficient of skewness for X_k
μ_{X_k}	Expected value of the k^{th} input random variable
$\xi_{k,1}$, $\xi_{k,2}$	Locations of concentrations
σ_{X_k}	Standard deviation of the k^{th} input random variable
Γ	Gamma function
a_r, b_r	Order of the AR and MA model
C_i	i^{th} decision criterion
C_{HPS}	Cost of hybrid power system
EE_d	Expected energy demand
ENS	Energy not supplied
EENS	Expected energy not supplied
EIR	Energy index of reliability
f_{X^k}	PDF for the k^{th} simulated random variable
G_{PV}	Net power generated by PV
G_W	Net power generated by wind
G_{PV_t}	Electric power generated by PV for time *t*
G_{W_t}	Electric power generated by wind for time *t*
G_{W_r}	Rated wind power
G'_{PV}	Power generated by PV
G'_W	Power generated by wind
H_0	Extra-terrestrial radiation on a horizontal surface
IC_{PV} / IC_W	Installation cost for PV/wind
L_t / L'_t	Load/modified load at time *t*
L_{I_t}/ L_{S_t}	Interrupted/shifted load at time *t*
OMC_{PV}	Cost of operation and maintenance for PV
OMC_W	Cost of operation and maintenance for wind
p	Parameter in the functional form for the $k(k_t)$
P	Power rating for the energy storage
P_t	Power of the energy storage at time *t*
q	Parameter in the functional form for the $k(k_t)$
r_d	Ratio, diffuse radiation in hour/diffuse in day
R_b	Geometric factor, the ratio of beam radiation on the tilted surface to that on a horizontal surface
S	Storage system capacity
SW, Sk, SL	Simulated wind speed, clearness index, load
S_t	Stored energy at time *t*

$x_{n,t}$	Sample for the n^{th} simulation and t^{th} scheduling period
X^k	k^{th} stochastic input variable
α_{PV}/ α_W	PV/wind capacity installation
θ_j/φ_i	Moving average/Autoregressive coefficient of the ARMA model
μ_k, σ_k	Mean and standard deviation for clearness index
μ_L, σ_L	Mean and standard deviation for the load
μ_W, σ_W	Mean and standard deviation for the wind speed
μ_{C_i}	Satisfaction level for the i^{th} decision criterion
μ_{r_i}	Reference level of achievement for the i^{th} decision criterion
ρ	Reflectance of the ground
Φ	Set of trade-off points

I. Chapter 1. Introduction

1.1 Background

The US is currently increasing its use of renewable energy and decreasing its reliance on imported fossil fuels. Renewable resources in the United States have become an important portion of generation mix with a capacity of 12.2% of net electricity generation at the end of 2012. State initiatives including federal production tax credit, Renewable Portfolio Standards (RPS), and the climate change concerns have resulted in a growth in renewable generation capacity of approximately 39% of national electric capacity additions in 2012 [1]. According to RPS targets, this growth will continue. For example, Arizona and Colorado will increase their renewable generations to 15% and 30% by 2025 and 2020, respectively [2]. The development of the smart grid will facilitate the integration of renewable energy sources into the power grid. Smart grid applications include transmission, distribution and distributed generation [3]. The "smarter" monitoring and control will create a more efficient energy management system for residential customers. Smart grid applications in distribution systems include smart metering technologies for efficient integration of distributed renewable generation applications, fair pricing mechanisms, remote monitoring and home automation and control of electrical power consumption. The stochastic nature of PV and wind energy resources makes them not dispatchable and complicates the integration of renewable generation applications. In addition, wind is often not correlated with load pattern and may be discarded sometimes when abundantly available [4], [5], and solar energy is only available during the day time. This can be dealt with over different time scales ranging from seconds to days corresponding to actions by the system

operator to maintain system balance between generation and load [6]. Regulation services which are provided by automatic generation control (AGC) maintain the system balance for short time scales (seconds to minutes). Installed wind capacity of 1500 MW and 3300 MW (15% and 10% penetration level) in the most recent wind integration projects in the United States has resulted in a modest increase of 8 MW and 36 MW regulation requirements, respectively [7]-[8]. This modest regulation impact of wind is due to the fact that wind and load are generally uncorrelated for short time scales [6]. Load following service maintains the system balance for both energy and capacity ranging from 10 minutes to a few hours. This service is provided by generating units with quick start capability or those that have been previously committed and have extra capacity [9]. Scheduling and unit commitment correspond to time scales that may range from several hours to days ahead of the real-time schedule to plan for the required quantity of generation and reserve capacity. These services increase the system operating cost by up to $5.00/MWh of wind generation with wind capacity penetrations between 20% and 30% [10].

The integration cost results from several studies undertaken in the United States reveal that the cost assigned to scheduling and unit commitment services accounts for a significant portion of the system operation cost increase when compared with the regulation and load following costs [7], [10]-[16]. Consequently, an adequate ramping requirement provided by the scheduling services may significantly affect the system operation cost. Accounting for increased variability of the system due to the intermittent nature of the renewable energy resources, there is a need for greater flexibility from the conventional generating units. This can be satisfied with greater ramping capability to compensate for wind power output variability and to maintain the system balance for a day ahead scheduling [15]. Taking advantage of the spatial diversity of

renewable energy resources, wind power generation can be spread over wider areas to reduce the wind power fluctuations [7]. This may result in reduced ramping requirements and system operation costs when compared with concentrated wind generation.

The US Department of Energy estimates that controllable loads, such as heating ventilation and air conditioning (HVAC) loads, account for 40 to 60% of the energy consumption in US commercial and residential buildings [17]. Utilities may have some agreements with consumers to shift part of their controllable loads during peak load hours. This agreement will provide the customer with economic incentives and prevent the need for additional conventional generation during these peak hours. For example, NV Energy's cool share program is associated with approximately 145 MW remote controlled air conditioning load. These loads can be dispatched by NV Energy through “raise/lower” thermostat commands as needed [18]. Because these time flexible loads may be deferrable for a few minutes or hours, their energy consumption can be adapted according to the renewable power supply fluctuation. This demand side flexibility can counterbalance renewable supply variations and efficiently integrate renewable generation. Energy efficiency can further be increased by storing energy when renewable power generation exceeds the load requirements then releasing it when renewable generation is insufficient to supply the load [19]. A smart strategy is required to implement the load shifting and reduce the mismatch between renewable generation and controllable loads. The efficiency of a hybrid system is dependent on the renewable generation efficiency, the self-discharge rates and roundtrip efficiencies of the energy storage units, and on the sizing of the system components [20], [21].

The design, simulation and optimization of hybrid power systems have been the subject of several studies [22]-[32]. Operating concepts, performance evaluation and economic analysis of such systems were investigated in [22]-[26] where the component sizing is either arbitrary or based on practical and experimental estimates, with no attempt at optimizing their parameter values. References [27]-[31] employed a variety of heuristic optimization techniques for the design and operation of the hybrid systems. However, none of these investigations focused on demand flexibility and controllable loads in particular, or on matching controllable loads with renewable energy sources without the need for supplementary conventional generations. Reference [32] presented an optimal component-sizing framework for the hybrid system, but the stochastic nature of wind/PV generation is not considered in the model. Emerging smart grid strategies can provide the distribution system with an opportunity to balance renewable generation and controllable loads for a residential feeder using energy storage systems.

The intermittent nature of renewable energy resources also reduces the reliability of power systems. A hybrid power system which is composed of energy storage and renewable generation can alleviate the issues associated with renewable power supply fluctuations and reliability. Storage of the excess renewable energy for later use offsets renewable energy variations and makes the renewable generation integration more reliable [33]. This is particularly true for flexible controllable loads which can be deferred and adopted based on renewable energy fluctuations. However, the large number of random variables and parameters in a hybrid power system makes its optimal design more challenging [34]. This optimization includes component-sizing for the hybrid system as well as the assessment of system performance to realize the best compromise between cost and reliability. The reliability study is based on stochastic models to

consider the uncertainties of the hybrid power system such as equipment failures and random variations in both generation and load [31].

Performance of isolated hybrid power systems have been studied in [22], [23], [27] and [29]. References [22] and [23] utilized practical and experimental estimates for component sizing and performance evaluation without optimizing their parameter values. Optimization techniques were employed in [27] and [29] to design and operate the stand-alone hybrid power systems. However, none of these studies evaluated the reliability of the hybrid power systems for grid-independent applications. Several studies have proposed probabilistic frameworks for optimal sizing and reliability analysis of hybrid power systems [34], [31], [35]-[40]. References [34], [31], [35] and [36] employed analytical methods to mathematically model the hybrid power system and used direct solutions to evaluate the reliability indices from its model. However, increasing the number of random parameters in a hybrid power system complicates the mathematical computations of the reliability indices. In addition, analytical methods do not properly represent the random nature of hybrid power systems and their component failures [37]. Monte Carlo simulation (MCS) randomly samples the system states, irrespective of event chronologies, to provide a detailed knowledge of the probability distributions of reliability indices. MCS has been used to evaluate the hybrid power system reliability [37]-[40]. None of these studies investigated load shifting and its potential impact on the hybrid system reliability/cost analysis. Also, the traditional derivative-based optimization methods cannot be used here due to terms such as “max” and “absolute value” that are utilized to calculate a dependent variable in the objective function. Therefore, an appropriate meta-heuristic method must be used to handle the non-convex and discontinuous optimization problem.

Recent developments in advanced energy storage technologies combined with the associated technical, economic and environmental benefits provide energy storage systems with a broad range of potential to optimize grid connected wind power resources [41]. Integration of wind generation with more than 20% penetration levels requires additional regulation and spinning reserve resources for grid stability purposes. These services incur some costs which have been the subject of several investigations in the U. S. and Europe [42]-[46]. This increased cost gives an opportunity for energy storage systems to provide all or some portion of these ancillary services. Rated capacity of the wind power is the determining factor in calculating the amount of grid capacity required to accommodate the full wind power resource. However, the average capacity of wind power is typically between 30% and 40% of rated capacity. This is due to the intermittent nature of wind power which makes it a variable and uncertain energy resource. Therefore, when compared with conventional generating technologies, more transmission capacity per unit of delivered wind energy is assigned to deal with wind power intermittency [41]. Wind power may be curtailed during high wind periods to avoid transmission congestion. This may impose an extra cost to the grid operators or a loss of revenue to the wind generators. Energy storage can be used to store the wind energy in excess of transmission capacity and dispatch it later when transmission capacity is available. Effective utilization of transmission capacity could be realized by optimizing the placement and scheduling of energy storage. This results in transmission congestion relief and/or transmission expansion deferral [47]. Adequate energy storage is also required to efficiently integrate renewable resources and justify the cost of storage deployment over the more conventional alternatives [48]. Therefore, application of large-scale energy storage for renewable integration calls for an economic assessment framework to

enhance grid operability and reduce operation cost [49]. This is particularly essential for transmission congestion relief application whose lack of operational practices limits the knowledge of operating, sitting, sizing, and optimal scheduling of energy storage technologies in power systems with renewable energy sources. This has been the subject of investigation in few publications [50], [51]. Wind uncertainties are not considered in [50], which questions the applicability of the proposed methodology for real world problems. In addition, the compressed air energy storage (CAES) is arbitrarily placed close to the wind resource and/or load center, with no attempt at optimizing its location and size to minimize congestion-related costs. Reference [51] concludes with installing storage systems at locations that are downstream from the point of congestion in a transmission system. This would allow for the transmission of energy for charging when there is no congestion. The stored energy can be later discharged to reduce transmission capacity requirements during peak load periods. However, this conclusion cannot be generalized for a transmission network where the presence of several transmission lines and load centers complicates the optimal placing problem.

The transmission system plays a key role in the successful transition of a regulated power system to a deregulated structure by providing a non-discriminatory competitive environment for power market participants [52]. An appropriate strategy for TNEP guarantees a fair competition within the market as the system load and generation grow. However, TNEP in a deregulated power system (DPS) should consider several objectives rather than the single objective of investment cost minimization which is taken into account in a traditional TNEP [53]-[55]. In a DPS, minimizing the investment cost of the transmission lines is more highlighted in the sense that the pricing mechanism of the transmission services is influenced by the investment cost.

This objective is required to lower the tariffs of transmission services for the market participants [53]. Market-based criteria should also be considered for TNEP to motivate the private investors and increase their participation in transmission projects [54]. In addition, successful trade in a competitive power market requires a desirable level of reliability which should be effectively implemented in TNEP [55].

Unlike other parts of the power system, the transmission section has not been sufficiently attractive to absorb private investments due to the transmission service pricing, tariffs and investment risk. The lack of economic incentives in recovering the investment cost is the main drawback for construction of the new transmission projects in the United States [56]. The situation is worse when the power system uncertainties increase with increasing penetrations of variable renewable energy sources such as wind and solar. With a nameplate installed capacity of 60,007 MW as of December 31, 2012, wind energy has become a significant resource in many electric utility systems across the United States [57]. In addition, favorable wind profiles in remote areas from the load centers necessitate the construction of new transmission lines which are less utilized due to the intermittent nature of wind power [57]. Therefore, the TNEP strategy in a restructured power market with renewable energy generation should address the private investors' concerns and provide economic incentives to encourage their investment in the transmission network.

The transfer capability of a transmission system is limited by the reliability criteria which are established by the North American Electric Reliability Council (NERC), Regional Reliability Council, or local jurisdiction (state or ISO). These criteria are determined by the stability limits, thermal limits, voltage collapse, and resource deficiency of the transmission lines [59].

Inefficient utilization of transmission infrastructure to accommodate electricity trades between different entities in a restructured market causes the transmission system to be operated closer to its physical constraints [60], [61]. Therefore, the secure and efficient operation of the transmission network is of significant importance to provide a desirable level of reliability and avoid congestion in a DPS. Towards this end, the TNEP strategy should offer transparent transmission prices while maintaining system reliability to support a competitive and non-discriminatory environment for the participants and circumvent the market power in a deregulated structure.

Two types of projects are proposed to alleviate the bottlenecks regarding the transmission expansion: reliability projects and market economic projects [61]. The reliability projects are regulatory requirements to satisfy the reliability criteria where an approved transmission rate is assigned to the investment recovery. In contrast, the cost recovery rate of the economic projects is not regulatory approved. Wind power intermittency and uncertainty regarding customer behaviors complicate the investment decision for merchant transmission projects. Thus, TNEP in a restructured power system should provide a proper strategy to consider the uncertainties of the system and maximize private investments absorption.

TNEP has been the subject of investigation in several studies [53], [62]-[71]. Deterministic methods were developed in [53] and [62]-[65] for TNEP problem without taking the power system uncertainties into account. While some studies have used stochastic models [66]-[67], none incorporated the reliability criteria into the modeling. Reference [68] proposed a probabilistic TNEP framework for the power systems with high wind penetration but did not consider the risk involved in transmission investments. A game-theory based TNEP was

proposed in [69] to manage the risk without incorporating the financial factors. References [53], [67], [68], [70] and [71] proposed multi-objective optimization framework to consider different criteria including investment cost, congestion cost and reliability for TNEP in deregulated power systems. However, none of these references addressed the financial aspects of transmission lines, which are the determining factors for the private investment. This is particularly essential in restructured power systems where the lack of economic incentives and measures for the transmission sector discourage private investment. Therefore, an appropriate strategy is required to determine the market economic projects and mitigate the monopoly power over the transmission network.

1.2 Dissertation Organization

This dissertation includes six chapters. Chapter one introduces the challenges/concerns of intermittent renewable generation. It also provides a comprehensive literature review regarding the studies performed for intermittent renewable generation integration. Chapter two provides an analysis regarding the effect of geographical distribution of wind farms on the ramping requirements in the IEEE 24-bus system. Probabilistic unit commitment (UC) based on unit de-commitment method and point estimate method is used to determine the ramping required to compensate for the wind power fluctuations and load uncertainty. A brief analysis is carried out regarding the system operation cost and the potential reduction of this cost due to dispersed wind generation. In chapter three, two stochastic methods are developed to meet the controllable heating, ventilation and air conditioning (HVAC) load with a hybrid renewable generation and energy storage system. The two methods size a hybrid power system with specific reliability and

confidence levels. Chapter four proposes a new strategy to evaluate the potential impact of co-locating wind and storage on operation and congestion costs of the IEEE 24-bus system. Different scenarios are studied to evaluate the economic advantage of wind and storage co-location over the cases where the wind and storage units are installed at different buses. Distributed storage and its potential to reduce the congestion cost of the system are also analyzed in this chapter. In chapter five, a multi-stage multi-objective transmission network expansion planning framework is developed to provide the investors with economic incentives and maximize the absorption of private investment. An NSGA II optimization is used to obtain a set of Pareto optimal solutions that are non-dominant with respect to all objective functions. The best final plan is then selected using a decision making method. Chapter six provides conclusions for each chapter and suggestions for future work.

II. Chapter 2. Distributed Wind Generation

2.1 Methodology

2.1.1 Probabilistic modeling of wind and load

The stochastic nature of wind and the load characteristics impose some degree of uncertainty on power systems with a high level of wind power generation. Variability of wind power output [72] and random changes in load [73]-[74] need to be modeled probabilistically in order to reflect their random characteristics. Several articles reported that the wind speed profile most closely follows a Weibull distribution over time [75]-[76]. Using curve fitting, the maximum likelihood estimates of the Weibull distribution parameters are calculated for historical hourly wind speed data. The Probability distribution function (PDF) for a Weibull distribution is given by:

$$f_v(v) = \left(\frac{k}{\lambda}\right)\left(\frac{v}{\lambda}\right)^{k-1} e^{-\left(\frac{v}{\lambda}\right)^k}, 0 \le v \le \infty \tag{2.1}$$

where v is the wind speed, c is the scale factor and k is the shape factor of the Weibull distribution.

The output power of a wind generator can also be characterized as a random variable through a transformation from wind speed to output power as stated below [77]:

$$G_W = \begin{cases} 0 & v_i > v \quad and \quad v > v_o \\ \dfrac{v - v_i}{v_r - v_i} G_{W_r} & v_i \le v \le v_r \\ G_{W_r} & v_r \le v \le v_o \end{cases} \tag{2.2}$$

where G_W , G_{W_r}, v_i, v_r and v_o are the wind output power, wind rated power, cut in wind speed, rated wind speed and cut out wind speed, respectively. The same procedure is applied to the

historical load data and a normal PDF is acquired using curve fitting and maximum likelihood estimation.

2.1.2 Probabilistic scheduling based on unit de-commitment and two-point estimate methods

Deterministic models of unit commitment cannot represent the effects of the stochastic wind power output and load variation on the dispatch results [78]. Uncertain factors such as wind power output and variable loads can be taken into account in unit commitment computations by using a probabilistic unit commitment (PUC). The proposed PUC is based on unit de-commitment and two-point estimate methods (PEM). Unit de-commitment provides a mechanism for completely shutting down the generators which are very expensive to operate and finding a least cost commitment and dispatch. This results in an economic operation of the system over the scheduling time period [79]. PEM has been regarded as an appropriate probabilistic method because of its accuracy, simplicity, and speed. The method was developed by Rosenblueth in the 1970s for calculating the moments of a random multi-variable quantity [80]. This section applies the two-point estimate method (2PEM), which is a variation on the original PEM, to model the uncertainties [81], [82]. Vectors of input and output random variables and the corresponding nonlinear function are given by:

$$X = [Wind\ Speed, Loads] \tag{2.3}$$

$$Y = [RR, OC] \tag{2.4}$$

$$Y = h(X) \tag{2.5}$$

where wind speed and loads are the input probabilistic variables, while ramping requirements (RR) and system operation cost (OC) are the output probabilistic variables. h is the multivariate nonlinear function corresponding to the proposed OPF based on unit de-commitment [82].

The moments of the random variables are derived using the wind and load distributions. Two estimate points are chosen from every distribution, and then the corresponding weighting coefficient and the probability concentration at each point are calculated. The deterministic optimal power flow (OPF) based on unit de-commitment is then used to dispatch the generation for every estimate point at each hour. As all the points are calculated, the results computed by every point and the corresponding probability concentration are used to derive the mean and standard deviation of the dispatch results [82]. The PUC algorithm based on unit de-commitment and 2PEM is outlined as follows:

1) Load the input data (wind speed and load)

2) For t=1 to t=24 do the followings

3) Assign appropriate PDF to each probabilistic variable including wind speed and loads

4) Set $E(Y) = E(Y^2) = 0$

5) Set k =1

6) Determine the necessary parameters of the 2PEM

$$\zeta_{k,i} = \sqrt{n + (\lambda_{k,3}/2)^2} \quad i = 1,2 \tag{2.6.a}$$

$$\xi_{k,i} = \lambda_{k,3}/2 + (-1)^{3-i}\zeta_{k,i} \quad i = 1,2 \tag{2.6.b}$$

$$P_{k,i} = \frac{(-1)^i \xi_{k,3-i}}{2n \times \zeta_{k,i}} \qquad i = 1,2 \tag{2.6.c}$$

where $\xi_{k,1}$, $\xi_{k,2}$, $P_{k,1}$ and $P_{k,2}$ are the locations and probabilities of concentrations. $\lambda_{k,3}$ is the coefficient of skewness of X_k.

7) Set the concentrations ($x_{k,1}$ and $x_{k,2}$) and run the deterministic optimal power flow based on unit de-commitment method using the input vector X.

$$x_{k,i} = \mu_{X_k} + \xi_{k,i}\sigma_{X_k} \quad i = 1,2 \tag{2.7}$$

where μ_{X_k}, σ_{X_k} are the expected value and standard deviation of the input variable (X_k), respectively.

8) Run the deterministic OPF based on unit de-commitment method using

$$Z = [\mu_{X_1}, \mu_{X_2}, ..., x_{k,i}, ..., \mu_{X_n}] \qquad i = 1,2 \tag{2.8}$$

Note that $\mu_{X_K}$is replaced by $x_{k,i}(i = 1,2)$ at each iteration.

9) Calculate RR and OC

10) Update $E(Y)$ and $E(Y^2)$

$$E(Y) \cong \sum_{k=1}^{n}\sum_{i=1}^{2}(P_{k,i} \times h([\mu_{X_1}, ..., x_{k,i}, ..., \mu_{X_n}])) \tag{2.9.a}$$

$$E(Y^2) \cong \sum_{k=1}^{n}\sum_{i=1}^{2}(P_{k,i} \times h^2([\mu_{X_1}, ..., x_{k,i}, ..., \mu_{X_n}])) \tag{2.9.b}$$

10) Set k=k+1and repeat steps 6, 7, 8, 9, and 10 until these steps are done for all random input variables.

11) Calculate the mean of Y using

$$\mu_Y = E(Y) \tag{2.10.a}$$

and its standard deviation using

$$\sigma_Y = \sqrt{E(Y^2) - \mu_Y{}^2} \tag{2.10.b}$$

2.1.3 Probabilistic Unit Commitment (PUC)

The proposed PUC method uses the probabilistic DC-OPF based on unit de-commitment and 2PEM to calculate the ramping requirements and operation cost of the system for each hour of the scheduling period. The objective function is composed of the generation costs and startup costs of individual units over the scheduling horizon, and is given by:

$$OC = Min\left\{\sum_{t=1}^{24}\sum_{i=1}^{n_g}\left(\left(a_i P_{g_i}^2(t) + b_i P_{g_i}(t) + c_i\right)\times U_i(t) + SU_i(t)\right)\right\} \tag{2.11}$$

where n_g is the number of generating units; a_i, b_i and c_i are the cost function coefficients of unit i; $p_{g_i}(t)$ is the unit i generation output at hour t; $U_i(t)$ and $SU_i(t)$ are the commitment state and startup cost of unit i at hour t, respectively.

The hourly UC constraints include the unit generation limits (2.12), system power balance constraints (2.13), unit ramping up limits (2.14), and unit ramping down limits (2.15):

$$P_{g_i,\min}\times U_i(t) \le P_{g_i}(t) \le P_{g_i,\max}\times U_i(t) \qquad (i = 1,2,...,n_g; t = 1,2,...,24) \tag{2.12}$$

where $P_{g_i,min}$ and $P_{g_i,max}$ are the lower and upper limits of power generation of unit i, respectively.

$$\sum_{i=1}^{n_g} P_{g_i}(t)\times U_i(t) = P_D(t) \quad t = 1,2,...,24 \tag{2.13}$$

where $P_D(t)$ is the system demand at hour t.

$$P_{g_i}(t) - P_{g_i}(t-1) \le UR_i \qquad (i = 1,2,...,n_g; t = 1,2,...,24) \tag{2.14}$$

where UR_i is the ramp-up rate limit of unit i.

$$P_{g_i}(t-1) - P_{g_i}(t) \le DR_i \qquad (i = 1,2,...,n_g; t = 1,2,...,24) \tag{2.15}$$

where DR_i is the ramp-down rate limit of unit *i*.

The ramping requirement of a generating unit is defined as the difference between the optimal dispatch of that unit for two sequential hours to compensate for the wind power output variability and load uncertainty. To this end, the expected value and standard deviation of the dispatch results are calculated using PUC without the ramping constraints (2.14), (2.15). The ramping rate of the i^{th} generating unit over a one hour interval at time *t* is calculated by the following equation:

$$RR_i(t) = \left| P_{g_i}(t) - P_{g_i}(t-1) \right| \quad t = 2,3,....,24 \tag{2.16}$$

where $RR_i(t)$ is the ramping rate of the i^{th} generating unit to compensate for wind power fluctuation and load variability over the one hour interval; $P_{g_i}(t)$ and $P_{g_i}(t-1)$ are the optimal dispatch of conventional unit *i* at hours *t* and *t*-1, respectively. The total ramping requirement of the system is calculated as follows:

$$RR_{Total} = \sum_{i=1}^{n_g} \sum_{t=2}^{24} RR_i(t) \tag{2.17}$$

The maximum ramping requirement of the system at each hour is defined as the ramping rate of the unit with the highest or lowest level of ramping for the given period and is formulated as follows:

$$RR_{\max}(t) = Max\left\{RR_1(t),\ RR_2(t),...RR_{n_g}(t)\right\} \qquad t = 2,3,....,24 \tag{2.18}$$

where $RR_{max}(t)$ is the maximum ramping requirement of the system at each hour. Applying this procedure over a 24 hours period determines the maximum ramping requirement of the system for the day ahead scheduling RR_{max} as given by

$$RR_{\max} = Max\left\{RR_{\max}(2),\ RR_{\max}(3),...,\ RR_{\max}(24)\right\} \tag{2.19}$$

The total maximum ramping requirement of the system is defined as the sum of the maximum ramping requirement at each hour for the 24 hours day ahead scheduling period:

$$RR_{\max-Total} = \sum_{t=2}^{24} RR_{\max}(t) \tag{2.20}$$

Figure 1 shows the flowchart for the proposed methodology. Using curve fitting, a PDF is assigned to each of the input variables. OPF based on unit de-commitment and 2PEM is utilized to derive the expected value and standard deviation of the dispatch results. Neglecting the ramping constraints of (2.14) and (2.15), ramping requirements of the system are calculated for the 24 hours day ahead scheduling period to compensate for the wind power variability and load uncertainty. Ramping limits of (2.14) and (2.15) are then applied considering the ramping requirements calculated in the previous step. UC is then utilized to derive the expected value and standard deviation of the generation outputs and calculate the optimal operation cost of the system over the scheduling horizon.

2.2 Case Studies

Different scenarios and associated simulation results are demonstrated in this section using the IEEE 24-bus system as shown in Figure 2. Penetration level in these scenarios is

defined as the ratio of the installed wind capacity to the peak load. The system has a maximum load of 3467 MW. Initially, all generating units are committed for each hour of the scheduling period. Using the OPF results, the generators with the least operation costs are then selected for being scheduled for the given hour. Generating units data for the IEEE 24-bus system are given in the Appendix.

Three different cases are evaluated in order to examine the impacts of dispersed wind generation on ramping capabilities required to deal with wind power fluctuations for the IEEE 24-bus system. Case I corresponds to a concentrated wind generating plant at bus 14. Dispersed wind generating plants at buses 14 and 10 are evaluated in Case II. Case III corresponds to the dispersed wind generating plants at buses 14, 10 and 20. The same installed wind capacity is considered for all cases.

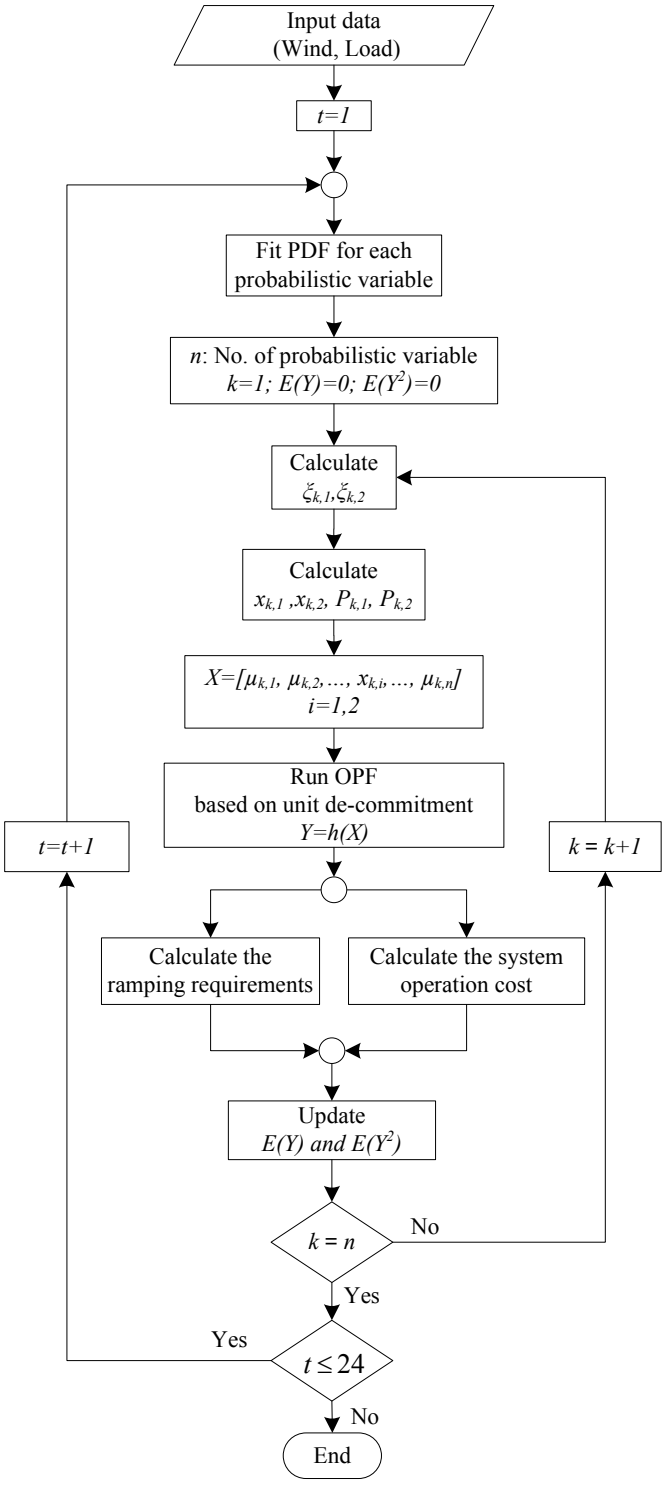

Figure 1. Flowchart for the proposed methodology

Figure 3 illustrates the maximum ramping requirements of the system at each hour ($RR_{max}(t)$) for Cases I-III over the 24 hours scheduling period with 40% wind penetration level. The magnitude of the ramping rates supplied by conventional generators increases due to the variable nature of wind generation [15]. The proposed unit commitment process provides a primary tool for scheduling sufficient resources to supply the load as well as respond to system changes such as ramping events. Figure 3 provides a qualitative representation of the wind dispersion impacts on the level of ramping rates that conventional generators need to supply. Accordingly, maximum ramping requirement of the system at each hour ($RR_{max}(t)$) is considered as an index to evaluate the ramping capability required to deal with wind power fluctuations and load uncertainty for the given period.

As shown in Figure 3, increasing the wind dispersion level from Case I with concentrated wind farm to Case II with two dispersed wind farms and Case III with three dispersed wind farms decreases the maximum ramping requirement of the system at each hour ($RR_{max}(t)$) for most of the scheduling period. This is due to the fact that the deviation of the average total output of the low or uncorrelated wind farms is lower than the deviation of the individual outputs. This will lead to a smoother output from the dispersed wind farms (Case II and Case III) compared to a concentrated one (Case I). Subsequently, the levels of ramping supplied by the conventional generators to compensate for wind power variability are highest for Case I followed by Case II and then Case III for most of the scheduling period.

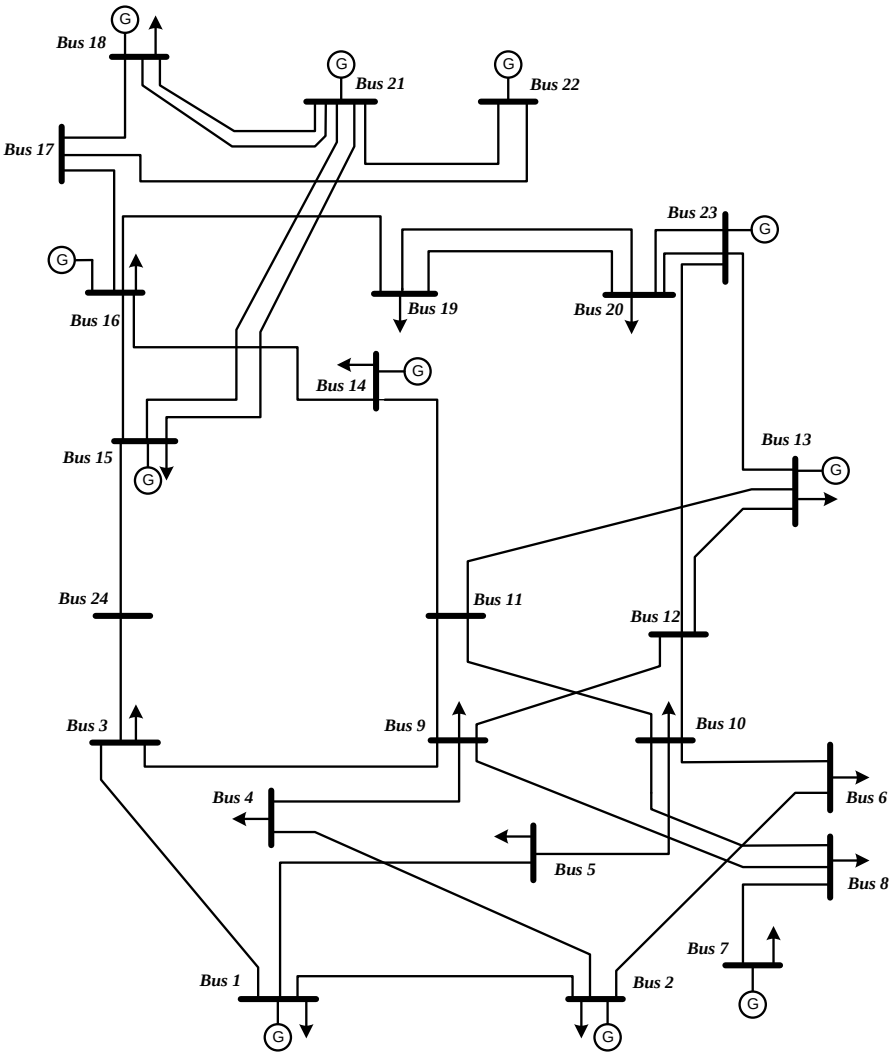

Figure 2. IEEE 24-BUS SYSTEM

The maximum ramping requirement (RR_{max}) and the total maximum ramping requirement ($RR_{max-Total}$) of the system for the 24 hours day ahead scheduling period are given in Table 1 with their corresponding means and standard deviations. These values are calculated for Cases I-III with different wind penetration levels. When considering 20% wind penetration with respect to the peak load, the mean total maximum ramping requirement of the system ($RR_{max-Total}$) decreases from 689.288 (MW/h) in Case I to 354.612 (MW/h) and 279.254 (MW/h) in Cases II

and III, respectively. The same trend is observed for the maximum ramping requirement of the system (RR_{max}) whose mean decreases from 64.86 (MW/h) in Case I to 43.582 (MW/h) in Case II and 29.392 (MW/h) in Case III. Distributed wind generation has the same impact on ramping requirements of the system with larger wind penetration levels (30% and 40%) and decreases the ramping required to compensate for wind power output variability. This is due to the wind diversity over the given geographical areas which lessens the variability of the output power for dispersed wind farms compared to concentrated ones.

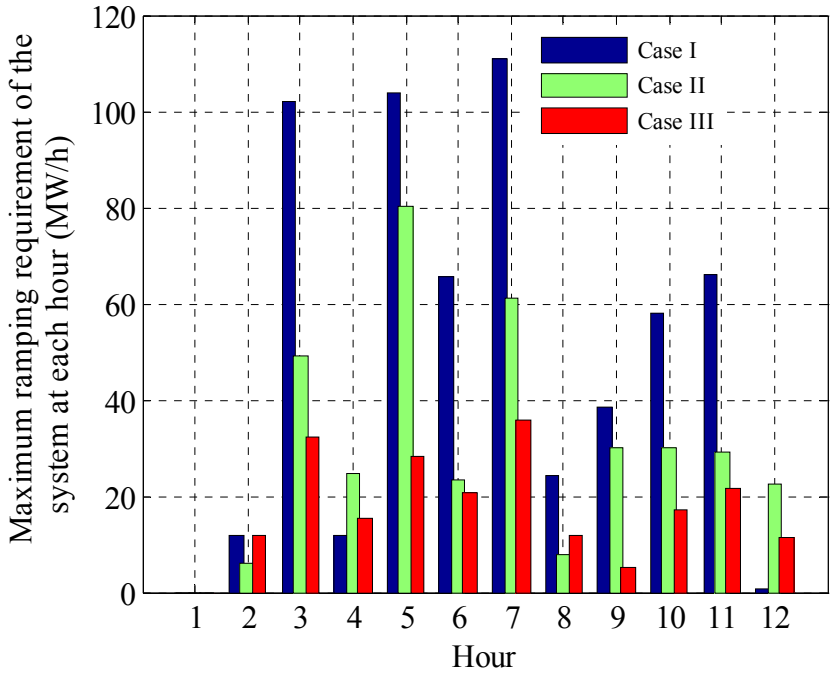

(a)

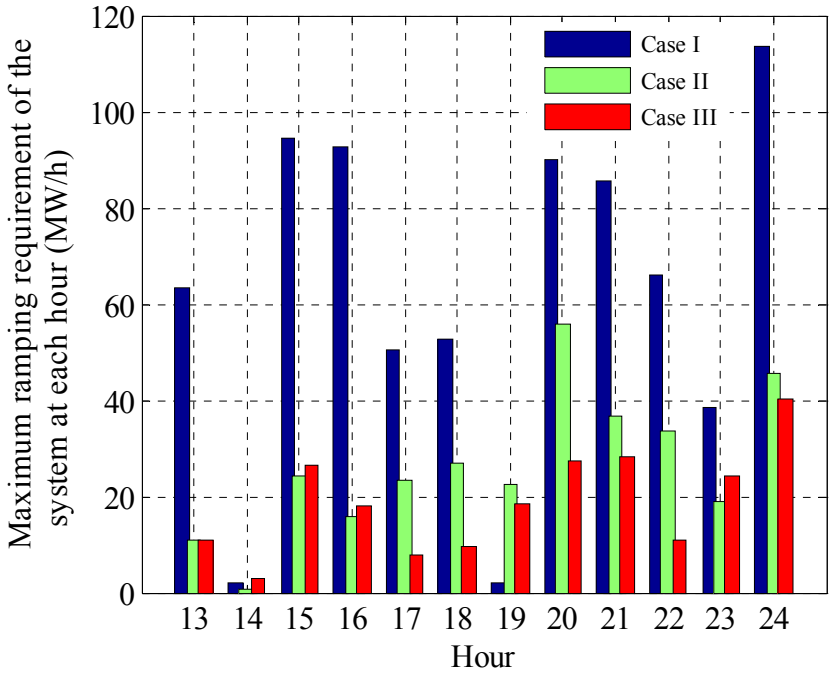

(b)

Figure 3. Mean maximum ramping requirements for 24 hours scheduling period and 40% wind penetration level. (a) t=1:12, (b) t=13:24

Table 1. System Ramping requirements for 24 hours scheduling period and different wind penetration levels

Penetration Level		$RR_{max-Total}(MW/h)$		$RR_{max}(MW/h)$	
		μ	σ	μ	σ
20%	Case I	689.288	165.877	64.86	26.634
	Case II	354.612	146.579	43.582	32.806
	Case III	279.254	84.463	29.392	6.3606
30%	Case I	1001.7	342.429	89.216	52.496
	Case II	503.888	313.301	61.903	65.642
	Case III	352.129	178.625	36.40	64.783
40%	Case I	1344.9	616.96	113.574	107.96
	Case II	678.12	609.67	80.2234	110.38
	Case III	435.433	334.812	40.2312	114.80

Comparing the ramping requirement of the systems with different wind penetration levels in Table 1, one can conclude that the ramping requirement for the 24 hours day ahead scheduling

increases with an increase in wind penetration level. This is due to the increased variability of wind for systems with larger wind penetration levels which requires greater flexibility to deal with. Greater flexibility can be provided by higher magnitude ramping rates as indicated in Table 1. The scale (λ) and shape (k) parameters of the Weibull distribution for the output random variables are estimated using least square method (LSM) and are given in Table 2.

Table 2. Scale and shape parameters of the Weibull distribution for system ramping requirements over 24 hours scheduling period and different wind penetration levels

Penetration Level		$RR_{max-Total}(MW/h)$		$RR_{max}(MW/h)$	
		λ	k	λ	k
20%	Case I	753.08	4.7365	73.0083	2.6177
	Case II	399.2498	2.5986	47.4785	1.3423
	Case III	309.5294	3.6803	31.8974	5.3203
30%	Case I	1123.9	3.2	100.187	1.7543
	Case II	563.5309	1.6512	60.2865	0.9435
	Case III	397.5224	2.0679	23.8823	0.5941
40%	Case I	1518	2.3131	115.89	1.052
	Case II	705.67	1.114	66.53	0.7387
	Case III	472.34	1.3122	14.137	0.4244

The expected total ramping requirement of the system (RR_{Total}) are calculated and given in Table 3. For 20% wind penetration, increasing the wind dispersion level from Case I with concentrated wind farm to Case II with two dispersed wind farms and Case III with three dispersed wind farms decreases the total ramping requirement of the system from 5285.6 (MW/h) to 2718.1 (MW/h) and 2101.5 (MW/h), respectively. When comparing the total ramping requirement of the systems with different wind penetration levels, it is concluded that an increase in wind penetration level increases the total ramping requirement of the system for the 24 hours day ahead scheduling period.

Table 3. Total system ramping requirements for 24 hours scheduling period and different wind penetration levels

Penetration Level		$RR_{Total}(MW/h)$
20%	Case I	5285.6
	Case II	2718.1
	Case III	2101.5
30%	Case I	7514.9
	Case II	3724.1
	Case III	2592.0
40%	Case I	9786.9
	Case II	4862.3
	Case III	3023.6

Figures 4 and 5 show the cumulative distribution functions of the system ramping requirements for 24 hours scheduling period and 40% wind penetration level. For a given ramping level in these figures, the probability that the ramping requirements of the system are less than that level is highest for Case III, followed by Cases II and I, respectively. Accordingly, increasing the wind dispersion level provides the system with more smoothing capability of wind power output and decreases the ramping required to compensate for wind power fluctuations and load variability.

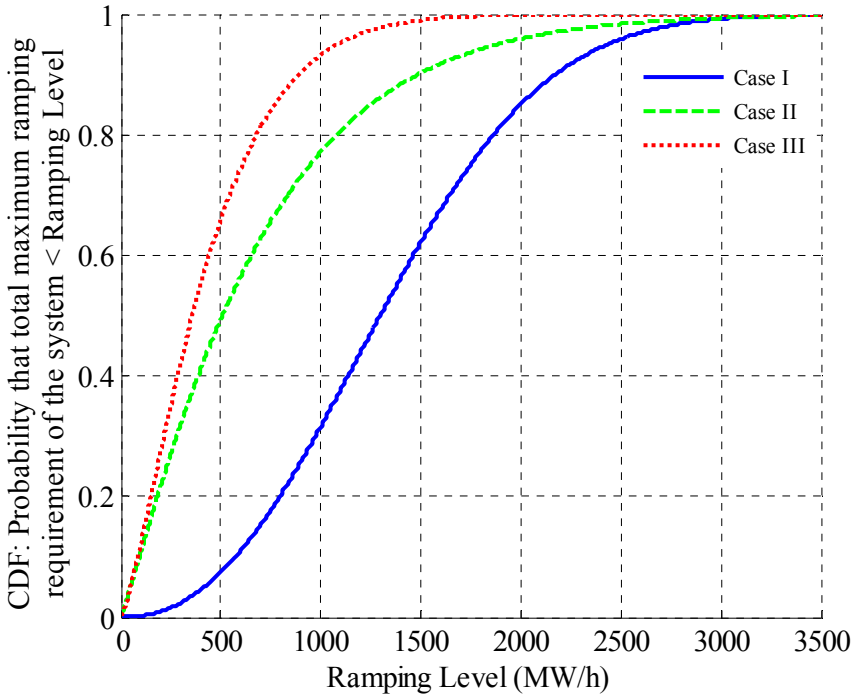

Figure 4. Cumulative distribution of system total maximum ramping requirement for 24 hours scheduling period and 40% wind penetration level

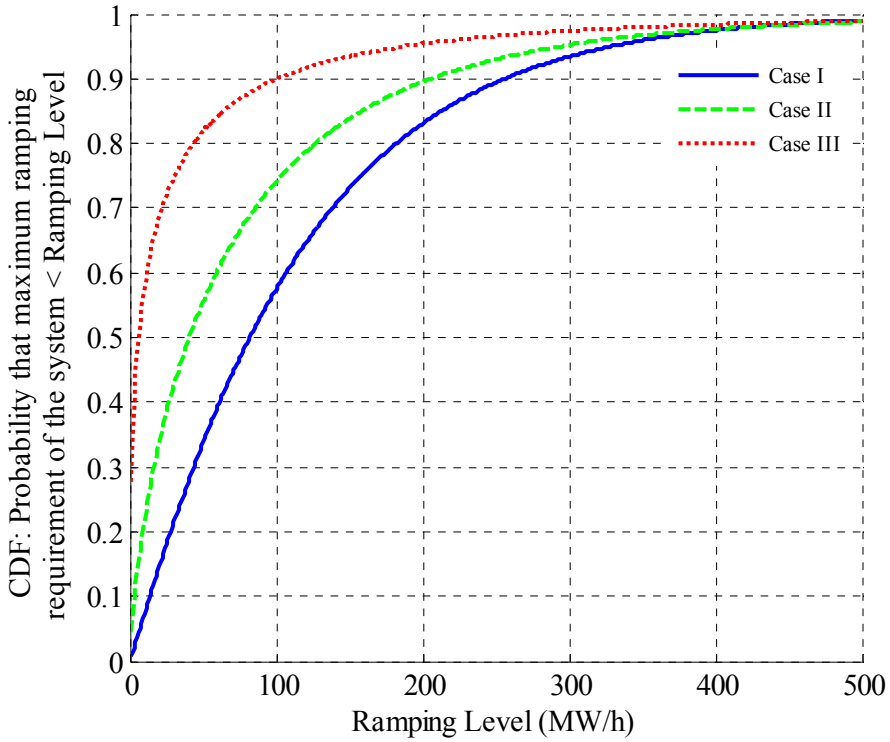

Figure 5. Cumulative distribution of system maximum ramping requirement for 24 hours scheduling period and 40% wind penetration level.

Considering the ramping requirements obtained by the unit de-commitment and two-point estimate methods, a unit commitment is performed over the 24 hours day ahead scheduling period for different wind penetration levels. System operation costs are calculated for Cases I-III and expected value of the results are given in Table 4. As indicated, increasing the wind dispersion level from Case I to Case II and Case III decreases the system operation cost for a certain wind penetration level. This is due to the lower ramping magnitudes required to compensate for the decreased wind variability in the dispersed wind farms compared to a concentrated one. An increase in wind penetration level increases the wind power output in scheduling process. This will decrease the required conventional generations for meeting the

load and lessen the system operation cost for the 24 hours day ahead scheduling. Also, the impact of wind distribution on system operation cost reduction will be more significant for the systems with higher wind penetration levels.

Table 4. System operation cost for 24 hours scheduling period and different wind penetration levels

Penetration Level (%)	Ramp rate limit (MW/h)	Case #	$OC(\$/24\ h)$
20	40	I	1.7563×10^6
		II	1.7188×10^6
		III	1.7075×10^6
30	60	I	1.6861×10^6
		II	1.6366×10^6
		III	1.6195×10^6
40	80	I	1.6188×10^6
		II	1.5538×10^6
		III	1.5297×10^6

2.3 Conclusion

This chapter evaluates distributed wind generation and its potential impact on ramping requirement in power systems with high levels of wind penetration. Using historical data and curve fitting, wind and load are stochastically modeled. Probabilistic unit commitment based on unit de-commitment and two point estimate methods is proposed to calculate the ramping requirements and system operation costs. This method is tested on the IEEE 24-bus system and different case studies are carried out to investigate the factors affecting the ramping requirement. Based on simulation results, distributing the wind generating plants throughout the IEEE 24-bus system decreases the ramping requirement for 24 hours day ahead scheduling. Furthermore, higher wind penetration levels increase the ramping requirement of the system due to the increased wind power variability. System operation cost analysis shows a reduction in cost when wind generation is spread over a wide geographical area. This reduction will be more significant

for the systems with higher wind penetration levels.

Table 5. Conventional generators data

Conventional Generator	Cost Function Coefficients			Startup Cost ($)
	$a_i(\$/MW^2h)$	$b_i(\$/MWh)$	$c_i(\$)$	
G_1	0.0073	21.05	1313.6	1000
G_2	0.0078	21.04	1168.1	1000
G_3	0.0080	16.19	1078.8	1000
G_4	0.0061	17.26	969.8	1000
G_5	0.0058	21.6	958.2	1000
G_6	0.0068	21.6	958.2	1000
G_7	0.0080	23.9	471.6	1000
G_8	0.0070	23.9	471.6	1000
G_9	0.0078	19.7	445.4	1000
G_{10}	0.0081	16.51	702.7	1000

III. Chapter 3. Optimal Sizing of Hybrid Power Systems

3.1. Methodology

3.1.1. Probabilistic modeling of generation and HVAC load

Hybrid generation systems are inherently uncertain because of the stochastic nature of wind speed, solar irradiance and load characteristics. The uncertainties of wind/solar generation are characterized using the probability density functions (PDFs) whose statistics are obtained from historical data of wind speed and solar irradiance [34], [83]. Fuzzy C-Means (FCM) clustering is used in this section to account for seasonal variation in the data [84]. Ten years of historical hourly data are utilized to produce three data sets for: wind speed, solar irradiance and load [85]. Each data point is specified by a membership grade between 0 and 1. The objective function of the FCM is to minimize the distance from any given data point to a cluster center weighted by that data point's membership grade. An iterative algorithm is used to update the cluster centers and the membership grades for each data point, which moves the cluster centers to the most appropriate location within the data sets. The elbow method is used to determine the number of clusters [86]. Accordingly, the days are grouped into 10 clusters with similar 24-hour wind speed, solar irradiance and load data. Maximum likelihood estimates of the distribution parameters are calculated for the historical hourly data within a cluster. Each cluster is then represented by three sets of 24 individual PDFs over the 24-hour period.

a) Hourly wind power modeling: Wind speed is statistically modeled using the Weibull distribution [34], [83]. The PDF for a Weibull distribution is given by:

$$f_v(v) = \left(\frac{k}{\lambda}\right)\left(\frac{v}{\lambda}\right)^{k-1} e^{-\left(\frac{v}{\lambda}\right)^k}, 0 \le v \le \infty \quad (3.1)$$

Using curve fitting, maximum likelihood estimates of the Weibull distribution parameters are calculated for historical hourly wind speed data. The output power of a wind generator is a function of wind speed and given by [77]:

$$G_W^{'} = \begin{cases} 0 & v \le v_i, v \ge v_o \\ \frac{v - v_i}{v_r - v_i} G_{W_r} & v_i \le v \le v_r \quad \infty \\ G_{W_r} & v_r \le v \le v_o \end{cases} \quad (3.2)$$

If the power electronic interface has an efficiency of η_w, the net wind power output is given by:

$$G_w = \eta_w . G_W^{'} \quad (3.3)$$

b) Hourly photovoltaic power modeling: Unlike wind speed, the uncertainty of solar irradiance cannot be directly modeled using a PDF. This is due to the fact that the solar irradiance has very strong diurnal patterns as at night time, the value of solar irradiance is certain to be zero [87]. Hence, this section uses the clearness index to characterize solar irradiance. The hourly clearness index (k_t) is defined as the ratio of the irradiance on a horizontal plane, I_t (kW/m^2), to the extraterrestrial total solar irradiance I_o (kW/m^2):

$$k_t = \frac{I_t}{I_o} \quad (3.4)$$

The clearness index is statistically modeled using the Beta distribution [83], [88]. The PDF for a Beta distribution over a time interval *t* is given by:

$$f_{ci}(k_t) = \frac{\Gamma(a+b)}{\Gamma(a)\Gamma(b)} . k_t^{a-1} . (1 - k_t)^{b-1} \quad (3.5)$$

Using curve fitting, maximum likelihood estimates of the Beta distribution parameters are

calculated for historical hourly clearness index data. Once the hourly clearness index is known, the irradiance on a surface with inclination β to the horizontal plane, I_β is calculated as:

$$I_\beta = T.k_t - T'.k_t^2 \quad (3.6)$$

where T and T' are parameters that depend on inclination, declination, reflectance of the ground, latitude, hour angle and sunset hour angle. The PV power output is a function of the clearness index and is given by [34]:

$$G'_{PV} = A_c.\eta'_{PV}.I_\beta A_c.\eta'_{PV}.(T.k_t - T'.k_t^2) \quad (3.7)$$

If the power electronic interface has an efficiency of η_{PV}, the net PV power output is given by:

$$G_{PV} = \eta_{PV}.G'_{PV} \quad (3.8)$$

The values for η_W and η_{PV} are calculated using the efficiency curves of the power converters [89], [90].

c) Hourly load modeling: This section uses a Gaussian distribution with specific lower and upper limits to model the hourly load variation [83]. Using curve fitting, maximum likelihood estimates of its parameters are calculated for historical hourly load data.

3.1.2. Optimization approach based on genetic algorithm

Optimization using genetic algorithms provides a powerful tool to obtain the optimal capacity for solar energy, wind energy and storage in a hybrid system. Generally, a set of initial solutions (initial populations), randomly selected from the feasible solution space, is used to start the genetic algorithm. The fitness function is evaluated for each solution, and the solutions are consequently ranked. The population then evolves through several operations such as reproduction, crossover and mutation to optimize the fitness function and obtain the final optimal

solution. The process is repeated until a termination criterion is satisfied. This evolutionary algorithm is preferred to classical optimization approaches because it can handle the non-linear, non-convex and non-smooth optimization problem of the component-sizing for the hybrid system. The non-convexity of the problem makes it difficult for classical optimization methods to obtain a global optimum. Genetic Algorithms, on the other hand, globally search the domain of possible solutions for an optimal solution [53], [91]-[92].

Several implementation provisions are considered in this section to avoid convergence to local minima. In this regard, the double vector representation rather than the binary one is used for chromosome codification to guarantee mutation coherence. Scaling the decision variables and using MW/MWh, instead of kW/kWh for the components sizing keeps the feasible solution space smaller and facilitates mutation. A large population size is selected to increase the possibility of convergence to the global minimum, but this significantly increases the computational burden. Two elitism children are maintained for each generation to ensure retaining desirable solutions. The balance between crossover and mutation offspring is kept at a desirable level by adjusting the crossover rate around 78%. To ensure satisfying the constraints, a large penalty factor is assigned to a solution that violates a constraint. Enhanced system efficiency, as well as the fewer number of variables provided by the GA, make it a better solution than classical optimization approaches for optimal component-sizing of hybrid systems. The parameters of the GA are given in Table 6.

Using historical hourly data for wind and PV generation and cooling load, we first normalize the PV and wind generation curves by dividing them by the maximum PV and wind generation. Next, we assign the scaling parameters (α_{PV}) and (α_{W}) to the normalized PV and

wind curves which show the installed capacities of PV and wind generation. We obtain the optimum scaling parameters α_{PV} and α_W, as well as the storage capacity by minimizing the cost function:

$$Min\ Cost = Min\ \{C_{PV}.\alpha_{PV} + C_W.\alpha_W + C_S.S + C_P.P\} \quad (3.9)$$

The last two terms are the capital costs needed for installing the storage system. The total capital cost of the storage system is composed of four components: the capital cost for energy, the capital cost for power, the system energy balance cost and the system power balance cost. The balance of system energy and power cost can be included in C_S and C_P, respectively [93]. Also, the inverter based interface cost for connecting the PV and wind to the network is considered part of C_{PV} and C_W.

Table 6. GA parameters

Parameter	Population Size	Max Generation	Crossover Rate	Mutation Rate	Elitism Number
Value	200	150	78%	20%	2

The optimization formula given in equation (3.9) is subject to several physical constraints on the parameters. The first constraint is an energy balance equation to guarantee that the combination of wind and PV generation meets the required HV or cooling load over the optimization period. Note that the efficiency of the storage system is always less than unity due to the losses. To compensate for these losses, additional generation is needed. Hence, the energy balance equation must be changed to the following inequality constraint:

$$\sum_{t=1}^{T} G_{PV,t} + \sum_{t=1}^{T} G_{W,t} \geq \sum_{t=1}^{T} L_t \quad (3.10.a)$$

$$E = \sum_{t=1}^{T} EE_t = \sum_{t=1}^{T} G_{PV,t} + \sum_{t=1}^{T} G_{W,t} - \sum_{t=1}^{T} L_t \quad (3.10.b)$$

The next constraint guarantees an instantaneous balance between the sum of the generated wind energy, PV energy, and stored energy, and the instantaneous load. The storage is charged when $G_{PV,t} + G_{W,t} - L_t + L_{S,t} \geq 0$ and discharged when $G_{PV,t} + G_{W,t} - L_t + L_{S,t} < 0$. The instantaneous energy balance in the storage system is as follows:

a) For charging:

$$S_t = (1-d)S_{t-1} + \eta_S\left(G_{PV,t} + G_{W,t} - L_t + L_{S,t}\right), \forall t \in T \quad (3.11.a)$$

b) For discharging:

$$S_t = (1-d)S_{t-1} + \left(G_{PV,t} + G_{W,t} - L_t + L_{S,t}\right), \forall t \in T \quad (3.11.b)$$

Utilities often have some intelligent control over HVAC loads including agreements with consumers to shift part of their HVAC loads during peak load hours if there is a problem in the operation of the transmission network. For example, NV Energy's cool share program is associated with approximately 145 MW remote controlled air conditioning load. These loads can be dispatched by NV Energy through "raise/lower" thermostat commands as needed and may include pool pumps, refrigerators, hot tubes, etc. which "need to run" but their exact time of operation is not critical. Load shifting can provide some flexibility regarding this problem. Because the hourly generation of wind farms and solar plants is not strictly under human control, load shifting can be useful during periods of insufficient generation. Implementing smart load control can reduce the mismatch between renewable generation and HVAC load. Load shifting is expressed as:

$$L'_t = L_t - L_{S,t} \quad (3.12.a)$$

$$L'_{t+1} = L_{t+1} + L_{S,t} \quad (3.12.b)$$

To ensure that the shifted load is positive and is less than the specific percentage of the load (δ) at each time *t*, we need:

$$0 \leq L_{S,t} \leq \delta . L_t \quad (3.13)$$

Storage systems have a minimum storage level, denoted by S_{min} that must be maintained to prolong lifetime. In addition, there is typically a maximum storage capacity that is dictated by the size of the renewable generation units, which we denote by S_{max}. The storage at time *t* is thus governed by:

$$S_{min} \leq S_t \leq S_{max} \quad (3.14)$$

The upper bound S_{max} is not known a priori and is optimally calculated in our solution.

The next constraint ensures that the capacity of the storage system is equal to the maximum storage capacity needed to maintain excess energy at hour *t*.

$$S = \max (S_t) \quad (3.15)$$

Assuming the same charge and discharge rate, the maximum power rating of the storage unit is given by:

$$P_t = G_{PV,t} + G_{W,t} - L_t + L_{S,t} \quad (3.16.a)$$

$$P = \max|P_t| \quad (3.16.b)$$

The optimization problem can be formulated as follows:

$$\min \{f(x,u)\} \quad (3.17)$$

$$s.t. \quad g(x,u) = 0 \quad (3.18)$$

$$h(x,u) \leq 0 \tag{3.19}$$

where *f(x, u)* is the objective function of (3.9), the decision variables (u) are α_{PV}, α_W, and the dependent variables (x) are EE, L'_t, L'_{t+1}, S_t, S, P_t, P. The equality constraints of (3.18) are given by (3.10.b), (3.11), (3.12), (3.15), and (3.16), while the inequality constraints of (3.19) are given by (3.13) and (3.14).

We first solve a simplified optimal component-sizing problem without load shifting for the hybrid system using a GA implemented in MATLAB. We then solve the same problem using discontinuous nonlinear programming (DNLP) in GAMS. Table 7 shows the simulation results for this problem. Comparing the GA-based results with the DNLP demonstrates the improved efficiency of the proposed methodology over the classical optimization approaches.

Table 7. Simulation results for GA-based and classical optimization approaches

Simulation Results	$\alpha_W(MW)$	α_{PV}(MW)	*S (MWh)*	*EE (MWh)*	Total Cost (M$)
GA (MATLAB)	1.9325	0	3.383	1.148	4.7792
DNLP (GAMS)	1.9350	0	3.392	1.171	4.786

3.1.3. Probabilistic optimization

The randomness of wind and PV power output and loads are taken into account by using stochastic optimization. The latter is performed using analytical methods or simulation methods [94]. Monte-Carlo simulation (MCS) is a simple and accurate simulation method that uses historical data to determine their PDFs. Random values from these PDFs are used to quantify the uncertainties. The large computational effort is the main obstacle for efficient use of this method. Several approximate methods have been proposed to reduce the computational burden including Taylor series expansion [95], first-order second-moment method (FOSMM) [96], cumulants

[97], and point estimation (PE) [80]. PE is a popular analytical method because of its accuracy, simplicity, and speed. Two-point estimation (2PE), a variation of PE, is applied in this section to model the uncertainties [81], [82]. Vectors of input and output random variables and the corresponding nonlinear function are given by equations (20), (21), and (22).

$$X = [Wind\ Gen., PV\ Gen., HVAC\ Load] \tag{3.20}$$

$$Y = [S_t, P_t, EE_t, L_{S,t}\ ] \tag{3.21}$$

$$Y = h(X) \tag{3.22}$$

Two concentrations of f_{X_k} ($x_{k,1}$, $x_{k,2}$) are used to replace f_{X_k} by matching its first three moments. The functional relation between X_k and $h(X_k)$ is then used to produce two estimates of Y variants ($Y_{k,i}$=$h(\mu_{X_1}, \mu_{X_2},\ldots, x_{k,i},.., \mu_{X_{n-1}}, \mu_{X_n})$ i=1, 2) from ($x_{k,1}$, $x_{k,2}$). $P_{k,1}$ and $P_{k,2}$ scale these estimates to compute the expected value and standard deviation of the output.

Figure 6 shows the flowchart for the proposed method. Ten years of historical hourly wind speed, solar irradiance and load data are the inputs. FCM is then used to cluster these data into clusters of days with similar data points. Next, the scaling parameters (α_{PV} and α_W) are initialized. The parameters of the 2PE shown in Figure 6 are:

$$\zeta_{k,i} = \sqrt{n + (\frac{\lambda_{k,3}}{2})^2} \qquad i = 1, 2 \tag{3.23.a}$$

$$\xi_{k,i} = \frac{\lambda_{k,3}}{2} + (-1)^{3-i}\zeta_{k,i} \quad i = 1, 2 \tag{3.23.b}$$

$$P_{k,i} = \frac{(-1)^i \xi_{k,i}}{2n \times \zeta_{k,i}} \qquad i = 1, 2 \tag{3.23.c}$$

$$x_{k,i} = \mu_{X_k} + \xi_{k,i}\sigma_{X_k} \qquad i = 1, 2 \tag{3.24}$$

Once the 2PE parameters are calculated for the input random variables, equations (3.2)-(3.3) and (3.7)-(3.8) are used to calculate these parameters for the normalized net wind and PV power outputs. The normalized outputs are then multiplied by the scaling parameters to calculate the hourly net PV and wind generation using vector Z. Note that μ_{X_k} in Z is replaced by $x_{k,i}$ $(i = 1, 2)$ at each iteration. The power rating of the storage system at time t (P_t) is then calculated by the energy management function (EMF). If P_t is positive, more generation is provided and the storage system is charged. If negative, the load exceeds generation and the storage system is discharged to supply the excess load. If the energy stored is less than S_{min}, part of the load is shifted to the next hour. If the energy stored is less than S_{min} after the maximum allowable load shifting (a specific percentage of the HVAC load (δ)), new scaling parameters are selected by GA to satisfy this constraint. The first and second moments of the output variables are then calculated by:

$$E(Y) \cong \sum_{k=1}^{n}\sum_{i=1}^{2}(P_{k,i} \times h([\mu_{X_1}, \dots, x_{k,i}, \dots, \mu_{X_n}])) \tag{3.25.a}$$

$$E(Y^2) \cong \sum_{k=1}^{n}\sum_{i=1}^{2}(P_{k,i} \times h^2([\mu_{X_1}, \dots, x_{k,i}, \dots, \mu_{X_n}])) \tag{3.25.b}$$

Given $E(Y)$ and $E(Y^2)$, we calculate the mean and standard deviation of the output variables.

$$\mu_Y = E(Y) \tag{3.26.a}$$

$$\sigma_Y = \sqrt{E(Y^2) - \mu_Y^2} \tag{3.26.b}$$

The fitness function is then evaluated and a confidence coefficient (γ) is allocated to the

probabilistic constraints:

$$P(X \geq X_{min}) \geq \gamma \tag{3.27}$$

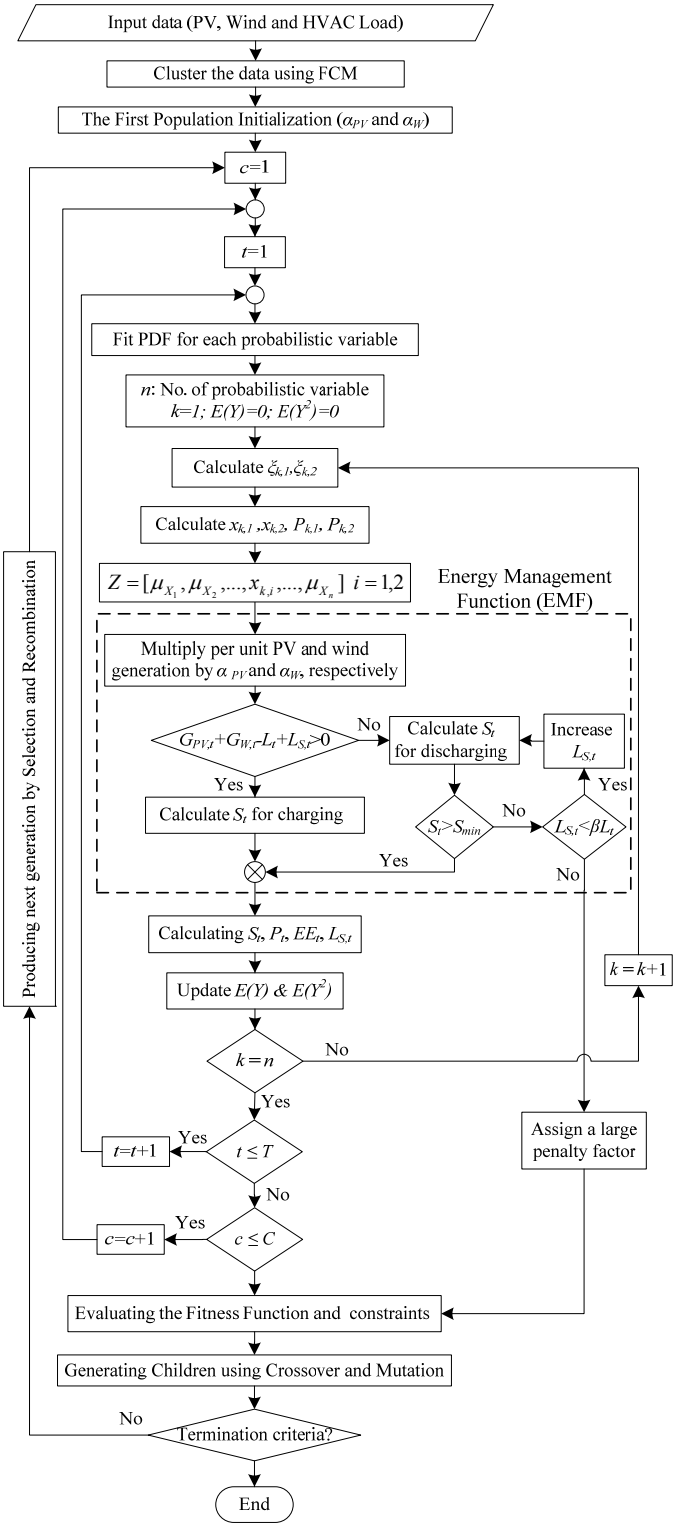

Figure 6. Flowchart for the probabilistic GA-based optimization approach using 2PE

Next, the constraints are checked for violation. If there is any violation, the violated constraints are assigned a large penalty factor (υ) and combined with the fitness function f to give:

$$f'(x,u) = f(x,u) + v[h(x,u)]^2 \tag{3.28}$$

This combination assigns a higher cost to an infeasible solution candidate than to a feasible one with the same objective values [91].

Implementing the crossover and mutation operators to the chromosomes, the offspring population is created and then used to produce the next generation by selection and reproduction. This evolutionary algorithm is repeated until reaching the termination criterion. Eventually, the best chromosome is selected as the optimal solution. The fitness function of the GA is a weighted sum of the hybrid system installation costs for all the clusters and is given by:

$$Fitness\ Function = Min\left\{\sum_{c=1}^{C} w_c.Cost_c\right\} \tag{3.29}$$

The weighting coefficient for each cluster (w_c) is defined as the ratio of the number of days within that cluster to the total number of days (365×10 days). Minimizing the installation cost of the hybrid system selects the optimum PV, wind generation, and storage capacity to supply the HVAC load at the desired confidence level without the need for supplementary generation.

3.2. Case Studies

In this section, we examine two scenarios for an energy management system combining renewable energy generation and energy storage. The first is a simplified deterministic scenario that allows us to better demonstrate the interplay between storage and renewable energy generation to meet an HVAC load. The second scenario is stochastic and includes the complexity

introduced by the uncertainties of renewable energy generation and cooling loads. We present simulation results for the optimal GA or GA-2PE solution subject to the constraints (3.10.b) and (3.11)-(3.16).

3.2.1. Scenario I: Deterministic wind/PV generation and cooling load

Scenario I corresponds to deterministic wind generation PV generation, and cooling load for a residential feeder over a single day [98]-[100]. The peak wind generation level is typically significantly less than the generation capacity as observed in this data set [98]. Two different cases are studied using GA-based optimization. Figure 7 shows the hourly generation of the PV system and wind system normalized based on the maximum installed capacities of PV and wind generation for a single day. Figure 8 shows the hourly cooling load for a residential feeder.

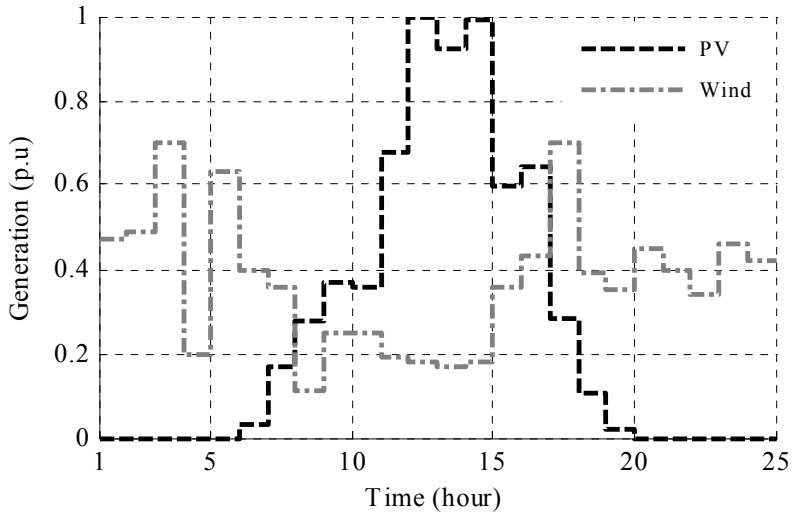

Figure 7. Normalized hourly PV generation and wind generation

Installation costs of the storage system for energy and power are 0.2 $/Wh, and 0.25 $/W [93]. Piece-wise linear cost functions are assigned to the PV and wind generation to calculate the associated installation costs [101], [102]. These are the average installation costs of the different

technologies for utility-scale (hundreds to thousands of kilowatts) systems.

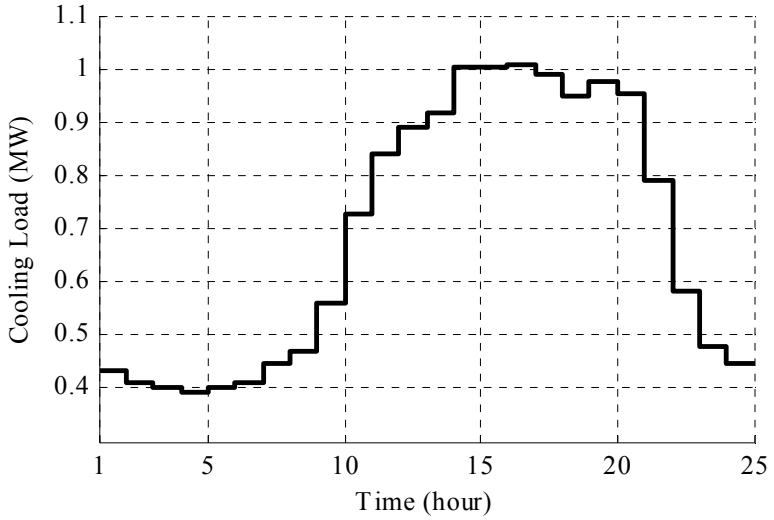

Figure 8. Hourly cooling load of a residential feeder for a single day

The minimum allowable charge of the storage system is 3% of its rated capacity [103]. This minimum charge, necessary for some storage technologies, is for ensuring a longer life time.

Case Study I: The optimization problem is solved for the normalized PV generation, wind power and cooling load as shown in Figures 7 and 8. The maximum allowable load shifting is 30% of the load for each hour. The simulation results in Figure 9 show that in the absence of load shifting the modified cooling load is the same as the cooling load during hours 1-15. Storage shows the state of charge of the storage system at each hour. At each hour, the energy stored in the storage system at time t can be calculated by adding two components; the energy stored in the storage system at time t–1 reduced to account for discharge over one hour, and the excess energy given by the difference between the generation and load over a one hour period scaled to account for the roundtrip efficiency of the storage system. As shown, wind generation is always included in the optimal solution since wind installation cost per MW is less than PV installation

cost. The storage system is charged in the early hours of the day when more energy is available and the load is low, then releases the energy stored when the load exceeds generation. During peak hours when the wind is low and the storage is not sufficiently charged, load shifting dispatches the flexible loads to hours when the wind energy is in excess of the load. This is evident for hours 17, 22, 23, and 24 where the shifted loads are fully met.

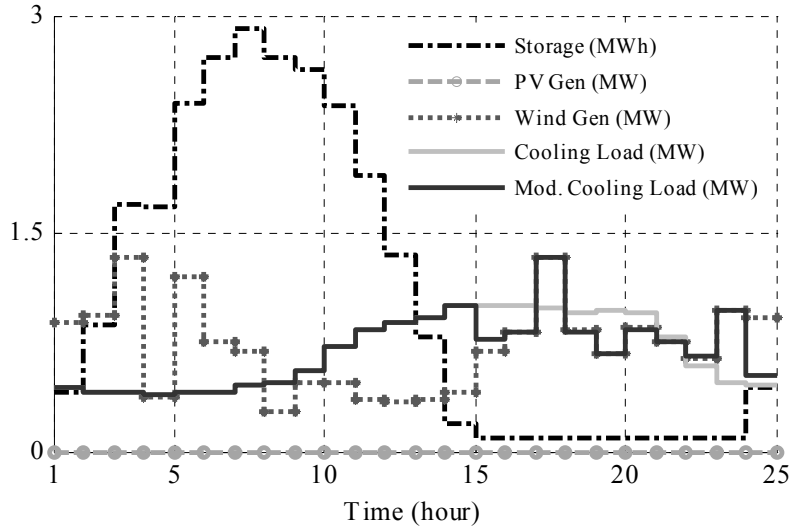

Figure 9. Simulation result for Case Study I (Scenario I)

For this case study, the optimum PV, wind installation and storage capacity are 0.0 MW, 1.9 MW and 2.92 MWh (with 0.93 MW). The excess energy, i.e. the amount of energy in excess of the load, is 0.85 MWh. Total installation cost of the system is $\$4.615\times 10^6$ ($\$3.80\times10^6$ for wind and $\$0.815\times 10^6$ for storage).

Case Study II: This case study evaluates the possibility of matching HVAC load and PV plants, which is particularly important for regions with poor wind speed profiles and an abundance of solar energy. The 24 hour simulation period starts at noon when solar energy is most readily available. The optimum PV, and storage capacity are 2.85 MW, and 6.4 MWh (with 1.81 MW)

and the excess energy produced is 4.58 MWh. Total installation cost of the system is minimized at $\$13.404\times 10^6$ ($\$11.671\times 10^6$ for PV $\$1.733\times 10^6$ for storage). The simulation results show that by installing more PV capacity and storage capacity the load can be fully supplied without wind energy generation. Another observation is that the storage capacity needed for this case study is larger than Case Study I where wind energy, is available during most hours of the day. This is because solar energy is only available during daylight hours and storage provides energy for the remainder of the day.

3.2.2. Scenario II: Stochastic wind/PV generation and cooling load

Scenario II corresponds to stochastic models of wind generation, PV generation, and cooling load. PDFs are obtained from historical hourly wind speed and solar irradiance using curve fitting [85]. Wind and PV power are derived based on equations (3.1)-(3.5). Similarly, we calculate the maximum likelihood estimates of the normal distribution parameters for historical hourly cooling load data for a residential feeder. GA-2PE stochastic optimization evaluates the efficiency of the hybrid system for 10%, 20%, 30%, 40% and 50% load shifting (L.S.).

Case Study I: The GA-based optimization problem is solved considering the probabilistic PV generation, wind generation and cooling load. Figures 10 and 11 show the cumulative distribution functions $F_S(s)$ of the storage capacity (S) and $F_{EE}(ee)$ of the excess energy (EE) for each load shifting.

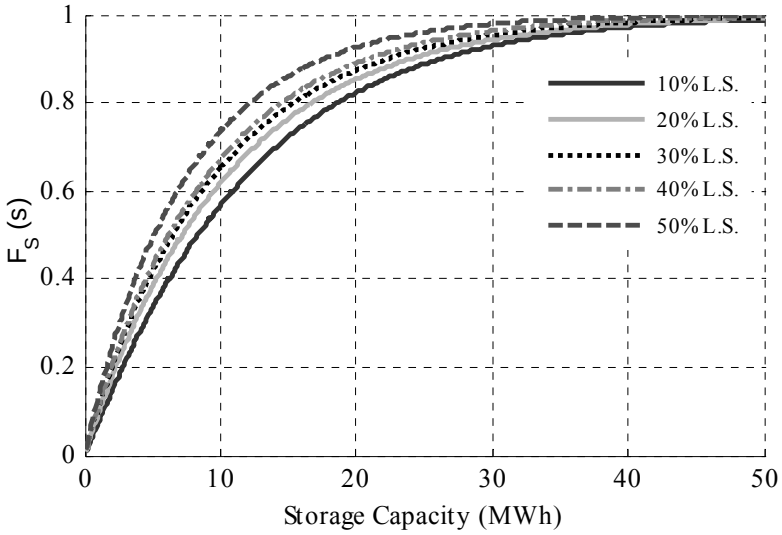

Figure 10. Cumulative distribution of the maximum capacity of the storage system for different load shifting percentages (Scenario II, Case Study I)

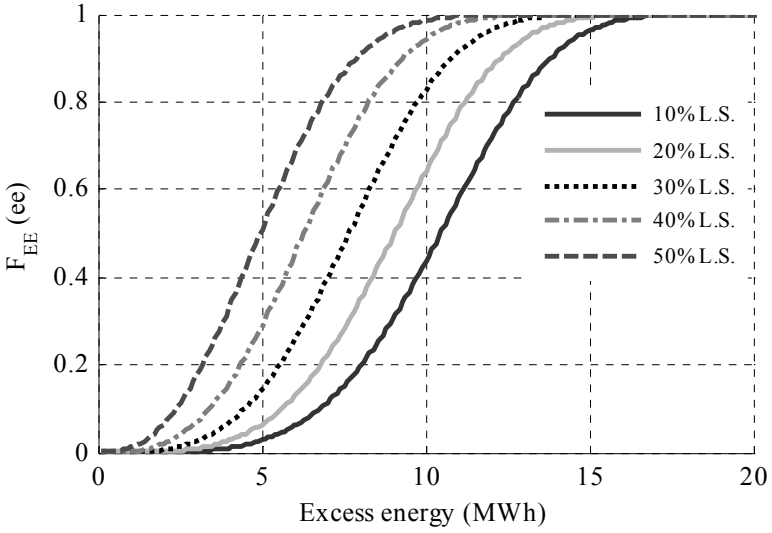

Figure 11. Cumulative distribution of the excess energy of the system for different load shifting percentages (Scenario II, Case Study I)

For both *S* and *EE,* the cumulative probabilities increase with load shifting. Thus, increasing the load shifting from 10 to 50 percent provides the system with more flexibility and reduces the storage capacity and excess energy of the system. This leads to a more efficient system with less energy dissipated due to the non-ideal characteristics of the storage system.

Case Study II: This case study evaluates the possibility of matching HVAC load and PV plants for regions with poor wind speed profiles and an abundance of solar energy. The CDFs, $F_S(s)$ of the storage capacity (*S)* and $F_{EE}(ee)$ of the excess energy (EE) for this case study show a similar trend to those of Case Study I and are not provided for brevity. For both S and EE, the cumulative probabilities increase with load shifting. Thus, increasing the load shifting from 10 to 50 percent provides the system with more flexibility.

Table 8. Installed wind and PV capacity, maximum storage capacity, and excess energy (Scenario II)

Load Shifting		10%	20%	30%	40%	50%
Case Study I	$\alpha_W(MW)$	2.611	2.478	2.347	2.219	2.096
	$\mu_S(MWh)$	11.630	10.309	9.004	7.735	6.576
	σ_S(MWh)	11.139	10.505	9.891	9.168	7.820
	$\mu_{EE}(MWh)$	10.364	9.000	7.655	6.340	5.068
	$\sigma_{EE}(MWh)$	2.712	2.563	2.421	2.255	2.110
	Wind Cost (M$)	5.222	4.956	4.695	4.439	4.191
	Storage Cost (M$)	2.510	2.232	1.955	1.685	1.441
Case Study II	α_{PV}(MW)	3.883	3.844	3.776	3.690	3.542
	$\mu_S(MWh)$	9.114	8.968	8.728	8.429	7.919
	$\sigma_S(MWh)$	4.251	4.208	3.488	3.409	3.274
	$\mu_{EE}(MWh)$	9.131	8.871	8.426	7.855	6.880
	$\sigma_{EE}(MWh)$	2.613	2.799	2.821	2.773	2.801
	PV Cost (M$)	15.922	15.760	15.483	15.128	14.522
	Storage Cost (M$)	2.467	2.429	2.366	2.286	2.151

Table 8 gives the installed wind and PV capacity, the expected value and standard deviation of storage capacity and excess energy. This table also provides optimal installation cost of the hybrid system for renewable energy generation and storage system.

Table 9 gives the cost of the hybrid system for different risk levels. Assigning a confidence coefficient (γ) to the probabilistic constraints, risk is defined as the percentage of the random variable violating the corresponding constraint:

$$Risk(\%) = 1 - \gamma \tag{3.30}$$

Table 9. Hybrid system cost for different risk levels (Scenario II)

Risk Level (%)		75	80	85	90	95
Case Study I	Wind Cost (M$)	3.769	4.191	4.799	6.121	9.279
	Storage Cost (M$)	1.059	1.441	2.070	3.471	6.835
Case Study II	PV Cost (M$)	14.341	14.522	15.256	17.265	18.626
	Storage Cost (M$)	2.111	2.151	2.315	2.782	3.102

As shown in Table 8, increasing load shifting from 10 to 50 percent decreases the expected value of *S* from 11.630 MWh to 6.576 MWh and decreases the expected value of *EE* from 10.364 MWh to 5.068 MWh for Case Study I. The same trend is observed for Case Study II, where the expected value of *S* decreases from 9.114 MWh to 7.919 MWh and the expected value of *EE* decreases from 9.131 MWh to 6.880 MWh as load shifting changes from 10% to 50%. Note that renewable energy sources have already been installed in many electric utility systems across the United States. Therefore, the total cost of the hybrid system will be significantly reduced if these resources are already in place. The proposed methodology provides electric utilities with an energy management tool to optimally utilize these resources and the

storage system to meet the HVAC load of the residential feeders at a desired confidence level. Case Studies I and II show the economic benefits of using wind power to supply the HVAC load. This is evident from the lower installation costs of the hybrid system in Case Study I with respect to Case Study II. In addition, optimal solutions for Case Study I require less wind power capacity than the PV power capacity of Case Study II. The simulation results summarized in Table 9 provide a quantitative representation of the compromise between cost and risk in the hybrid system.

3.3. Conclusions

This section evaluates the efficiency of a hybrid system that combines renewable energy generation and energy storage to meet a controllable HVAC load. Using historical data and curve fitting, wind and PV generation and cooling loads are stochastically modeled. FCM clustering provides ten data clusters that properly represent the effects of seasonal variations. GA-based optimization is proposed to minimize the cost and increase the efficiency. This method is tested on a residential feeder and different case studies are carried out to investigate the factors affecting the energy efficiency of the system. Simulation results show that increasing the load shifting percentage gives the system more flexibility and may lead to less excess energy and more efficiency. Our results show the compromise between risk of failure to meet demand and cost for different wind and PV generation levels. Case studies demonstrate the economic benefits of using wind power to supply the HVAC load. In addition, the proposed methodology provides utility companies with an energy management tool to optimally utilize the installed renewable energy sources and the storage system to meet the flexible loads of the residential/commercial

/industrial feeders.

3.4. Methodology for reliability calculation

The main objective of this section is to match HVAC loads with renewable energy sources without the need for supplementary conventional generations or grid-connection strategies. This will expand the use of renewable energy to reduce greenhouse gases associated with conventional generation. An isolated stand-alone hybrid energy system including storage, wind, and PV generation is designed to economically and reliably supply the HVAC load. Load shifting is used to provide the demand flexibility and meet the objective.

3.4.1. ARMA model for wind speed, solar irradiance and load

The SMCS requires sampling from sequences of distributions to chronologically simulate the random behavior of the system [104]. Time series methods are used to provide such sequences and model the uncertainties for the sequential analysis. Several references used ARMA as a time series model to characterize random variations of wind and solar generation. An a^{th}-order AR and b^{th}-order MA model represents the long-term wind/solar/load characteristics [105], [106]:

$$y_t = \sum_{i=1}^{a_r} \varphi_i \, y_{t-i} + \sum_{j=0}^{b_r} \theta_j \, \varepsilon_{t-j} \tag{3.31}$$

where ε_t is the white noise with zero mean, zero autocorrelation and unity variance. Ten years of historical hourly wind speed, clearness index, and load data are used to calculate the autoregressive and moving average coefficients and obtain a statistical model that accounts for a long-term scheduling period. This model uses the randomly generated value of ε_t and the

previous values of y and ε to provide a time series representation for y and generate hourly samples for the one-year scheduling period. Since wind, PV and load follow specified patterns and the utilized ten-year data is more likely to cover all states that may occur for wind, PV and load profiles, the modeling technique properly represents the system's behavior for the scheduling period. The time series (y_t) is shifted using the mean and scaled using the standard deviation of the historical data to obtain hourly data for wind speed, clearness index and load [107]:

$$SW_t = \mu_{W_t} + y_{W_t} \cdot \sigma_{W_t} \tag{3.32}$$

$$Sk_t = \mu_{k_t} + y_{k_t} \cdot \sigma_{k_t} \tag{3.33}$$

$$SL_t = \mu_{L_t} + y_{L_t} \cdot \sigma_{L_t} \tag{3.34}$$

The simulated wind speed is used to calculate the wind power output [77]:

$$G_W^{'} = \begin{cases} 0 & v \le v_i \, , v \ge v_o \\ \frac{v - v_i}{v_r - v_i} G_{W_r} & v_i \le v \le v_r \\ G_{W_r} & v_r \le v \le v_o \end{cases} \tag{3.35}$$

Assuming an efficiency of η_w for the power electronic interface, the net wind power output is:

$$G_w = \eta_w . G_W^{'} \tag{3.36}$$

A single-row layout with sufficient distance between the individual turbines is assumed for the wind farm to avoid the wake effects in the prevailing wind direction.

Solar irradiance is stochastically modeled using the clearness index (k_t) which is described as the quotient of the irradiance on a flat level, I_t (kW/m^2), and the extraterrestrial solar irradiance, I_o (kW/m^2) [87]:

$$k_t = \frac{I_t}{I_o} \tag{3.37}$$

The irradiance with an inclining angle of β with respect to the horizontal plane, I_β is given by:

$$I_\beta = T.k_t - T'.k_t^2 \tag{3.38}$$

T and T' are given by:

$$T = \left[\left(R_b + \rho \cdot \frac{1 - cos\beta}{2}\right) + \left(\frac{1 + cos\beta}{2} - R_b\right) \cdot p\right] \cdot r_d \cdot \frac{H_0}{3600} \tag{3.39}$$

$$T' = \left(\frac{1 + cos\beta}{2} - R_b\right) \cdot q \cdot r_d \cdot \frac{H_0}{3600} \tag{3.40}$$

p and q are parameters defining the correlation of the diffuse fraction (k) with the clearness index (k_t) as follows [34]:

$$k = p - qk_t \tag{3.41}$$

The simulated clearness index is used to calculate the PV power output by:

$$G'_{PV} = A_c.\eta'_{PV}.I_\beta = A_c.\eta'_{PV}.(T.k_t - T'.k_t^2) \tag{3.42}$$

Assuming an efficiency of η_{PV} for the power electronic interface, the net PV power output is:

$$G_{PV} = \eta_{PV}.G'_{PV} \tag{3.43}$$

The efficiency curves of the converters are used to calculate η_W and η_{PV} [89], [90].

3.4.2. Optimization problem

Wind and PV capacity installations, α_W and α_{PV}, are multiplied by the normalized renewable generation to represent the electric power generated by renewable resources. These parameters as well as the power rating and capacity of the storage system are included in the objective function to minimize the sum of installation, operation and maintenance costs of the hybrid energy system.

The optimization problem can be formulated as follows:

$$\min \{f(\bar{x}, \bar{u})\} \tag{3.44}$$

$$s.t. \quad g(\bar{x}, \bar{u}) = 0 \tag{3.45}$$

$$h(\bar{x}, \bar{u}) \leq 0 \tag{3.46}$$

where $f(\bar{x}, \bar{u})$, $g(\bar{x}, \bar{u})$, $h(\bar{x}, \bar{u})$, $\bar{x}$ and $\bar{u}$ are the objective function, equality constraint, inequality constraint, dependent and decision variables, respectively.

The objective function of (14) is given by:

$$Min\ C_{HPS} = Min\ \{(IC_{PV} + OMC_{PV}).\alpha_{PV} + (IC_W + OMC_W).\alpha_W + C_S.S + C_P.P\} \tag{3.47}$$

The last two terms of C_{HPS} $(C_s.S + C_P.P)$ indicate the storage cost. The balance-of-system (BOS) costs for energy and power are included in C_S and C_P, respectively [93].

The power electronic interface cost for connecting the PV and wind to the network is considered part of C_{PV} and C_W. The constraints of (3.45) and (3.46) include design, load and reliability constraints which are discussed next.

3.4.3. Design Constraints

Because of the physical limits existing in operation of the hybrid system, any feasible solution of the optimization problem must satisfy the following constraints:

Storage constraints: These constraints must satisfy an instantaneous energy balance between the sum of the generated and stored energy and the load. The balance of energy for charging and discharging of the energy storage system is given by (3.48.a) and (3.48.b), respectively.

$$S_t = (1-d)S_{t-1} + \eta_S\left(G_{PV_t} + G_{W_t} - L_t + L_{S_t} + L_{I_t}\right), \forall t \in T \tag{3.48.a}$$

for $G_{PV_t} + G_{W_t} - L_t + L_{S_t} + L_{I_t} \geq 0$

$$S_t = (1-d)S_{t-1} + \left(G_{PV_t} + G_{W_t} - L_t + L_{S_t} + L_{I_t}\right), \forall t \in T \quad (3.48.b)$$

for $G_{PV_t} + G_{W_t} - L_t + L_{S_t} + L_{I_t} < 0$.

The storage at time *t* satisfies the minimum and maximum capacity requirements as:

$$S_{min} \leq S_t \leq S_{max} \quad \forall t \in T \quad (3.49)$$

The storage system capacity (S) is defined as the maximum of the storage capacities over the scheduling period.

$$S = \max\ \{S_t\} \qquad t \in T \quad (3.50)$$

Assuming P_{max} as the power rating, then for each hour, the storage system must satisfy:

$$P_t = G_{PV_t} + G_{W_t} - L_t + L_{S_t} + L_{I_t} \quad \forall t \in T \quad (3.51.a)$$

$$|P_t| \leq P_{max} \quad \forall t \in T \quad (3.51.b)$$

The storage power rating is:

$$P = \max|P_t| \quad t \in T \quad (3.52)$$

Load constraints: Limited human control on the generation of the intermittent renewable resources may lead to a significant mismatch between renewable generation and HVAC load in a hybrid power system. Load shifting and interruption provide some flexibility to reduce this mismatch, especially during periods of insufficient generation and/or peak load. This is particularly true for HVAC loads such as refrigerators, pool pumps and hot tubes, which have a flexible time of operation. Load shifting and interruption are implemented as:

$$L_t^{'} = L_t - L_{S_t} - L_{I_t} \quad \forall t \in T \quad (3.53.a)$$

$$L_{t+1}^{'} = L_{t+1} + L_{S_t} \quad \forall t \in T \quad (3.53.b)$$

The shifted load is supplied at the earliest opportunity when the renewable generation is in

excess of the required load. The following inequality constraint ensures that the shifted load remains between the minimum and maximum allowable load shifting for time *t*:

$$0 \leq L_{S_t} \leq \delta . L_t \quad \forall t \in T \tag{3.54}$$

If $G_{PV_t} + G_{W_t} - L_t + L_{S_t} + L_{I_t} \geq 0$, (3.48.a) is used to charge the storage system. If $G_{PV_t} + G_{W_t} - L_t + L_{S_t} + L_{I_t} < 0$, the storage system is discharged using (3.48.b) to supply the excess load. If the stored energy is less than S_{min}, part of the load is shifted to the next hour using (3.53.a) and (3.53.b). If the maximum allowable load shifting ($\delta . L_t$) cannot satisfy the minimum capacity requirement specified by (3.49), the load is interrupted to balance the hybrid power and load.

Reliability constraints: Reliability assessment evaluates the quality of meeting load in a composite power system. During periods of generation deficiency or peak load when the hybrid power system cannot supply the load, load shifting is applied to balance the hybrid power and load. The load is interrupted if the maximum allowable load shifting cannot meet this objective. Reliability assessment of the hybrid power system considers the system uncertainties contributing to the load interruption. These uncertainties include equipment failure rates and random changes in both renewable generation and load. Equipment failure and repair characteristics provide the two-state models for each individual generating unit. The reliability models of wind turbines and PV arrays in a hybrid power system are the combination of these two-state models and power output models defined by (3.36) and (3.43). The wind/PV power output from each individual wind turbine/PV panel is then added to calculate the total power generated by the wind turbines/PV units within a wind/PV farm. Figure 12 shows the reliability

model for a wind/PV generator.

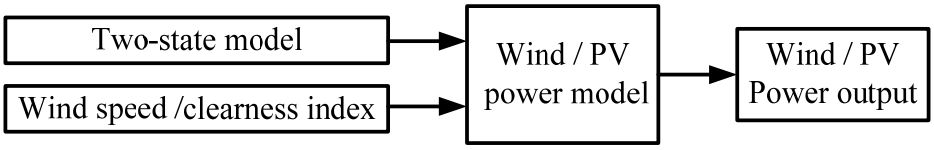

Figure 12. Reliability model for Wind/PV generator.

The equipment unavailability or equipment forced outage rate (FOR) is the statistically calculated forced outage probability of the unit for a long time period:

$$FOR = \frac{r}{r+m} \tag{3.55}$$

where *r* is the down time and *m* is the up time of each unit. Both are exponentially distributed. An up-down sequence is generated for the scheduling period. This sequence is used with the wind speed/clearness index - power curves to obtain the generating capacity sequence [108].

The energy not supplied (ENS) over a scheduling period (*T*) is:

$$ENS = \sum_{t=1}^{T} L_{I_t} \tag{3.56}$$

The expected energy not supplied (EENS) is a probabilistic index for the reliability analysis of the hybrid power system and is expressed as:

$$EENS = \frac{\sum_{n=1}^{N} ENS_n}{N} \tag{3.57}$$

The reliability of the hybrid power system is measured using the energy index of reliability (EIR) as follows:

$$EIR = 1 - \frac{\sum_{n=1}^{N}\sum_{t=1}^{T} L_{I_t}}{\sum_{n=1}^{N}\sum_{t=1}^{T} L_t} = 1 - \frac{EENS}{EE_d} \tag{3.58}$$

where EE_d is the expected energy demand of the hybrid power system design candidates over the

scheduling period.

A reliability constraint guarantees that the energy index of reliability (or expected energy not supplied) satisfies the desired reliability level for the hybrid power system. This constraint can be expressed by either of the following inequalities:

$$EENS \leq EENS_{des} \tag{3.59.a}$$

$$EIR \geq EIR_{des} \tag{3.59.b}$$

3.4.4. Sequential Monte Carlo Simulation

SMCS is used in this chapter to deal with uncertainties of the hybrid power system. The method simulates the chronological progress of the system by generating the random sequential samples of system states. ARMA models of renewable energy generation and HVAC loads are used to simulate these sequences. This process is repeated for many trials to obtain distributions for the output random variables [108], [109]. The output and input random vectors are related by:

$$Y = h(X) \tag{3.60}$$

SMCS produces a sample ($x_{n,t}^{(k)}$) for each input random variable ($x^{(k)}$) using its ARMA model. The functional relation between $x^{(k)}$ and $h(x^{(k)})$ is then used to produce the output for each sample. It repeats this process for a specified number of simulation (N) over a scheduling period (T). Using the sample outputs for the k^{th} input random variable ($y_{n,t}^{(k)}$), the distribution for the k^{th} output random variable ($f_{Y(k)}$) can be derived [110].

Mathematically, SMCS includes a set of algorithms that produce a collection of N weighted random samples $\left\{\omega_n^{(k)}, x_{n,t}^{(k)}; n = 1,2, \dots, N\right\}$ where $\omega_n^{(k)} > 0$ and $\sum_{n=1}^{N} \omega_n^{(k)} = 1$ at each time instance such that for the function $h(x_{n,t}^{(k)})$:

$$\lim_{N\to\infty}\sum_{n=1}^{N}\omega_n^{(k)}\,h(x_{n,t}^{(k)}) \rightarrow \int h(x_{n,t}^{(k)})f_{X^{(k)}}(x_{n,t}^{(k)})dx_{n,t}^{(k)} \tag{3.61}$$

3.4.5. Pattern search

A PS-based optimization technique is utilized in this chapter to optimally size wind generation, PV generation and adequately size energy storage capacity in a hybrid power system, while satisfying a specified reliability level. Generally, an initial starting point supplied by the user is used to start the algorithm. A mesh, a set of points, is then established around the present point of the algorithm. The present point is added with a set of vectors, called direction vectors, which are scaled with a scalar coefficient to make the mesh. The scalar is called the mesh size and its default value is unity for the first iteration. This is illustrated in Figure 13 where [0 1], [1 0], [-1 0] and [0 -1] are the direction vectors and X_0 is the initial point. The mesh points are polled by the algorithm based on their fitness function values. If a point improves the fitness function value over the present point, it is chosen as the present point (X_1) for the next iteration and the poll is successful. Upon a successful poll, the algorithm expands the existing mesh size with an expansion coefficient (default value of 2) and uses the new mesh size to form the expanded mesh around the present point. This results in 2*[1 0] + X_1, 2*[0 1] + X_1, 2*[-1 0] + X_1 and 2*[0 -1] + X_1 as the mesh points for iteration 2. A successful poll of the mesh points by the algorithm gives X_2 as the present point and the current mesh size is multiplied by 2 to get a mesh size of 4 at the third iteration. Otherwise, if the poll is unsuccessful for iteration 2, the present point is retained ($X_2 = X_1$) and the mesh size is reduced for the next iteration. Towards this end, the algorithm multiplies the current mesh size by a contraction factor (0.5) and polls the next

iteration with a smaller mesh size.

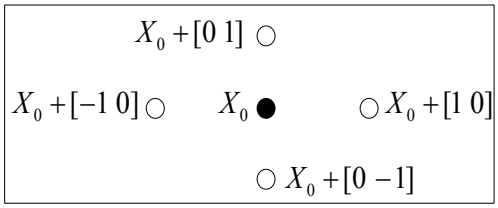

Figure 13. Formation of mesh for PS.

The process halts upon the satisfaction of a termination criterion with one of the following situations:

- The mesh size is smaller than a specified value for the mesh tolerance.
- The iteration number is greater than a specified value.
- The distance between the points found at two consecutive successful polls is less than a specified tolerance.

This evolutionary algorithm is appropriate to solve the non-linear, non-convex and non-smooth problem of the optimal hybrid power system design where the classical optimization methods cannot handle the non-convexity and discontinuity of the objective function. Moreover, uncertain factors considered for the reliability assessment of the hybrid power system make our optimization problem a stochastic program that cannot be solved by the traditional derivative-based optimization methods.

A genetic algorithm is used to generate the initial solution because of its global search ability which ensures the convergence of the optimization to the global optimum. Direct search tools such as PS are faster than GA to locally find the optimal solution. The search capability of the population-based evolutionary algorithms such as GA is highly dependent on the population size which significantly increases the computational burden if used in combination with SMCS

for the whole optimization process. Thus, the GA-based SMCS optimization necessitates a compromise between the number of simulations and population size to make its computational time reasonable. This compromise may result in an in-convergence state or non-optimal solution. Local search ability and high speed of PS make it an efficient direct search tool to resume the optimization process from the initial solution generated by GA and improve the computational efficiency [111], [112].

We first ran the optimization problem using our proposed method (PS-based SMCS) and then solved the same problem using GA with the population size of 50 and generation number of 20. Table 10 of the Appendix shows the simulation results for the PS based optimization as well as the GA results for 1000 simulations. These results demonstrate the improved efficiency of the proposed PS-based SMCS over the GA-based SMCS optimization.

Table 10. Simulation results for PS-based and GA-based SMCS

Method	$EENS_{des}$ (MWh)	α_{PV} (MW)	α_{W} (MW)	C_{Inv} $(M\$)$	*Simulation Time (Sec)*
PS-based SMCS	0.10	0.000	2.9250	8.4341	358.65
GA-based SMCS	0.10	0.221	2.6821	8.5631	2598.67

3.4.6. PS-based SMCS optimization

Figure 14 presents the flowchart for the developed method. The vectors of input and output random variables are:

$$X = [Wind\ Speed, Clearness\ Index, HVAC\ Load] \tag{3.62}$$

$$Y = \left[S, P, L_{S_t}, L_{I_t}, EIR\right] \tag{3.63}$$

Ten years of hourly load, clearness index and wind speed data are used to characterize the

uncertainties of the HVAC load and solar/wind generation by their ARMA models. The scaling parameters (α_{PV} and α_{W}) are initialized using GA then used as the initial solutions to start the PS algorithm. For each sample, a large penalty coefficient (υ) is enforced on the violated constraints to assign a higher cost to an infeasible solution [91]. The combination is given by:

$$f'(\bar{x},\bar{u}) = f(\bar{x},\bar{u}) + v[h(\bar{x},\bar{u})]^2 \quad (3.64)$$

PS optimization obtains the optimal sizing of the hybrid system components for a specified number of simulations (N) over a scheduling period (T). The optimal configuration of the hybrid power system ensures that the system reliability requirements are met with minimum investment cost.

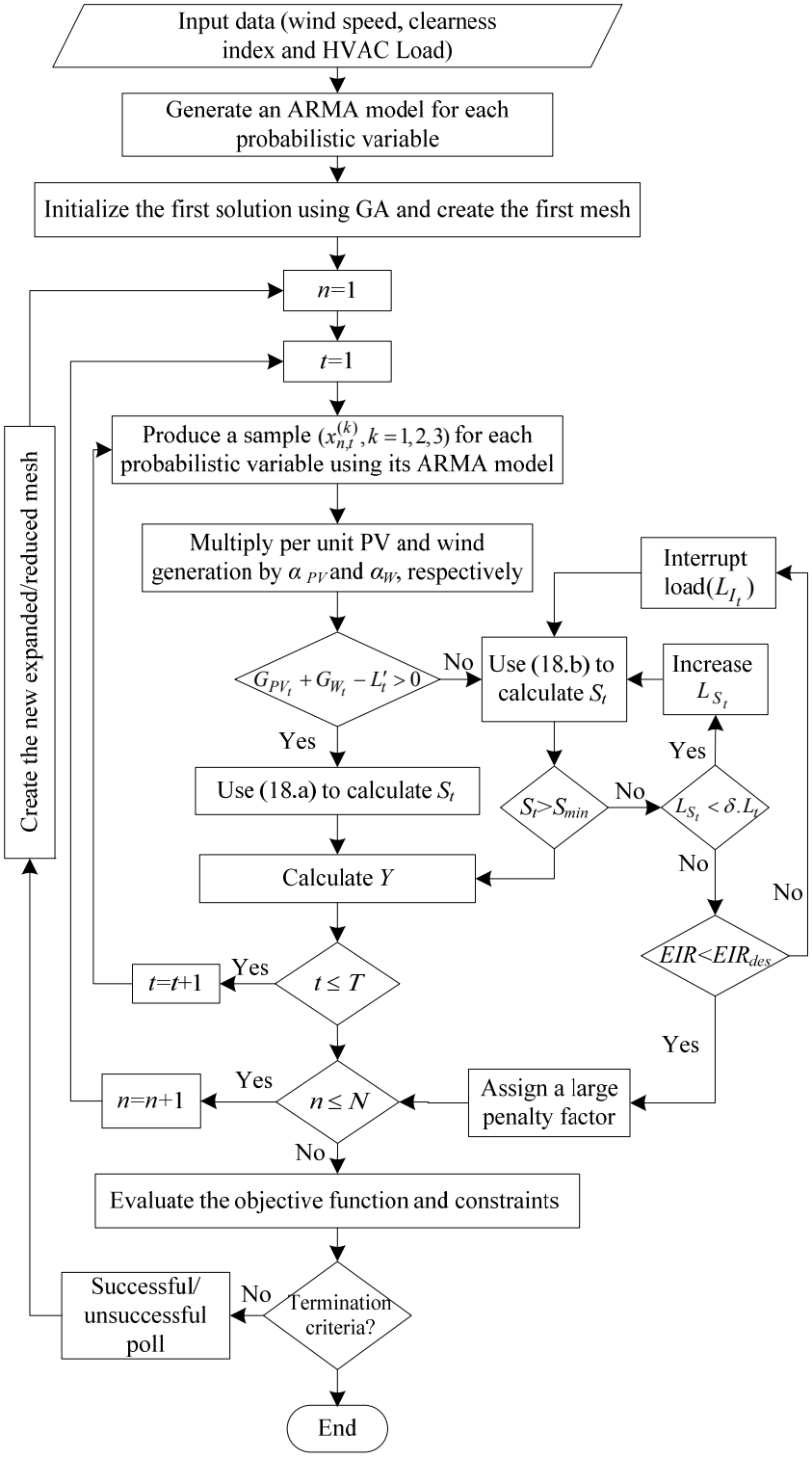

Figure 14. Flowchart for the PS-based SMCS optimization.

3.4.7. Sensitivity analysis

The proposed methodology minimizes the investment cost of the hybrid power system for a specified level of reliability. Sensitivity analysis of the cost with respect to the reliability level helps the investors make a rational decision that is a compromise between the cost and reliability. An Epsilon-constraint approach is used to determine the trade-off region for the hybrid power system where the cost minimization is the objective function and the reliability criteria is the constraint. Towards this end, $EENS_{des}$ is changed by ε values and the objective function is calculated for the desired reliability level. An efficient decision-making method is then required to realize the best compromise between the reliability and cost for a hybrid power system. We use a compromise solution that minimizes the normalized Euclidian distance between the potential optimal and utopia points. The utopia point is the point which is close enough to the minimum point. We solve the minimization [113]:

$$\min_{U\in\Phi}\left\{\sum_{i=1}^{2}\left|F_i(U)-F_i^0\right|^2\right\}^{\frac{1}{2}} \tag{3.65}$$

$F_i(U)$ is the normalized function for each decision criterion C_i and is given by:

$$F_i(U)=\frac{C_i^{max}-C_i(U)}{C_i^{max}-C_i^{min}} \tag{3.66}$$

where, $C_i^{max}$and $C_i^{min}$are the maximum and minimum values of C_i and $F_i^0$is the normalized utopia point. By solving (3.65) with $F_i^0=1$, each criterion would be as close as possible to its minimum point. Normalization is necessary because different criteria have different units.

3.5. Case Studies

Two cases are evaluated in this section for an optimal design of the hybrid power system. The first case considers no load interruption and provides the sizing requirements of the hybrid power system for worst-case scenarios. It also gives the probability distributions of the output random variables. Based on the design parameters, it then calculates the reliability index of the hybrid power system. The second case provides a stochastic framework to optimally satisfy the system reliability requirements with the minimum investment cost. This scenario examines the load shifting strategy and its potential impacts on the hybrid system reliability/cost evaluation. The wind speed, clearness index and load data are from the Bonneville Power Administration authority and Mesonet [114], [85]. Capital costs for energy and power of the storage system are 0.2 $/Wh, and 0.25 $/W [93]. Capital costs for wind and PV generation and the values of the system parameters for the case studies are provided in Table 11. The parameters for the wind, PV and load ARMA models are provided in Table II.

Table 11. Installation costs of wind and PV generation and values of the system parameters [34], [37], [89], [90], [101], [102]

Wind Generation (kW)	< 100	100-1000	1000-1750	≥ 1750
Installation Cost ($/kW)	4000	2300	2200	2000
OMC ($/kW)	100			
PV Generation (kW)	≤ 2		$> 1{,}000$	
Installation Cost ($/kW)	9800		5200	
OMC ($/kW)	60			
$v_i = 3\ m/h$	$v_r = 17\ m/h$	$v_i = 3\ m/h$	$v_r = 17\ m/h$	
$\eta_S = 89\%$	$\eta_{PV} = 95\%$	$\eta_S = 89\%$	$\eta_{PV} = 95\%$	
$I_O = 1367\ W/m^2$	$\beta = 0^0$	$I_O = 1367\ W/m^2$	$\beta = 0^0$	
$p = 0.9$	$q = 0.1$	$p = 0.9$	$q = 0.1$	

3.5.1. Case I: Hybrid power system design without the reliability constraints

Case I uses PS optimization to size the hybrid power system components for each

simulation with no load interruption. Figure 15 shows the PDFs for the installed storage, wind and PV capacities as well as the storage power and cost for 30% load shifting. These capacities fully meet the hybrid system load without the need to interrupt the load even for the worst-case scenarios of insufficient wind and PV generations. However, this design may result in a high investment cost for the hybrid power system. Using the expected values of these capacities avoids cost overestimation.

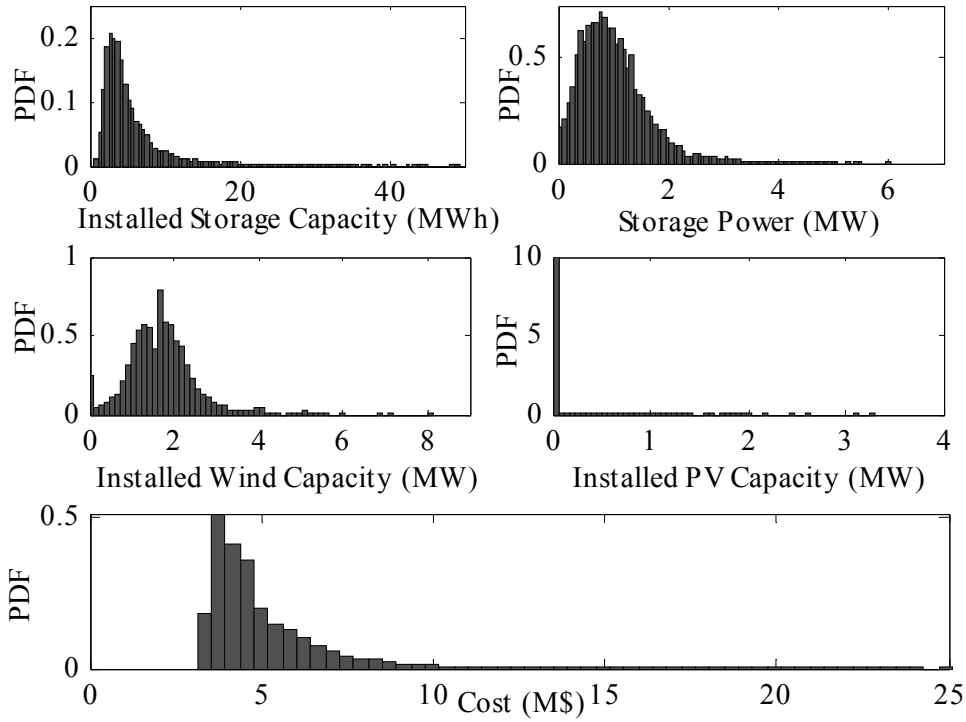

Figure 15. PDFs for the installed storage, wind and PV capacities, storage power and cost of the hybrid power system

Table 12. Wind, PV and Load ARMA parameters

a_r/φ	φ_1	φ_2	φ_3	φ_4	φ_5	φ_6
Wind (a_r = 4)	0.824	1.063	0.793	-0.094	-	-
PV (a_r = 6)	4.579	-8.647	8.368	-4.079	0.728	-0.051
Load (a_r = 4)	2.287	-2.693	2.172	0.7772	-	-
b_r/θ	θ_0	θ_1	θ_2	θ_3	θ_4	θ_5
Wind (b_r = 3)	1	0.192	-0.977	-0.201	-	-
PV (b_r = 4)	1	3.604	5.15	-3.447	0.913	-
Load (b_r = 3)	1	-0.978	1.237	-0459	-	-

Figure 16 shows the expected value of the storage capacity and energy index of reliability (EIR) for 10,000 simulations. The convergence state is reached after about 6,000 simulations. The EIR is calculated for the scheduling period based on the design parameters to evaluate the reliability of the hybrid system. This figure shows the extent to which the reliability requirements are met using the expected values of the PDFs for the installed storage, wind and PV capacities. This design avoids the cost overestimation associated with designing the hybrid power system based on the maximum values of these PDFs. However, the reliability level may not seem appropriate for the hybrid power system. Designing the system based on the cost distribution is a post-optimization process which may not necessarily satisfy the desired reliability level. The cost distribution design is based on trial and error with no attempt at optimizing the parameter values. This demonstrates the necessity of hybrid system design with the reliability constraints, which is the subject of investigation for Case II.

3.5.2. Case II: Hybrid power system design with the reliability constraints

Case II uses the proposed method to optimally size the hybrid system components while satisfying the desired reliability level for the hybrid power system. We evaluate the potential impacts of reliability level on the component sizing. The reliability constraint for EENS is set at

a desired level and the hybrid system component-sizing problem is solved to minimize the investment cost and meet the desired level. Table 13 shows the wind, PV and storage capacity installations and power for different reliability levels. Optimal costs for renewable energy generation and storage system are also given in this table.

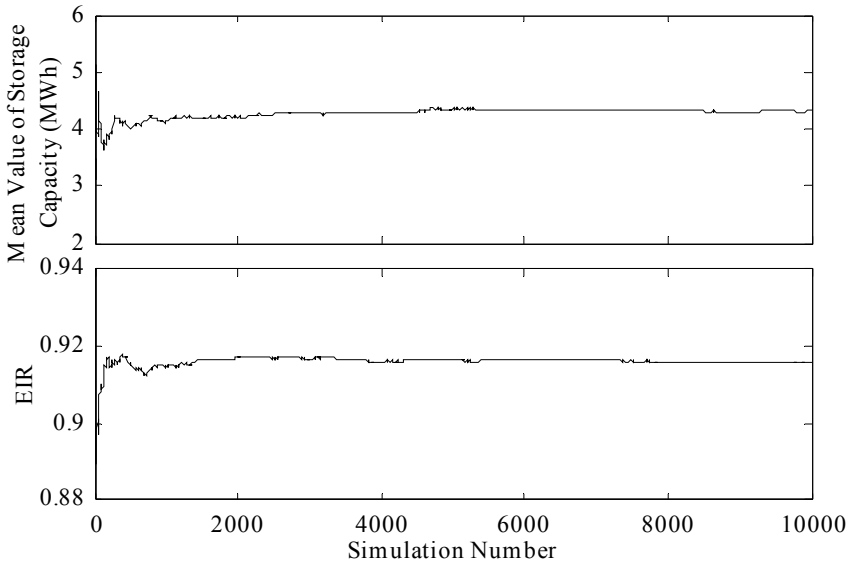

Figure 16. Expected value of the storage capacity and energy index of reliability

Table 13. Wind, PV and storage capacity installations for 30% load shifting and different reliability levels

$EENS_{des}$(MWh)	0.3	0.25	0.2	0.15	0.10	0.05	0.01
EIR_{des} (%)	98.18	98.48	98.79	99.09	99.39	99.70	99.94
$\alpha_W(MW)$	2.340	2.394	2.450	2.560	2.741	3.100	2.900
α_{PV} (MW)	0	0	0	0	0	0	0.750
S (MWh)	6.241	6.626	7.106	8.006	9.005	12.14	14.99
P (MW)	0.955	1.079	1.131	1.215	1.772	2.032	0.364
Renewable Cost (M$)	4.914	5.027	5.145	5.376	5.757	6.510	9.210
Storage Cost (M$)	1.487	1.595	1.704	1.905	2.244	2.936	3.089

As shown in Table 13, increasing the desired reliability level (EIR_{des}) from 98.18% to 99.94% increases the cost of the hybrid power system for both energy storage and renewable

generation. Optimum solutions show no PV installation for lower reliability levels while the wind installation is always contained within the optimal solutions. This is because wind energy, when available, can be generated for most periods of the day while PV energy is generated during the daylight periods. Thus, more storage capacity is needed to provide energy during the hours when no solar energy is available. In addition, installation cost of wind energy is less than the installation cost for PV generation. The increased variability of higher wind generation requires more storage capacity to deal with the uncertainties and sustain the higher reliability levels. This increases the cost of the hybrid wind and storage system. Therefore, optimal design of the hybrid power system for higher reliability levels requires both wind and PV generation to be installed within the system. This is due to less fluctuations of PV generation which decreases the storage capacity and cost for the hybrid wind, PV and storage system when compared to the hybrid wind and storage system. Higher investment costs for higher reliability levels can be offset by an appropriate load shifting strategy for the hybrid power system. This is even more pronounced for HVAC loads which can be deferred and adjusted according to the renewable energy variations. Table 14 gives the installed wind, PV and storage capacities for energy index reliability of 99.39% (EENS=0.1 MWh) and different load shifting percentages. As shown in Table 14, increasing load shifting from 0 to 50 percent decreases the renewable and storage capacity installations for the hybrid power system.

The epsilon-constraint approach is used to determine the compromise between the cost and reliability (EENS) shown in Figure 17. Using least-squares curve fitting, a curve is fitted on the trade-off points. Then the best compromise is adopted as the final solution utilizing the compromise-solution method. Table 15 shows the final optimal plan for this trade-off for

different values of the utopia point close to 1 (F_1^0 for cost and $F_2^0$for EENS). Two decision criteria are considered for our problem: the cost (C_1) and reliability index (C_2). The maximum and minimum values of each criterion ($C_i^{max}$and C_i^{min}) are obtained from the trade-off points of Figure 6 to calculate the normalized function of (36). For a certain value of F_1^0 , increasing F_2^0 increases the reliability level (decreases EENS) for the hybrid power system. This is evident for higher values of F_2^0 where the EENS decreases from 0.0915 MWh for F_1^0 =0.9 & F_2^0 =0.95 to 0.0869 MWh for F_1^0 =0.9 & F_2^0 =1. The same trend is observed for F_1^0 =0.95 and F_1^0 =1, where the EENS decreases from 0.0964 MWh to 0.0919 MWh and 0.1011 MWh to 0.0966 MWh as F_2^0 increases from 0.95 to 1. Increasing the utopia value for reliability (F_2^0) from 0.95 to 1 requires an investment cost increase from 8.1853, 8.0783 and 7.9803 M$ to 8.2953, 8.1773 and 8.0733 M$ for F_1^0 =0.9, F_1^0 =0.95 and F_1^0 =1, respectively. Another observation is that increasing the utopia value for cost from 0.9 to 1 with the same F_2^0 decreases the reliability and cost of the system.

Table 14. Wind, PV and storage capacity installations for EIR of 99.39% and different load shifting percentages

Load Shifting	0%	10%	20%	30%	40%	50%
$\alpha_W(MW)$	3.390	3.130	2.910	2.741	2.570	2.420
$\alpha_{PV}\ (MW)$	0	0	0	0	0	0
S (MWh)	14.597	12.358	10.463	9.005	7.5669	6.7878
P (MW)	2.3445	2.1157	1.9216	1.7704	1.6157	1.077
Renewable Cost (M$)	7.1190	6.5730	6.1110	5.7565	5.3970	5.0820
Storage Cost (M$)	3.5052	3.0009	2.5730	2.2436	1.9173	1.6268

Table 15. Final decision making for the hybrid power system

Utopia Values	F_1^0	0.9	0.9	0.95	0.95	1	1
	F_2^0	0.95	1	0.95	1	0.95	1
Criteria Values	*Cost (M$)*	8.185	8.295	8.078	8.177	7.980	8.073
	EENS (MWh)	0.092	0.087	0.096	0.092	0.101	0.097

3.6. Conclusions

This chapter proposes a stochastic framework for performance assessment of a hybrid power system to supply a deferrable HVAC load. ARMA models are used to characterize uncertainties of PV and wind power as well as HVAC loads. PS-based SMCS optimization is proposed to optimally size the hybrid system components and satisfy the reliability requirements. Optimal design of the hybrid power system is calculated for a residential feeder under different case studies. Simulation results for lower reliability levels show wind generation with no PV installation in the optimal solutions. Optimal design of the hybrid power system for higher reliability levels requires both wind and PV generation. A load shifting strategy is developed to offset the higher investment costs for higher reliability levels. Simulation results show the trade-off between system cost and reliability for a hybrid power system. The best compromise is realized using a compromise-solution method. The decision-making process is performed for different values of the utopia point to determine the final optimal plan based on the decision's maker preferences.

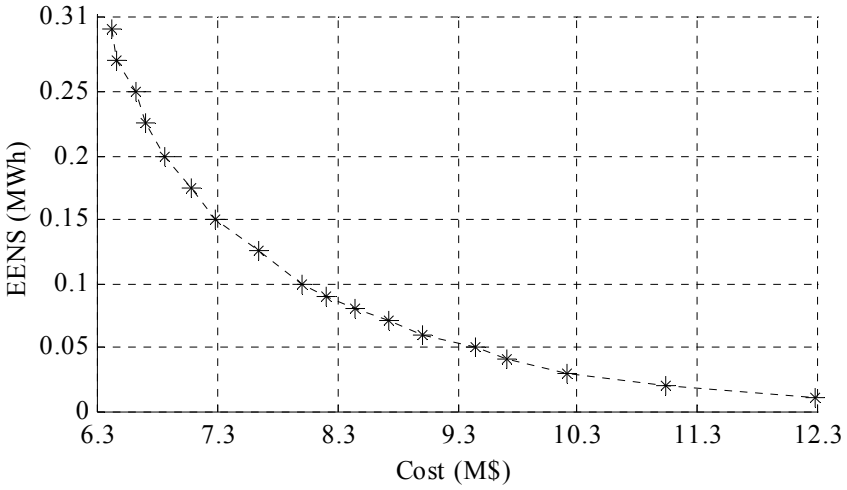

Figure 17. Trade-off points for the compromise solution of the hybrid system

IV. Chapter 4. Optimal Placement of Energy Storage Units

4.1. Stochastic modelling of wind and load

The stochastic nature of wind and the load characteristics impose some degree of uncertainty on power systems with wind energy resources. Wind uncertainties [115] and random changes in load [116] need to be modelled stochastically in order to reflect their characteristics. Wind speed variation is characterized using the Weibull distribution [116]:

$$f_V(v) = (\frac{\alpha}{\varphi})(\frac{v}{\varphi})^{\alpha-1} e^{-(\frac{v}{\varphi})^{\alpha}}, \ 0 \le v \le \infty \tag{4.1}$$

where, v is the wind speed, φ is the scale factor and k is the shape factor of the Weibull distribution. Using curve fitting and Maximum Likelihood Estimation (MLE), parameters of the PDF are estimated for historical wind speed data. The power output of a wind generator is calculated by [117]:

$$G_W = \begin{cases} 0 & 0 \le v < v_i, \ \ v > v_o \\ (B + B' \times v + B'' \times v^2) \times G_{W_r} & v_i \le v \le v_r \\ G_{W_r} & v_r \le v \le v_o \end{cases} \tag{4.2}$$

where G_W, G_{W_r}, v_i, v_r and v_o are the wind output power, wind rated power, cut in wind speed, rated wind speed and cut out wind speed, respectively. The constants B, B' and B'' depend on v_i, v_r and v_o as expressed in equations (4.2.a)-(4.2.c):

$$B = \frac{1}{(v_i - v_r)^2} \left\{ v_i(v_i + v_r) - 4 v_i v_r \left[\frac{v_i + v_r}{2 v_r} \right]^3 \right\} \tag{4.2.a}$$

$$B' = \frac{1}{(v_i - v_r)^2}\left\{4(v_i + v_r)\left[\frac{v_i + v_r}{2v_r}\right]^3 - (3v_i + v_r)\right\} \tag{4.2.b}$$

$$B'' = \frac{1}{(v_i - v_r)^2}\left\{2 - 4\left[\frac{v_i + v_r}{2v_r}\right]^3\right\} \tag{4.2.c}$$

Load variation is characterized using the Gaussian distribution as [116]:

$$f_L(l) = \frac{1}{\sqrt{2\pi\sigma^2}} e^{-\frac{(l-\mu)^2}{2\sigma^2}} \tag{4.3}$$

Using curve fitting and MLE, parameters of the PDF are estimated for historical load data.

4.2. Modelling of storage system

The CAES is used in this chapter for renewable integration due to its long life, large power capacity, and low capital and operation costs [118]. This large scale storage technology stores the excess wind energy that would otherwise be curtailed. The energy balance of the storage system for charging and discharging is:

a) For charging:

$$S_t = (1 - d_S)S_{t-1} + \eta_S^c L_{S_t} \qquad \forall t \in T \tag{4.4}$$

where L_{S_t} is the variable load of the storage satisfying the following inequality:

$$0 \le L_{S_t} \le \min(S_{\max} - (1 - d_S)S_{t-1}, P_R^c) \qquad \forall t \in T \tag{4.5}$$

where S_t, G_{W_t}, P_R^c and L_{S_t} are the energy stored in the storage system, generation of wind, Power rating of the storage system for charging and load demand at hour *t*; while η_S and d_S are the roundtrip efficiency and hourly self-discharge rate of the storage system. For each hour, the

following constraint ensures that the power of the storage system does not exceed the power rating for charging.

$$\left|P_t\right| \le P_R^c \quad \forall t \in T \tag{4.6}$$

b) For discharging:

$$S_t = (1-d_S)S_{t-1} - \eta_S^d G_{S_t} \qquad \forall t \in T \tag{4.7}$$

where G_{S_t} is the generation capacity of the storage satisfying the following inequality:

$$0 \le G_{S_t} \le \min((1-d_S)S_{t-1} - S_{\min}, P_R^d) \qquad \forall t \in T \tag{4.8}$$

For each hour, the following inequality constraint ensures that the power of the storage system does not exceed the power rating for discharging.

$$\left|P_t\right| \le P_R^d \quad \forall t \in T \tag{4.9}$$

The storage power rating is calculated by:

$$P_R = \max(P_R^c, P_R^d) \tag{4.10}$$

where, P_R, P_R^c and P_R^d are Power rating of the storage system, Power rating of the storage system for charging and Power rating of the storage system for discharging. For each hour, the energy stored in the storage system must remain between the minimum and maximum storage capacities as:

$$S_{\min} \le S_t \le S_{\max} \quad \forall t \in T \tag{4.11}$$

Ramp up and ramp down constraints associated with the storage generating capacity are:

$$G_{S_t} - G_{S_{t-1}} \le RU_S \qquad \forall t \in T \tag{4.12.a}$$

$$G_{S_{t-1}} - G_{S_t} \le RD_S \quad \forall t \in T \tag{4.12.b}$$

where G_{S_t} is the generation capacity for the storage system at time *t* and RU_S and RD_S are the ramp up and ramp down of the storage system.

4.3. Economic Characteristics

The investment cost for CAES includes the energy and power costs. The cost of energy is the sum of the reservoir and balance of plant (BoP) expenses. The cost of power is the combined turbine and compressor expenses. These costs are \$53/kWh and \$425/kW for energy and power, respectively [119].

$$IC_S = C_S \cdot S_{\max} + C_C \cdot P_R^c + C_T \cdot P_R^d \tag{4.13}$$

where, IC_S, C_S, $S_{\max}$, C_C, P_R^c, C_T, and P_R^d are Total investment cost for the storage system, Cost of reservoir for CAES, Maximum storage capacity, Cost of compressor for CAES, Power rating of the storage system for charging, Cost of turbine for CAES, and Power rating of the storage system for discharging, respectively. The operational cost of CAES for each hour is composed of two components: the fuel and fixed operation and maintenance (O&M) costs [119]:

$$OC_{S_t} = HR \cdot G_{S_t} \cdot C_{NG_t} + C_{OM} \cdot P_R \qquad \forall t \in T \tag{4.14}$$

where, OC_S, HR, G_{S_t}, C_{NG}, C_{OM} and P_R are Operation cost of the storage system, Heat rate of turbine for CAES, Generation capacity associated with the storage at time *t*, Natural gas cost for CAES, Operation and maintenance cost for CAES and Power rating of the storage system, respectively. *HR*, C_{NG}, and C_{OM} are 4300 Btu/kWh, \$5/MBtu and \$2.5/kW-year, respectively [119].

The investment cost and heat rate for the gas-fired conventional generator are $695/kW and 9000 Btu/kWh, respectively [120].

The annual equivalent cost for an investment is calculated as:

$$A = \frac{d(1+d)^N}{(1+d)^{N+1}-1} \cdot IC \tag{4.15}$$

where A, d, N *and* IC are Equivalent annual cost of the investment, Discount rate, Life time of the investment and Investment cost for an equipment. d and N are 10% and 30 years, respectively.

4.4. Optimal power flow

Optimal power flow (OPF) studies are used to find the optimal operating state of the system which minimizes the operation cost and satisfies the performance constraints. The objective function of the OPF is:

$$Min\{Objective\,Function\} = Min(OC_t) = Min\{\sum_{i=1}^{n_g}(a_i P_{g_{i,t}}^2 + b_i P_{g_{i,t}} + c_i)\} \qquad \forall t \in T \tag{4.16}$$

where, n_g is the number of generating units; a_i, b_i and c_i are the cost function coefficients of unit *i*; and $p_{g_{i,t}}$ is the unit *i* generation output at hour *t.* The performance constraints include the following formulations.

For the power balance equation using a DC OPF, we have:

$$\sum_{i=1}^{n_b} P_{g_{i,t}} = \sum_{i=1}^{n_b} P_{d_{i,t}} \qquad \forall t \in T \tag{4.17}$$

where, n is the number of buses and $p_{d_{i,t}}$ is the demand at bus i at hour t. The inequality constraint for the power generation is:

$$P_{g_{i,t}-min} \le P_{g_{i,t}} \le P_{g_{i,t}\text{-}max} \quad \forall t \in T \tag{4.18}$$

where p_{g_i-min} and $p_{g_i\text{-}max}$ are the lower and upper generation limits for generating unit i.

Generator ramp up and ramp down are:

$$P_{g_{i,t}} - P_{g_{i,t-1}} \le RU_i \quad \forall t \in T \tag{4.19.a}$$

$$P_{g_{i,t-1}} - P_{g_{i,t}} \le RD_i \quad \forall t \in T \tag{4.19.b}$$

The following inequality gives the limitation for the power flowing through a transmission line:

$$\sum_{i=1}^{n_b} H_{r-i} \times (P_{g_{i,t}} - P_{d_{i,t}}) \le \overline{f}_r \qquad r \in \Omega \,\&\, \forall t \in T \tag{4.20}$$

where, H_{l-i} is the generalized distribution factor of line l with respect to bus i and $\overline{f}_l$ is the maximum flow of line l and L is a set of transmission lines. The Lagrange function of the OPF is [65]:

$$\begin{aligned} LF_t = OC_t + \lambda_t \left(\sum_{i=1}^{n_b} P_{d_{i,t}} - \sum_{i=1}^{n_b} P_{g_{i,t}} \right) + \sum_{i=1}^{n_g} \mu_i^{\max} \left(P_{g_{i,t}} - P_{g_{i,t}\text{-}max} \right) + \sum_{i=1}^{n_g} \mu_i^{\min} \left(P_{g_{i,t}\text{-min}} - P_{g_{i,t}} \right) \\ + \sum_{r=1}^{\Omega} \gamma_{r,t} \left(\sum_{i=1}^{n_b} H_{r-i} \times (P_{g_{i,t}} - P_{d_{i,t}}) - \overline{f}_r \right) \qquad r \in \Omega \,\&\, \forall t \in T \end{aligned} \tag{4.21}$$

where, $\lambda_{i,t}$, $\mu_i^{\max}$, $\mu_i^{\min}$ and $\gamma_{l,t}$ are Lagrange multipliers of sets of constraints including the load-generation balance, the lower and upper limit for the i^{th} generating unit and the transmission constraint for line l. For an OPF problem, the LMP of a bus at hour t is the marginal cost of

serving the next increment of demand at that bus ($\lambda_{i,t}$). The market-clearing price (MCP) governs the entire system when there is no congestion. Transmission congestion results in different marginal prices which are generally referred as the locational marginal prices (LMPs). For an OPF problem, the LMP of a bus at hour *t* is the marginal cost of serving the next increment of demand at that bus. Using the Karush–Kuhn–Tucker (KKT) optimal conditions, the LMP at each bus is obtained by calculating the first-order derivative of the Lagrangian function with respect to $P_{d_{i,t}}$ [65], [121]:

$$LMP_{i,t} = \frac{\partial LF_t}{\partial P_{d_{i,t}}} = \lambda_t - \sum_{r=1}^{\Omega} \gamma_{r,t} H_{r-i} \quad \forall t \in T \tag{4.22}$$

Congestion cost of the system for each hour is calculated as follows:

$$CC_t = \sum_{(i,j)\in\beta} f_{ij,t}(LMP_{j,t} - LMP_{i,t}) \quad \forall t \in T \tag{4.23}$$

where, CC_t, $f_{ij,t}$ and $LMP_{i,t}$ are the congestion cost, power flow from bus i to bus j and local marginal price of bus i at hour t and B is a set of buses.

4.5. Probabilistic OPF

A deterministic OPF cannot represent the effects of the stochastic factors associated with wind generation and load variation on the dispatch results [122]. A probabilistic OPF (POPF) considers uncertainties of wind power output and loads in power flow computations. Two point estimation (2PE) is used in this section to perform the probabilistic analysis in POPF problems [81], [82]. Vectors of random input and output variables and the corresponding nonlinear function are given by equations (4.24), (4.25), and (4.26), respectively.

$$X = [Wind\ Speed, Loads] \tag{4.24}$$

$$Y = [OC, CC] \tag{4.25}$$

$$Y = h(X) \tag{4.26}$$

where, wind speed and loads are the input probabilistic variables, while system operation cost (*OC*) and congestion cost (*CC*) are the output probabilistic variables and *h* is the multivariate nonlinear function corresponding to the POPF with energy storage integration and wind generation.

The proposed method uses DC-OPF based on unit de-commitment to dispatch the generation for each hour. More expensive generators are shut down which results in the least costly dispatch and most economic operation for the system over the scheduling period [79]. Base load plants are always committed during this period. Energy storage is incorporated into the OPF model to store the extra wind power that would otherwise be curtailed. This occurs when $G_{W_t} - L_{M_t} > 0$ or the transmission network is congested. The stored energy is discharged when $G_{W_t} - L_{M_t} < 0$ or transmission capacity does not confine the power transfer. For each hour, the modified load (L_{M_t}) is defined as the difference between the total and base loads:

$$L_{M_t} = L_{T_t} - L_{B_t} \qquad \forall t \in T \tag{4.27}$$

The proposed POPF algorithm is outlined as follows:

1) Load the input data (wind speed and load)

2) Set *t*=1

3) Assign appropriate PDF to each probabilistic variable

4) Set $E(Y) = E(Y^2) = 0$

5) Set $k = 1$

6) Determine the necessary parameters for the 2PEM

$$\zeta_{k,i} = \sqrt{n + (\lambda_{k,3} / 2)^2} \quad i = 1, 2 \tag{4.28.a}$$

$$\xi_{k,i} = \lambda_{k,3} / 2 + (-1)^{3-i} \zeta_{k,i} \quad i = 1, 2 \tag{4.28.b}$$

$$P_{k,i} = \frac{(-1)^i \xi_{k,3-i}}{2n \times \zeta_{k,i}} \quad i = 1, 2 \tag{4.28.c}$$

where, $\xi_{k,1}$, $\xi_{k,2}$, $P_{k,1}$ and $P_{k,2}$ are the locations and probabilities of concentrations, and $\lambda_{k,3}$ is the coefficient of skewness of X_k.

7) Set the concentrations ($x_{k,1}$ and $x_{k,2}$) using the input vector X.

$$x_{k,i} = \mu_{X_k} + \xi_{k,i} \sigma_{X_k} \quad i = 1, 2 \tag{4.29}$$

8) Calculate $Z = [\mu_{X_1}, \mu_{X_2}, ..., x_{k,i}, ..., \mu_{X_n}] \quad i = 1, 2$

Note that μ_{X_k} is replaced by $x_{k,i}$ (i=1, 2) at each iteration.

9) If $G_{W_t} - L_{M_t} > 0$ or the transmission network is congested, the storage serves as a variable load with constraint (4.5) to store the excess wind power. Otherwise, the storage serves as a generator with constraint (4.8) to discharge the stored energy.

10) Run the deterministic OPF incorporating the storage system as either the variable load or generator using Z.

11) Calculate the state of charge (S) using equations (4.4) and (4.7)

12) Calculate OC_t and CC_t

13) Update *E(Y)* and $E(Y^2)$

$$E(Y) \cong \sum_{k=1}^{n} \sum_{i=1}^{2} (P_{k,i} \times h([\mu_{X_1}, ..., x_{k,i}, ..., \mu_{X_n}])) \quad (4.30.a)$$

$$E(Y^2) \cong \sum_{k=1}^{n} \sum_{i=1}^{2} (P_{k,i} \times h^2([\mu_{X_1}, ..., x_{k,i}, ..., \mu_{X_n}])) \quad (4.30.b)$$

14) Set *k=k+1* and repeat steps 6-13 until these steps are done for all random input variables.

15) Calculate the mean and standard deviation

$$\mu_Y = E(Y) \quad (4.31.a)$$

$$\sigma_Y = \sqrt{E(Y^2) - \mu_Y{}^2} \quad (4.31.b)$$

Figure 18 shows the flowchart for the POPF with energy storage integration and wind generation.

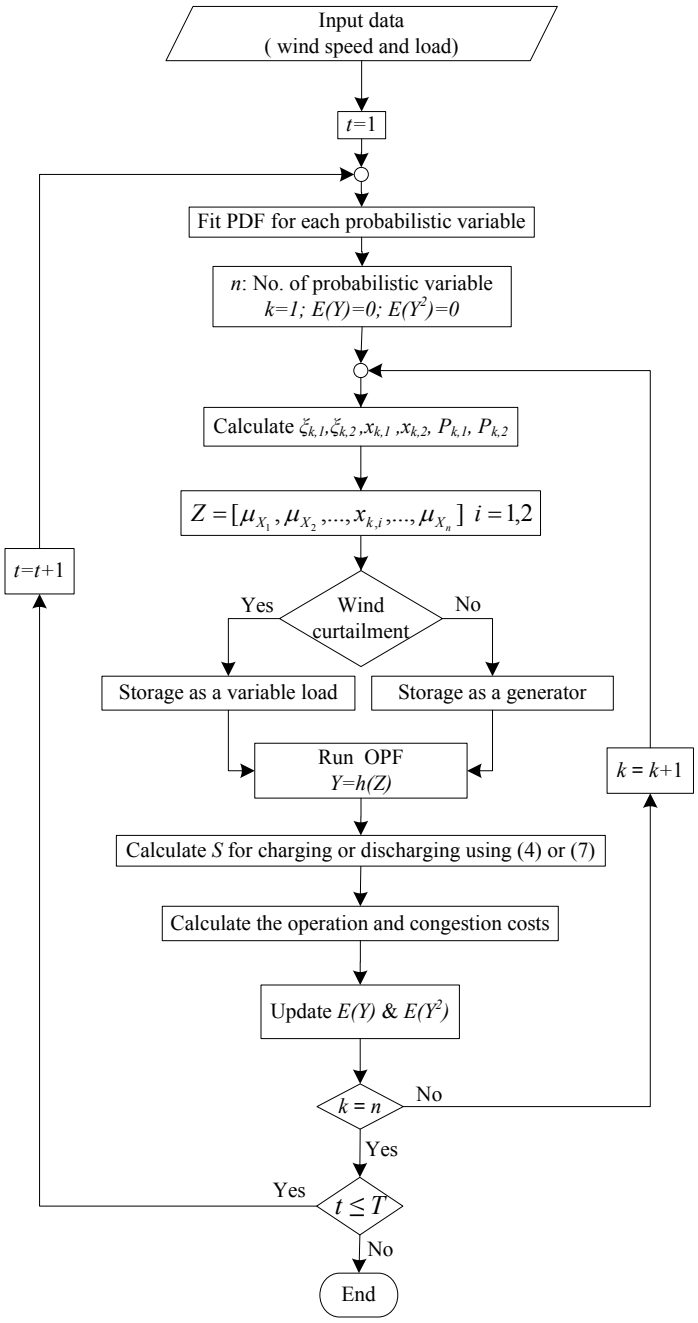

Figure 18. Flowchart for the POPF with energy storage integration.

The above POPF algorithm minimizes the system operation cost while satisfying the constraints for each hour over the scheduling period (T).

4.6. Particle swarm optimization

PSO is used in this section to optimally place and adequately size the energy storage which minimizes the social cost of the system for the scheduling period. The social cost is defined as the sum of operation and congestion costs. This evolutionary algorithm provides a more flexible and robust procedure than traditional derivative-based methods to solve the non-linear, non-convex, and mixed-integer optimization problem of the storage placement and sizing. PSO uses probabilistic transition rules to solve stochastic problems where the classical optimization methods cannot handle uncertain factors such as load variation and wind intermittency [123]. Generally, particles and their initial velocities are randomly generated to start the algorithm. Each particle moves with an adaptable velocity within the *q*-dimensional search space and retains a memory of the best position attained. Each particle updates its velocity and position using the following equations:

$$V_j^{m+1} = wV_j^m + c_1 r_1 (Pbest_j^m - U_j^m) - c_2 r_2 (Gbest^m - U_j^m) \tag{4.32}$$

$$U_j^{m+1} = U_j^m + V_j^{m+1} \tag{4.32}$$

where U_j^m and V_j^m are *q*-dimensional vectors for the position and velocity of the *j*th particle at the *m*th iteration as:

$$U_j^m = (u_{j,1}^m, u_{j,2}^m, ..., u_{j,q}^m) \tag{4.33}$$

$$V_j^m = (v_{j,1}^m, v_{j,2}^m, ..., v_{j,q}^m) \tag{4.33}$$

$Pbest_j^m$ is the vector of best position attained by the *j*th particle at the *m*th iteration and given by:

$$Pbest_j^m = (pbest_{j,1}^m, pbest_{j,2}^m, ..., pbest_{j,q}^m) \tag{4.34}$$

$Gbest^m$ is the vector of global best position attained among all particles in the swarm at the mth iteration and given by:

$$Gbest^m = (gbest_1^m, gbest_2^m, ..., gbest_q^m) \tag{4.35}$$

Figure 19 shows the flowchart for the proposed PSO-enhanced POPF. The fitness function of the proposed optimization method is:

$$Fitness\ \ Function = Min \sum_{t=1}^{T} (OC_t + CC_t) = Min \sum_{t=1}^{T} SC_t \tag{4.36}$$

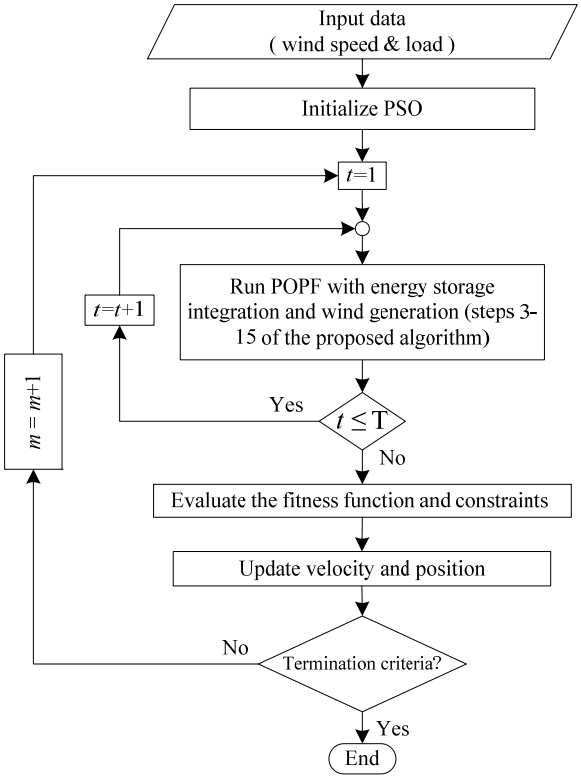

Figure 19. Flowchart for the proposed PSO-enhanced OPF.

The particles and their velocities are initialized to optimally locate and adequately size

the storage systems and minimize the fitness function for the scheduling period. Using the POPF, the minimum operation cost of the system for each hour is calculated based on optimal locations and adequate sizes of the storage systems. The velocities are updated at each iteration and the positions are changed accordingly. This evolutionary algorithm is repeated until a termination criterion is satisfied. Eventually, the global best position is selected as the optimal solution for the problem.

4.7. Case Studies

The proposed POPF is used in this section to optimally place and adequately size energy storage within the IEEE 24-bus system shown in Figure 20. Different wind penetration (WP) levels are considered for this study where the wind penetration is defined as the ratio of the installed wind power capacity to the system peak load. The system peak load is 3700 MW and the generation capacity of the baseload plants is 800 MW. Storage applications for social cost and transmission congestion relief are evaluated under two scenarios. For both scenarios, the primary energy source is a wind farm installed at bus 14. Buses 2, 9, 10, 11, and 17 are arbitrarily excluded from the candidate locations to represent the geological restrictions for CAES deployment. A control strategy is used to restrict discharging of the storage to the peak hours. This strategy decreases the installed conventional generation required to meet the peak load. The cost-benefit analysis evaluates the economics of storage technologies and alternative gas-fired generators for different WPs. OC_S and IC_S are the operation cost and equivalent investment cost of the storage system for a 24-hour scheduling period. OC_G and IC_G are the operation cost and equivalent investment cost of the alternative gas-fired generators for the

scheduling period. The social cost (*SC*) of the system is the sum of the congestion and total operation costs. Historical data from the BPA authority and Pacific Northwest are used for the system load and wind speed, respectively [125], [126]. Cost function coefficients of the generating units are given in Table 16.

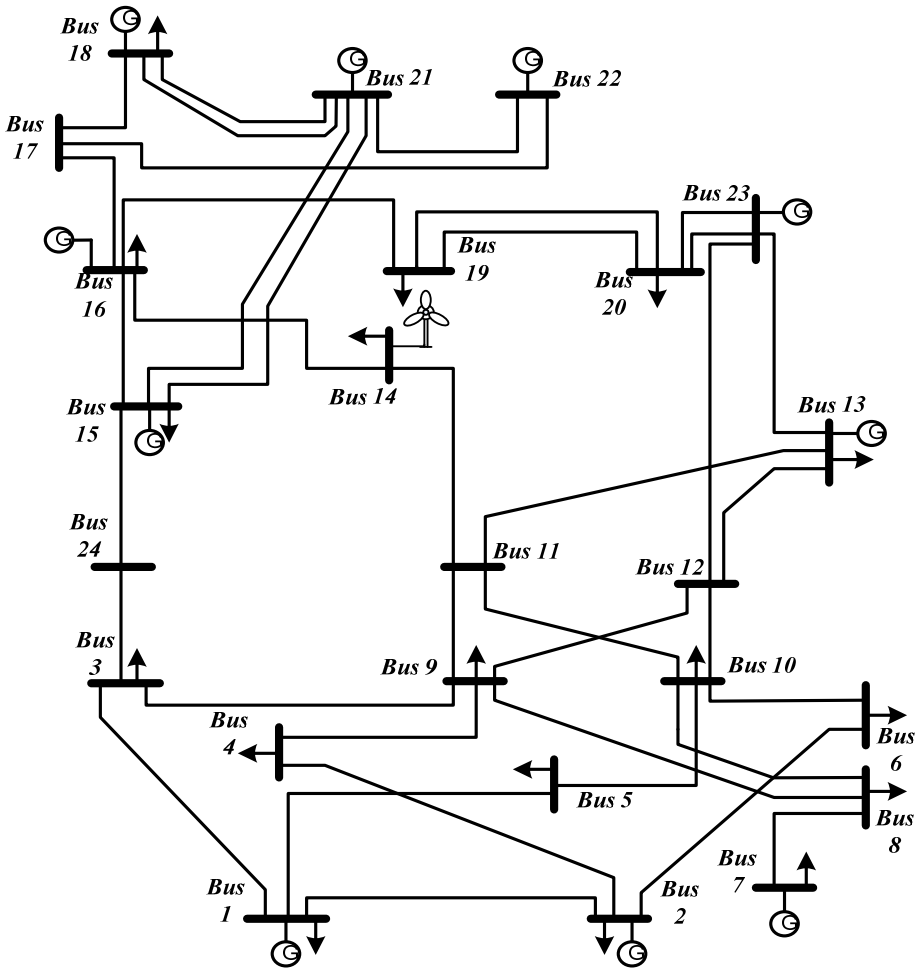

Figure 20. The IEEE 24-bus test system with wind installed at bus 14.

Table 16. Cost function coefficients of the generating units

Conventional Generator	Cost Function Coefficients		
	$a_i(\$/MW^2h)$	$b_i(\$/MWh)$	$c_i(\$)$
G_1	0.103	48.05	1313.6
G_2	0.108	48.04	1168.1
G_3	0.080	43.19	1078.8
G_4	0.081	44.26	969.8
G_5	0.068	23.6	958.2
G_6	0.068	23.6	958.2
G_7	0.090	50.90	471.6
G_8	0.080	50.90	471.6
G_9	0.088	46.70	445.4
G_{10}	0.091	43.51	702.7

4.7.1. Scenario I: Storage application for social cost relief

This scenario evaluates the storage application for social cost relief in a power system with high wind penetration. Case studies and their simulation results are summarized in Table 17. First, storage units are placed and sized using the PSO-enhanced POPF to minimize the social cost. Next, an adequate gas-fired generation capacity is used as an alternative to efficiently integrate the wind power. For this alternative, $P_{\max}$ denotes the power capacity of the gas-fired generators. The results show that for WP levels of 30%, 35%, 40% and 45%, the storage system is placed at bus 14 to minimize the social cost. Co-locating wind generation and energy storage significantly reduces the total operation cost of the system for these WPs where the transmission congestion is not significant. This is because the extra wind power can be directly stored without being curtailed due to the transmission congestion. The stored energy is released when the

transmission capacity is available. For higher WP of 50%, placing the storage system at the wind bus would significantly increase the congestion cost of the system when discharging the stored energy. Therefore, the storage system needs to be placed at a bus other than the wind bus which maintains a compromise between the operation cost increment and congestion cost decrement to realize the best optimal solution. This is evident from the simulation result for 50% WP where bus 16 is the optimal solution for the storage placement. Summing the congestion, operation and investment costs for the systems with storage and without storage in Table 17 shows the economic advantages of the storage application for wind integration over its gas-fired alternative. Optimal placement and adequate sizing of the storage within the IEEE 24-bus system decreases the wind curtailment when compared to the system with no storage. Wind integration for higher WPs is not as efficient as lower WPs where the wind curtailment is maintained at an acceptable level using the storage system. This is the case for 50% WP where 21.49% of the wind is curtailed even with the storage utilization. Simulation results for 50% WP are shown in Figure 21. All figures provide average hourly values for a 24-hour scheduling period. The storage is charged during the periods when the demand is low and wind generation is high. The stored energy is discharged during the mid-day peak hours when the transmission system is not congested. In order to increase the efficiency of wind integration for higher WP (50%), the storage is distributed to utilize the transmission capacity more effectively and avoid the costly solution of transmission expansion. Table 18 shows the results for 50% WP with two distributed storage systems. The results for the centralized storage are repeated for comparison. Optimal storage distribution between buses 14 and 23 decreases the social cost and wind curtailment from $\$ 2.260 \times 10^6$ and 21.49% with centralized storage to $\$ 2.214 \times 10^6$ and 12.94% with distributed

storage, respectively. Co-location of the first storage unit and wind generation for the distributed storage system significantly reduces the total operation cost from $\$ 2.165 \times 10^6$ with centralized storage to $\$ 2.087 \times 10^6$ which offsets the increase in congestion of the system with distributed storage. Cost-benefit analysis shows the economic merits of distributed storage system compared to the system with no storage. This is justified by the decrease in the sum of the operation, investment and congestion costs from $\$ 42.8787 \times 10^4$ with distributed storage to $\$ 42.967 \times 10^4$ with no storage. Figure 22 shows the simulation results for 50% WP and 2-unit distributed storage system.

Table 17. Simulation results for centralized storage-scenario I.

WP (%)		**Optimal Placement (*Bus #*)**	S_{max} **(*MWh*)**	P_{max} **(*MW*)**	OC_S **(10^4\$)**	IC_S **(10^4\$)**	OC_G **(10^4\$)**	IC_G **(10^4\$)**	CC **(10^4\$)**	**SC (10^6\$)**	**Wind Curtailment (%)**
30	*CS*[*]	14	1668.5	448.19	4.617	7.329	----	----	0.991	2.456	5.6
	NS[**]	----	----	221.22	----	----	8.444	4.04	0.919	2.493	19.66
35	*CS*	14	2429.1	546.91	6.753	9.490	----	----	4.817	2.385	6.87
	NS	----	----	449.64	----	----	12.350	8.211	4.415	2.436	24.65
40	*CS*	14	3071.4	561.94	8.457	10.552	----	----	6.029	2.311	9.76
	NS	----	----	435.58	----	----	15.468	7.954	4.988	2.370	29.48
45	*CS*	14	3457.2	566.67	9.418	11.143	----	----	8.194	2.273	13.65
	NS	----	----	421.76	----	----	17.225	7.702	5.973	2.328	33.38
50	*CS*	16	3015.7	609.18	8.407	11.002	----	----	9.522	2.260	21.49
	NS	----	----	445.29	----	----	15.375	8.132	9.321	2.327	36.82

[*]Centralized storage

[**]No storage

Table 18. Simulation results for distributed storage-scenario I.

WP (%)	Optimal Placement (*Bus #*)	S_{max} (*MWh*)	P_{max} (*MW*)	OC_S (10^4\$)	IC_S (10^4\$)	OC_G (10^4\$)	IC_G (10^4\$)	CC (10^4\$)	SC (10^6\$)	Wind Curtailment (%)
CS	16	3015.7	609.18	8.407	11.002	----	----	9.522	2.260	21.49
NS	----	----	445.29	----	----	15.375	8.132	9.321	2.327	36.82
DS[*]	14	3600.5	566.67	9.146	11.342	----	----	12.664	2.214	12.94
	23	1282.4	393.14	3.550	6.176	----	----			
NS	----	----	570.85	----	----	23.221	10.425	9.321	2.286	36.82

[*]Distributed storage

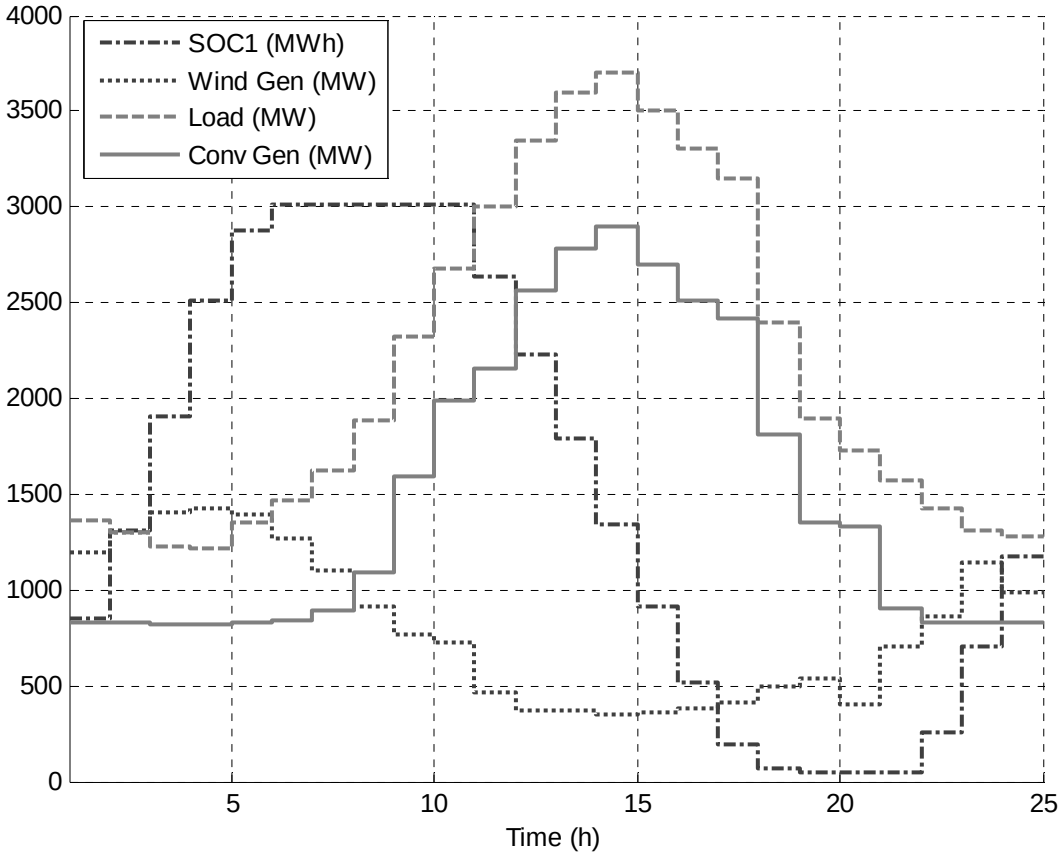

Figure 21. Simulation results for centralized storage-scenario I.

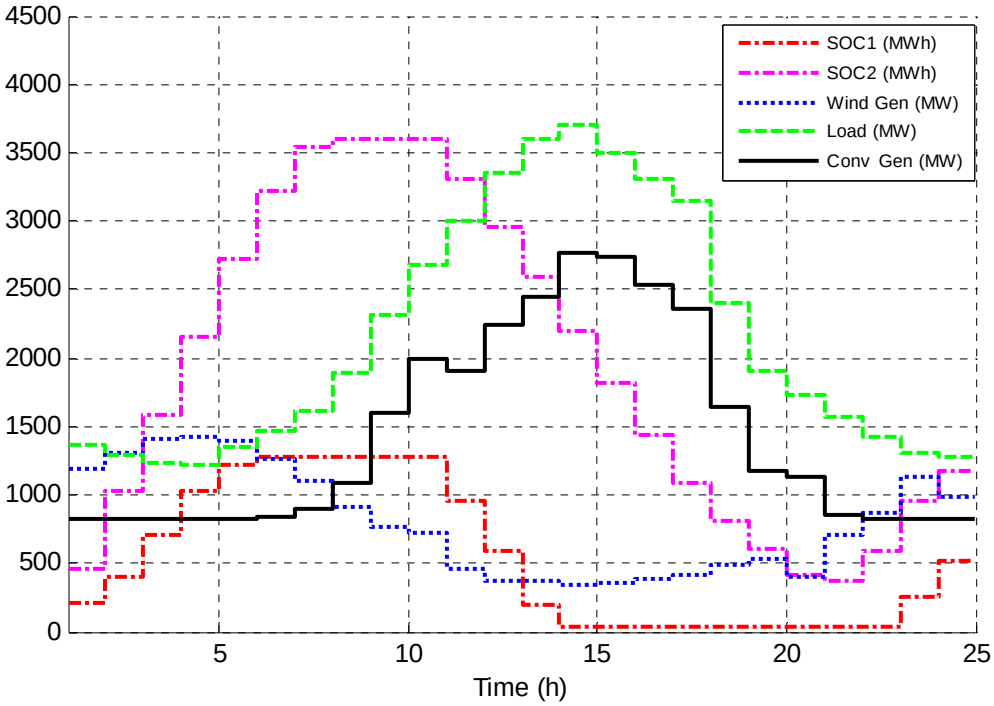

Figure 22. Simulation results for distributed storage-scenario I.

4.7.2. Scenario II: Storage application for transmission congestion relief

This scenario evaluates the distributed storage application for transmission congestion relief of wind integration with higher WPs. First, the storage systems are optimally placed and adequately sized to minimize the congestion cost of the system where the operation cost is excluded from the objective function. Next, an adequate gas-fired generation capacity is used as an alternative to efficiently integrate wind power. Simulation results for the 2-unit storage system and 50% WP are shown in Table 19. Optimal storage distribution between buses 7 and 8 with 753.29 MWh and 422.08 MWh capacities and 249.76 MW and 261.4 MW power ratings decreases the congestion cost from $\$ 9.321 \times 10^4$ with no storage to $\$ 7.389 \times 10^4$ with distributed storage. The decrease in wind curtailment from 36.82% with no storage to 32.31% with distributed storage shows the efficiency enhancement of wind integration when applying the

storage system for congestion relief purposes. The social cost of the system is also reduced as a result of this application when compared to the system with no storage. The sum of the operation, investment, and congestion costs decreases from $\$ 19.782 \times 10^4$ for the system with no storage to $\$ 18.034 \times 10^4$ for the system with 2-unit distributed storage which economically justifies the CAES deployment and its advantage over the gas-fired alternative.

Table 19. Simulation results for distributed storage-scenario II.

WP (%)	**Optimal Placement (*Bus #*)**	S_{max} **(*MWh*)**	P_{max} **(*MW*)**	OC_S **(10^4\$)**	IC_S **(10^4\$)**	OC_G **(10^4\$)**	IC_G **(10^4\$)**	CC **(10^4\$)**	**SC (10^6\$)**	**Wind Curtailment (%)**
DS	7	753.29	249.76	2.132	3.838	----	----	7.389	2.377	32.31
	8	422.08	261.4	1.168	3.507	----	----			
NS	----	----	242.285	----	----	6.037	4.424	9.321	2.424	36.82

Table 20. Transmission flow limitations.

From Bus #	To Bus #	Flow Limit (MW)
1	2	175
1	3	175
1	5	175
2	4	175
2	6	175
3	9	175
3	24	400
4	9	175
5	10	175
6	10	175
7	8	175
8	9	175
8	10	175
9	11	400
9	12	400
10	11	400
10	12	400
11	13	500
11	14	500
12	13	500
12	23	500
13	23	500
14	16	500
15	16	500
15	21	500
15	24	500
16	17	500
16	19	500
17	18	500
17	22	500
18	21	500
19	20	500
20	23	500
21	22	500

4.8. Conclusions

A technical framework is proposed to evaluate the energy storage application, its optimal placement and economic advantage for the social cost and transmission congestion relief of wind

integration with higher penetration levels. Wind generation and load are stochastically modeled using historical data and curve fitting. The storage system is incorporated into the POPF model to store the extra wind power that would otherwise be curtailed. A particle swarm optimization is proposed to optimally place and adequately size the energy storage for minimizing the sum of operation and congestion costs over a scheduling period. The proposed method was tested on the IEEE 24-bus system under two scenarios with different wind penetration levels. Simulation results have demonstrated the advantage of co-locating wind and storage for its social cost relief application. This advantage was due to the decreased operation cost of the system for lower wind penetrations where the transmission congestion was not significant. For higher wind penetrations, the storage system was placed at a bus other than the wind bus which maintained a compromise between the operation cost increment and congestion cost decrement to realize the best optimal solution.

V. Chapter 5. Transmission Network Expansion Planning

5.1. Wind and Load Modeling

Probability density functions (PDFs) are used to model the uncertainties associated with wind speed and load demand [83]. The behavior of wind speed is stochastically characterized using the Weibull distribution:

$$f_{wd}(v) = \left(\frac{\alpha}{\beta}\right)\left(\frac{v}{\beta}\right)^{\alpha-1} e^{-\left(\frac{v}{\beta}\right)^{\alpha}}, 0 \le v \le \infty \quad (5.1)$$

where, α, β, v and f_{wd} are the shaping, scaling coefficients, wind speed and PDF of wind speed, respectively. The power-speed curve is used to calculate the wind power as [77]:

$$P_W = \begin{cases} 0 & v \le v_i, v \ge v_o \\ \dfrac{v - v_i}{v_r - v_i} P_{W_r} & v_i \le v \le v_r \\ P_{W_r} & v_r \le v \le v_o \end{cases} \quad (5.2)$$

where, v_i, v_r, v_o, P_{W_r} and P_W are the cut-in, rated, cut-out wind speeds, rated and output wind powers, respectively. The variation of load demand is modeled by the Gaussian distribution as:

$$f_{ld}(l) = \frac{1}{\sqrt{2\pi\sigma^2}} exp\left[-\frac{(l-\mu)^2}{2\sigma^2}\right] \quad (5.3)$$

where, l, μ, σ, f_{ld} are the load, mean value, standard deviation and PDF of the load, respectively. Maximum Likelihood Estimation (MLE) is used to obtain the parameters of PDFs for historical wind speed and load data.

5.2. Transmission Financial Modeling

5.2.1. Transmission pricing

An appropriate transmission pricing mechanism is required to calculate the cost of transmission services based on the extent of use of transmission resources. A well-organized and fair pricing method creates economic signals and incentives for the essential reinforcement and expansion of the transmission network. Postage-stamp rate and contract path are traditional methods for the recovery of transmission costs. The postage-stamp rate method charges transmission users based on an average embedded cost where the real extent of use of transmission facilities by each user is not considered. The contract path method restricts the transaction to a specified path which may differ from the actual path taken in reality. The MW-mile method recovers the transmission costs based on the actual use of the transmission network calculated by DC power flow. This strategy cannot provide a fair pricing mechanism because it

recovers all the costs regardless of the extent of use of transmission line capacity [127]. The unused transmission capacity method is an enhanced version of MW-mile method to charge the users based on the percentage utilization of the transmission facility. The cost equation for this method is given by:

$$TC_t = \sum_{k=1}^{K} \frac{C_k \cdot L_k \cdot |f_{k,t}|}{|\bar{f}_k|} \tag{5.4}$$

where TC_t is the cost of transmission service and $f_{k,t}$ is the flow of line k for transaction t. C_k, L_k and $\bar{f}_k$ are the cost per MW per unit length, length, and maximum capacity for line k, respectively .

5.2.2. Rate of return and investment risk evaluation

Rate of return and risk are the most important determining factors for the investment in transmission projects. Power system uncertainties increase the risk level and make transmission investment less attractive to the private investors. Modern portfolio theory (MPT) provides a mathematical model to select an economic portfolio based on risk-return trade-offs and efficient diversification [128]. Here, the return rate of an investment is a random variable whose mean value indicates the expected profitability. The variance of the return is an indication of the risk involved which shows the deviation from the expected return. The mean-variance criterion is the basis of MPT for investment choice under uncertainties [129]. An economic portfolio or project gives the highest rate of return with a desirable level of risk. The return rate of an investment is calculated by solving the following equation for *i*:

$$\sum_{n=1}^{N} \frac{A_n}{(1+i)^n} = I_C - P_S \tag{5.5}$$

where I_C is the investment cost, P_S is the present worth of the salvage value, A_n is the annual revenue and i is the return rate of the investment.

Figure 23 shows the cash flow diagram for an investment.

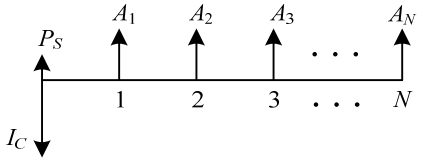

Figure 23. Cash flow diagram for an investment

5.3. Methodology

A multi-stage posterior method is used in this section for transmission expansion planning in a deregulated environment. A set of Pareto optimal solutions is obtained which provides more flexibility when compared to one optimal solution for the single objective formulation. A compromise-solution method is used to find the best solution based on the planner's preferences.

5.3.1. Objective Functions

a) Investment cost minimization

Minimizing the transmission investment cost in a deregulated environment decreases the cost of transmission services for market participants. The transmission investment cost IC is minimized using:

$$Min\ IC = Min \sum_{(i,j)\in\Omega} c_{ij} \cdot n_{ij} \tag{5.6}$$

where IC is the total investment cost of a candidate plan, $c_{ij}$is the cost of an added line and n_{ij} is the number of added lines to the corridor *i-j*, and Ω is the set of all corridors.

b) Private investment maximization

Power system uncertainties and the obstacles facing merchant transmission projects in a restructured electricity market discourage private investment in TNEP [130]. Insufficient transmission capacity mitigates the non-discriminatory competitive environment for market participants resulting in a monopoly power over the transmission network. An appropriate transmission expansion strategy is required to maximize private investment and eliminate monopolies in a deregulated environment.

Based on the revised unused transmission capacity method, the periodic revenue for transmission line *l* is calculated by:

$$A_n^l = \alpha . TC_l \tag{5.7}$$

where A_n^l is the periodic revenue, α is the annual return, and TC_l is the total cost of transmission service for the transmission line *l*. A_n^l and (5.5) are then utilized to calculate the rate of return (*i*) for each new transmission investment.

The rate of return for each transmission line is a probabilistic variable since it is determined using the power flow with random inputs. The mean value and standard deviation of the rate of return, defined as the expected rate of return (ROR_l) and investment risk ($Risk_l$), are used as two viable criteria to evaluate the investment in transmission projects [54]. These two parameters are then compared with the minimum attractive rate of return (*MARR*) and desirable

risk level ($Risk_d$) to determine whether the transmission projects are attractive for private investors [54]. A transmission project is attractive if the following inequality constraints are satisfied:

$$ROR_l \geq MARR \tag{5.8.a}$$

$$Risk_l \leq Risk_d \tag{5.8.b}$$

where ROR_l is the rate of return and $Risk_l$ is the and risk of investment for the transmission line l. Attractive transmission projects which satisfy (5.8) can absorb private investment. We maximize private investment PI^{AL} for the determined attractive lines:

$$Max\ PI^{AL} = Max \sum_{l=1}^{L} PI_l^{AL} \tag{5.9}$$

where PI^{AL} and PI_l^{AL} are the absorbed private investment for the attractive lines and l^{th} attractive line, respectively. L is the set of attractive lines determined by constraint (5.8).

c) Reliability maximization

Traditional transmission planning for conventional generation with firm capacities typically uses the deterministic n-1 security criterion for reliability analysis. This type of analysis is not appropriate for non-firm wind generation which is unlikely to exceed the n-1 firm transfer capacity. This results in an under-utilized transmission system as the high voltage transmission lines are usually available with high probability while the chance of wind generation curtailment when the n-1 contingency occurs is small. Therefore, a probabilistic reliability analysis is required to include both adequacy and security criteria for the expansion planning of transmission systems with wind generation. The probabilistic analytical state enumeration

method is used here to calculate the reliability index [131]. This method uses the interrupted load and probability for every contingency to calculate the reliability index of a transmission network. Expected energy not supplied (EENS) is utilized as an energy index to represent the reliability level of transmission network. The reliability index of a transmission network can be calculated using:

$$EENS_T = \sum_{i\in\phi}\sum_{j\in\Theta} IL_i^j . P_j \tag{5.10}$$

where $EENS_T$ is the expected energy not supplied for the transmission network, IL_i^j is the interrupted load at bus *i* due to the contingency *j*, P_j is the occurrence probability of contingency *j*, Θ represents the load buses, and ϕ is the set of contingencies. The occurrence probability (P_j) for each contingency *j* is obtained by multiplying the probability of component *j* not being available by the probability of other components being available. The following linear programming sub-problem which minimizes the total interrupted load is solved to calculate the interrupted load (IL_i^j) for each contingency:

$$Obj.Fun = \min_{j\in\Theta} \sum_{i\in\phi} IL_i^j \tag{5.11}$$

This objective function is subject to the following physical constraints of the network:

$$\sum_{i=1}^{n_b} P_{g_i} = \sum_{i=1}^{n_b} P_{d_i} \tag{5.12.a}$$

$$f_{jk} = B_{jk}(n_{jk} + n_{jk}^{ex.})(\theta_j - \theta_k) \tag{5.12.b}$$

$$\left|f_{jk}\right| \le (n_{jk} + n_{jk}^{ex.})\overline{f}_{jk} \tag{5.12.c}$$

$$\underline{P}_{g_i} \leq P_{g_i} \leq \overline{P}_{g_i} \tag{5.12.d}$$

$$\underline{P}_{d_i} \leq P_{d_i} \leq \overline{P}_{d_i} \tag{5.12.d}$$

$$0 \leq n_{jk} \leq \overline{n}_{jk} \quad \forall (j,k) \in \Omega \tag{5.12.e}$$

$$IL_i^j = \overline{P}_{d_i} - P_{d_i} \tag{5.12.f}$$

where f_{jk}, B_{jk} and $\overline{f}_{jk}$ are the power flow, susceptance and power flow limit of the line in corridor *j-k*. θ_j and θ_k are the voltage phases at bus *j* and *k*. $n_{jk}^{ex.}$, n_{jk} and $\overline{n}_{jk}$ are the number of existing lines, number of new transmission lines and maximum number of added lines in corridor *j-k*. P_{g_i}, $\underline{P}_{g_i}$and $\overline{P}_{g_i}$are the power output, lower and upper generation limits for the i^{th} generating unit. P_{d_i}, $\underline{P}_{d_i}$and $\overline{P}_{d_i}$are the supplied load, lower load limit and load demand for the i^{th} bus. IL_i^j, the interrupted load at bus *i* due to the contingency *j*, is calculated by the taking the difference of the demand and the supplied load at each bus [59]. To reduce the simulation time of the reliability analysis, we use a contingency selection strategy that (a) ranks contingencies based on the product of their probability and interrupted load and (b) neglects contingencies for which this value is very small.

5.3.2. NSGA II Optimization

Generally, there are multiple optimum solutions for the multi-objective optimization of TNEP. A set of Pareto optimal solutions that are non-dominant with respect to all the objective functions is used. Several evolutionary algorithms have been proposed to solve a multi-objective optimization problem using the non-dominancy concept [132]. Elitist Non-dominated Sorting Genetic Algorithm (NSGA II) is an efficient evolutionary algorithm to handle the non-linearity,

non-convexity and discontinuity of TNEP [132]. NSGA II is initialized using a set of randomly selected initial solutions. The initialized population is sorted into sets of Pareto solutions called Pareto fronts. The Pareto fronts are ranked based on their non-dominancy levels where the individuals of the first front are assigned the highest fitness value and so on. Crowding distance is calculated for each individual as a measure of proximity to its neighbors. The average crowding distance represents population diversity. A binary tournament algorithm is used to select parent populations based on their non-dominancy rank and crowding distance. Crossover, mutation and selection operators are then utilized to generate offsprings from the selected population for the next iteration. This process halts upon the satisfaction of a termination criterion [133].

5.3.3. Market-based Optimal Power Flow

A one-sided auction market is incorporated into the OPF where the market participants submit their hourly price bids in the form of marginal generation costs. The hourly social cost (HSC) is minimized in an electricity market-based OPF using [67]:

$$Obj.Fun = Min\left\{\sum_{i=1}^{n_g} P_{g_i}(t_h)\left(a_i P_{g_i}(t_h) + b_i\right) + \sum_{i=1}^{n_b} \alpha_i(\overline{P}_{d_i} - P_{d_i})\right\} = Min\ (HSC) \qquad (5.13)$$

where α_i is a large penalty cost assigned to the interrupted load at each bus i. This objective function is subject to the constraints (5.12.a)-(5.12.f) for normal operating conditions.

5.3.4. Market-based Probabilistic OPF

Due to the stochastic nature of wind power and load in TNEP, it is necessary to use probabilistic OPF analysis. Simulation, analytical and approximate methods are commonly used

to perform probabilistic OPF (POPF) [134]. To avoid the computational burden of Monte Carlo simulation and mathematical calculations associated with analytical methods, we use Hong's approximate but efficient point estimation (2*m*+1)-scheme [135]. Note that although the mapping function from inputs to outputs is not known explicitly for our problem, the successive operators corresponding to this mapping, equations (5.5), (5.7) and (5.12.a-5.12.f) and (5.13), are all continuous with continuous derivatives which satisfy the conditions required for Hong's (2*m*+1) method to converge.

In a $K \times m$ scheme, statistical information of the random input variables is represented by K points called concentrations. A location $x_{i,k}$ and a weight $w_{i,k}$ are used to form the k^{th} concentration of the i^{th} random variable. The location is determined by:

$$x_{i,k} = \mu_{x_i} + \xi_{i,k} \cdot \sigma_{x_i} \tag{5.14}$$

where μ_{x_i}, σ_{x_i} and $\xi_{i,k}$ are the mean, standard deviation and standard location of the k^{th} concentration for the random input variables x_i.

The weight and standard location are calculated by solving the following nonlinear system of equations:

$$\sum_{k=1}^{K} w_{i,k} = 1/m \tag{5.15.a}$$

$$\sum_{k=1}^{K} w_{i,k} \cdot (\xi_{i,k})^j = \lambda_{i,j}, \qquad j = 1, \dots, 2K-1 \tag{5.15.b}$$

The j^{th} standard central moment of the i^{th} random variable, $\lambda_{i,j}$, is :

$$\lambda_{i,j} = \frac{M_j(x_i)}{(\sigma_{x_i})^j} \tag{5.16}$$

The j^{th} central moment of the i^{th} random variable, $M_j(x_i)$, is given by:

$$M_j(x_i) = \int_{-\infty}^{\infty} (x_i - \mu_{x_i})^j \cdot f_{x_i} dx_i \tag{5.17}$$

where $f_{x_i}$is the probability density function of the random variable x_i.

Upon obtaining all concentrations ($x_{i,k}$,$w_{i,k}$), the vector of random output variables $Z(i,k)$ is calculated for each point $(\mu_{x_1}, \mu_{x_2}, \dots, x_{i,k}, \dots, \mu_{x_m})$ using the nonlinear input-output function F as follows:

$$Z(i,k) = F(\mu_{x_1}, \mu_{x_2}, \dots, x_{i,k}, \dots, \mu_{x_m}) \tag{5.18}$$

The j^{th} moments of the random output variables are then estimated by:

$$E[Z^j] \cong \sum_{i=1}^{m} \sum_{k=1}^{K} w_{i,k} \cdot (Z(i,k))^j \tag{5.19}$$

Setting K=3 and $\xi_{i,3} = 0$ yields $x_{i,3} = \mu_{x_i}$ in (5.18) and results in the same point of $(\mu_{x_1}, \mu_{x_2}, \dots, \mu_{x_i}, \dots, \mu_{x_m})$ for m of the 3m locations.

$$\xi_{i,k} = \frac{\lambda_{i,3}}{2} + (-1)^{3-k} \sqrt{\lambda_{i,4} - \frac{3}{4}{\lambda_{i,3}}^2} \quad k = 1,2, \xi_{i,3} = 0 \tag{5.20.a}$$

$$w_{i,k} = \frac{(-1)^{3-k}}{\xi_{i,k}\left(\xi_{i,1} - \xi_{i,2}\right)} \quad k = 1,2, w_{i,3} = \frac{1}{m} - \frac{1}{\lambda_{i,4} - {\lambda_{i,3}}^2} \tag{5.20.b}$$

Instead of using $w_{i,3}$ for each location, the weight w_0 is used and updated for the m locations in the (2m+1)-scheme as $\xi_{i,3} = 0$ and $x_{i,k} = \mu_{x_i}$ are the same for m of the 3m points:

$$w_0 = \sum_{i=1}^{m} w_{i,3} = 1 - \sum_{i=1}^{m} \frac{1}{{\lambda_{i,4} - \lambda_{i,3}}^2} \tag{5.21}$$

To perform a POPF, the non-linear input-output function F in (5.18) is replaced with the OPF equations (5.13) and (5.12.a)-(5.12.f).

5.3.5. Decision Making

A set of Pareto optimal solutions is obtained as the result of solving the multi-stage posterior TNEP problem. Once the non-dominated set is determined, a rational decision needs to be made by the planner to find the final optimal plan. The decision making represents a compromise between different objectives based on the planner's preferences. We use a compromise solution as an efficient decision-making method to realize the best solution among the set of Pareto optimal solutions. This method minimizes the normalized Euclidian distance between the potential optimal and utopia points. The utopia point is defined as a point which is sufficiently close to the minimum point. The Euclidian distance for our multi objective TNEP is minimized as follows [113]:

$$\min_{U \in \Phi} \left\{ \sum_{i=1}^{n_o} \left| F_i(U) - F_i^0 \right|^2 \right\}^{\frac{1}{2}} \tag{5.22}$$

$F_i(U)$ is the i^{th} normalized objective function given by:

$$F_i(U) = \frac{f_i^{max} - f_i(U)}{f_i^{max} - f_i^{min}} \tag{5.23}$$

where $f_i^{max}$and $f_i^{min}$are the maximum and minimum values for the i^{th} objective function. $f_i(U)$ and $F_i^0$are the i^{th} objective function value and normalized utopia point. Φ is the set of Pareto

optimal solutions. Setting $F_i^0 = 1$ in (5.22) makes each objective function as close as possible to its minimum point. Normalization is required for a multi objective problem where the objective functions have different units.

5.3.6. Proposed Algorithm

Figure 24 shows the flowchart of the proposed algorithm for the multi-objective multi-stage TNEP problem. The algorithm begins with initializing the first population as the candidate transmission lines. The investment cost is determined for each plan using (5.6). Probabilistic OPF is used to calculate the line flows under normal operating conditions. The revenues for the transmission lines are obtained based on the line flow results and (5.7). Solving (5.5) for i gives the rate of return for the investment for each line in a plan. The ($2m$+1) point estimate scheme is utilized to perform the POPF and calculate the rate of return for each transmission line. The input-output function F in (5.18) is the composition of the OPF equations (5.12.a-5.12.f) and (5.13), periodic revenue (5.7), and rate of return equation (5.5). The mean-variance criterion is used to calculate ROR_l and $Risk_l$ from the investment for each line obtained in the previous step (the mean value and standard deviation of the return rate give the expected ROR_l and investment risk $Risk_l$). These two parameters are evaluated using equations (5.8.a) and (5.8.b) to determine whether the transmission line is attractive for private owners. The absorbed private investment is then evaluated for each plan based on (5.8). If these constraints are satisfied for a transmission line, the line is attractive and the associated investment is considered as the absorbed private investment. The absorbed private investment is calculated for all attractive transmission lines using (5.9). The reliability index (EENS) for each plan is calculated using (5.10)-(5.12).

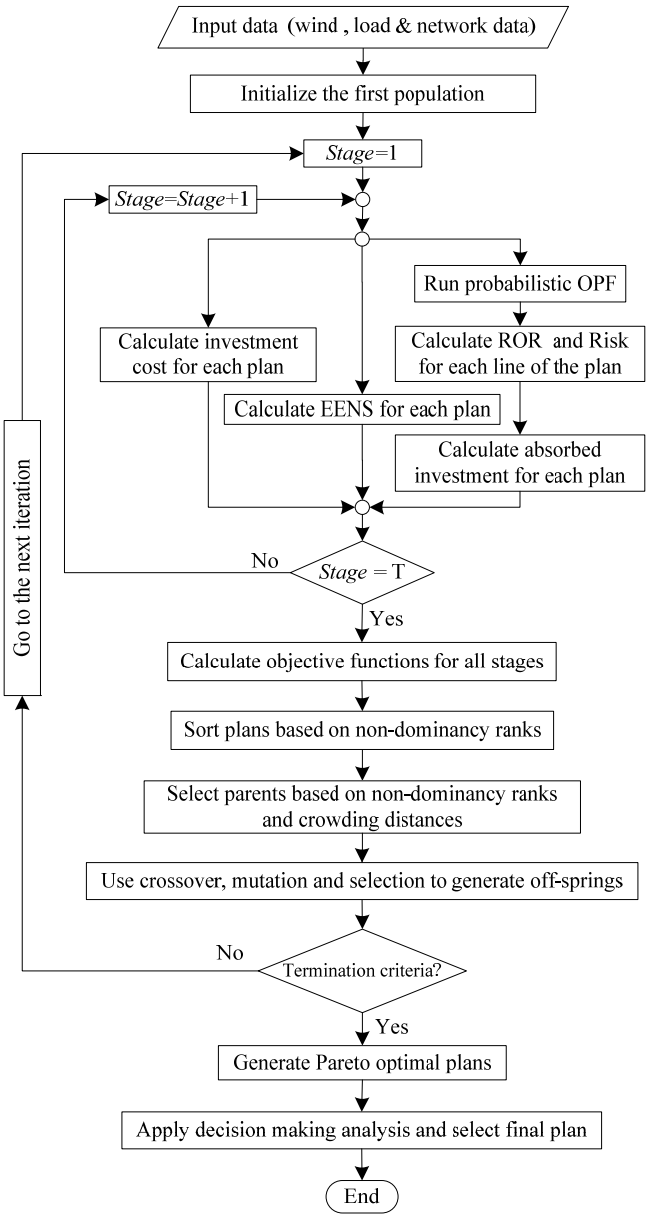

Figure 24. Flowchart for the proposed TNEP framework.

Once all the plans are obtained for the planning horizon, the solutions are ranked and the parent population is selected using a binary tournament algorithm. Crossover, mutation and selection generate the off-spring population for the next iteration. This process is iterated until the termination criterion is satisfied. Upon obtaining the Pareto

optimal plans from NSGA II, the decision maker uses an algorithm to select the final optimal solution based on the planner's preference.

5.4. Case Studies

The proposed framework is used to determine the new transmission lines, their locations and the stages when the transmission reinforcement takes place within the IEEE 24-bus reliability test system (RTS) shown in Figure 25 [136]. The OPF problem is solved using MATLAB [137]. Four stages, five years each, are considered for the 20-year planning horizon. Ten new right-of-ways as well as the existing 34 corridors are the candidate solutions for transmission installation. Transmission installation cost is $1000/MW-mile. Investment costs for the new transmission lines are given in Table 21 [53].

Table 22 shows the generation companies' (GenCos') bid coefficients. Load and generation growth rates of 7% and 6% per year are considered for the 20-year planning horizon. A wind farm is installed at bus 14 with an initial capacity of 500 MW. This capacity is increased to 750, 1000, 1250 and 1500 MW at the end of stages 1, 2, 3 and 4. The values of the discount rate, MARR, desirable risk level, and annual return are d=10%, MARR=15% $Risk_d$=5% and α= 25%.

Table 21. Investment cost of new lines

From	To	Investment Cost (M$)	From	To	Investment Cost (M$)
1	8	3.15	13	14	15.5
2	8	2.89	14	23	21.5
6	7	4.36	16	23	28.5
6	8	1.58	19	23	21
7	2	2.19	20	22	9

Table 22. Generation Companies' Bid coefficient

Generators	a_i	b_i	Generators	a_i	b_i
G1	0.01131	12.145	G7	0.00667	9.2706
G2	0.01131	12.145	G8	0.00028	5.345
G3	0.0122	17.924	G9	0.00028	5.345
G4	0.003	20.023	G10	0.001	0.5
G5	0.001	4	G11	0.00392	8.919
G6	0.00667	9.2706	-	-	-

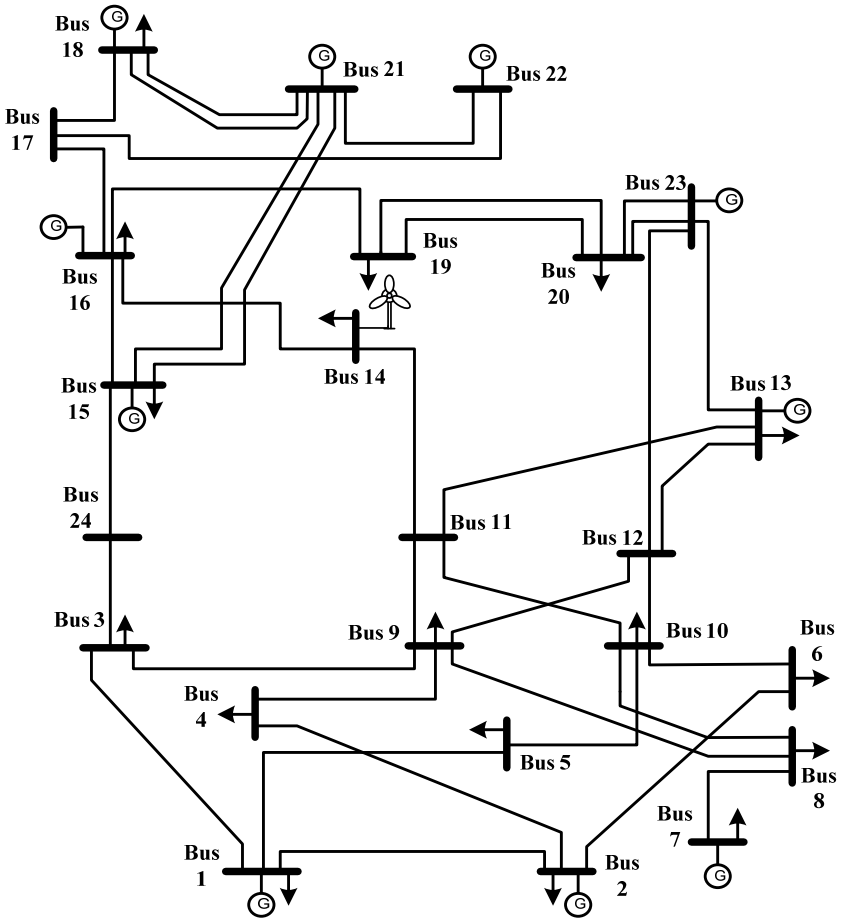

Figure 25. The IEEE 24-bus test system with wind installed at bus 14.

Figures 26(a)-(c) show the Pareto optimal solutions for TNEP. Each figure represents the trade-off region between the two objective functions. Figure 26(a) shows a supportive relation between the investment cost and absorbed private investment. Increasing the capital investment for transmission installation increases the capacity of the corridors that transfers the generated power to the load centers. This decreases the reliability index (EENS) of the system. As a result, more load is supplied which requires an increment in power flow through the transmission lines. Increased utilization of transmission capacity raises the revenue and rate of return for the transmission lines and makes the investment more attractive for the private sector. However, the

symbiotic relation between these two criteria comes to a saturation state for investment costs of M$220 and above. This is due to the fact that there is no significant reliability enhancement as the investment cost increases above M$220, which results in constant or even reduced absorption of private investment.

Figure 26(b) shows the trade-off region between the EENS as the reliability index and investment cost of the system. The optimal plans have a reliability index in the range of 0-0.35 p.u which corresponds to an investment cost of 0-455 M$. As shown, the reliability of the system is significantly enhanced by increasing the investment cost up to M$ 220 but is almost constant for larger investment costs.

Figure 26(c) gives a quantitative representation of the trade-off between the reliability criterion and absorbed private investment for the IEEE RTS. An increase in the absorbed private investment implies an investment cost increment, which provides more transmission capacity and decreases the interrupted load and EENS of the system.

The optimal solutions given by Figures 26(a)-(c) are non-dominant with respect to each other. Based on the planner preferences, the most appropriate solution is adopted as the final plan using the compromise-solution method. Table 23 shows the final optimal plan for two sets of utopia points represented by Cases I and II (F_1^0 for investment cost, F_2^0 for absorbed private investment and F_3^0 for reliability index). The values of utopia points can be selected based on different factors such as available budget and desired security level of the system.

Table 23. Decision Making for TNEP

	Utopia Values			Objective Function Value		
Case	F_1^0	F_2^0	F_3^0	IC [a]	PI[b]	EENS[c]
I	0.75	0.4	0.98	107.55	89.8	0.0126
II	0.7	0.45	0.98	115.075	97.325	0.002

[a]: Investment cost (M$)

[b]: Absorbed private investment (M$)

[c]: Expected Energy Not Supplied (p.u)

TNEP results for the final plans of Table 23 are given in Table 24. This table shows the new added transmission lines, rate of returns and risks of investment for each new line and the stages when the expansion takes place within the IEEE 24-bus RTS. The results include two types of transmission lines: reliability and merchant transmission lines. Transmission lines with $ROR_l \geq 15\%$ and $Risk_l \leq 5\%$ are the merchant transmission lines that provide private investors with economic incentives. The remainder includes the reliability transmission lines required to meet regulatory reliability criteria. The EENS of the transmission system for the final plan is calculated for different stages and given in Table 25. The system is simulated for the last year of stage 4. Based on the simulation, there is a low probability (0.031) that wind power exceeds the transmission limit during the year.

5.5. Conclusions

This chapter presents a stochastic framework for transmission network expansion planning in deregulated power systems with wind generation. The proposed method describes a multi-stage multi-objective model to satisfy reliability requirements and provide economic incentives for private investors. A NSGA II-based POPF was used to determine trade-offs

between reliability measures, absorption of private investments and installation costs for different solutions. The decision-making process was performed for different values of the utopia point to determine the final optimal plan based on the planner's preferences. The final plans clearly show two groups of merchant and reliability transmission lines. Note that the simulation time for real large-scale networks with many uncertain variables can be reduced by: (a) parallel processing, (b) reduced number of contingencies, (c) smart initialization of GA, and (d) use of MATLAB's MEX-files instead of M-files.

Table 24. TNEP Results for the Final Plans

Corridor		**Case I**					**Case II**				
From	To	I [a]	RoR_l [b] (%)	$Risk_l$ [c] (%)	Stage	Merchant Transmission	I [a]	RoR_l [b] (%)	$Risk_l$ [c] (%)	Stage	Merchant Transmission
3	24	✓	23.03	0.99	2	✓	✓	22.71	0.99	2	✓
6	10	✓	24.28	1.79	2	✓	✓	24.53	1.68	2	✓
8	10	-	-	-	-	-	✓	17.84	1.35	3	✓
10	11	✓	15.68	0.8	3	✓	✓	15.42	0.79	3	✓
10	12	✓	1.45	0.17	3	-	✓	1.42	0.17	2	-
15	24	✓	18.06	1.57	2	✓	✓	19.47	1.37	2	✓
16	17	✓	16.97	1.36	3	✓	✓	18.93	1.61	3	✓
18	21	✓	23.85	0.89	2	✓	✓	24.9	0.89	2	✓
6	7	✓	7.93	2.07	3	-	✓	1.67	1.79	3	-

[a]: Installation status for transmission line *l*
[b]: Rate of return of investment for transmission line *l*
[c]: Risk of investment for transmission line *l*

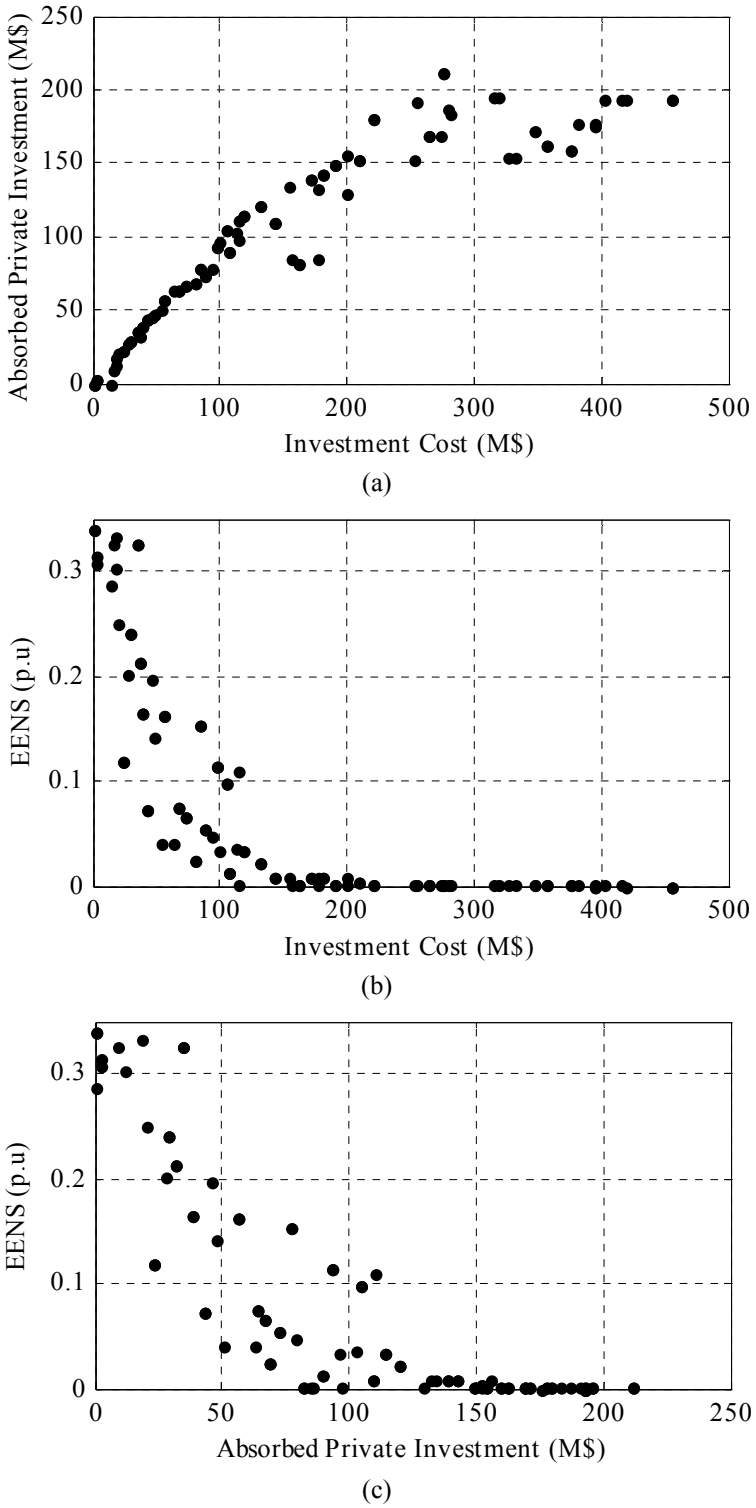

Figure 26. Pareto optimal solutions for IEEE RTS and trade-offs between (a) absorbed private investment and investment cost. (b) EENS and investment cost. (c) EENS and absorbed private investment.

Table 25. Reliability Results for the Final Plans

Stage		1	2	3	4
EENS (p.u)	**Case I**	0.0026	0.0016	0.0007	0.0126
	Case II	0.0026	0.0001	0.0002	0.0020

VI. Chapter 6. Conclusion and Future work

This dissertation proposes several methodologies to remove the barriers of extending intermittent renewable generation. These methods decrease renewable generation uncertainties using the geographical distribution of renewable resources, energy storage units, load shifting strategies, and network expansion planning. Several case studies have been performed to show the feasibility of the proposed methods.

In Chapter 2, a method has been developed to evaluate distributed wind generation and its potential impact on ramping requirement in power systems with high levels of wind penetration. This method is tested on the IEEE 24-bus system and different case studies are carried out to investigate the factors affecting the ramping requirement. Simulation results show that distributing the wind generating plants throughout the IEEE 24-bus system decreases the ramping requirement and integration costs for 24 hours day ahead scheduling.

In Chapter 3, two new methods have been proposed for optimal sizing of a hybrid power system including wind/PV/energy storage system. Using historical data and curve fitting, wind and PV generation and cooling loads are stochastically modeled. A smart-grid strategy is developed to shift the load and match the renewable energy generation and cooling load. In the first method, a GA-based optimization is proposed to minimize the cost and increase the efficiency. In the second method, a PS-based SMCS optimization is proposed to optimally size the hybrid system components and satisfy the reliability requirements. Simulation results show the trade-off between system cost and reliability for a hybrid power system. The best compromise is realized using a compromise-solution method. The proposed methodologies

enable electric utilities to efficiently utilize the installed renewable resources and storage capacities for supplying the controllable flexible load, such as the HVAC load. The proposed procedures can be applied for any controllable deferrable load, such as HVAC load.

In Chapter 4, a new technical framework is proposed to evaluate the energy storage application, for the social cost and transmission congestion relief of wind integration. Optimal storage distribution and its application for transmission congestion relief utilized the transmission capacity more effectively and increased the efficiency of wind integration when compared with the conventional alternatives. The cost-benefit analysis has shown the economic justification and advantage of storage application for both social cost and transmission congestion relief over the gas-fired alternatives. Simulation results have demonstrated the advantage of co-locating wind and storage for its social cost relief application.

In Chapter 5, a new stochastic framework for transmission network expansion planning in deregulated power systems with wind generation has been presented. The proposed method describes a multi-stage multi-objective model using a NSGA II-based POPF to satisfy reliability requirements and provide economic incentives for private investors. The decision-making process was performed for different values of the utopia point to determine the final optimal plan based on the planner's preferences. This is critical in a restructured power market with renewable energy generation where the stochastic nature of renewable resources and deregulation policies increase the investment risk and decrease the rate of return involved in transmission projects. The proposed strategy provides valuable insights for both private investors and transmission network operators. It also mitigates the monopoly power over transmission networks. Simulation

results for the IEEE 24-bus RTS demonstrate the feasibility and practicality of the developed planning algorithm.

For future work, we will apply the proposed method for matching the renewable energy sources with other controllable loads such as plug-in electric vehicles. Other applications of energy storage units such as hedging against forecast uncertainties and reducing network expansion expenses will also be explored. Moreover, application of the energy storage units for reliability improvement of power networks should be evaluated. For this purpose, a comprehensive reliability model must be developed for energy storage units.

VII. References

[1] REN21.2013. *Renewables* 2013 *Global Status Report*.

[2] http://dsireusa.org/incentives/incentive.cfm?Incentive_Code=CO24R&re=1&ee=1

[3] http://www.ita.ucla.edu/news/presentations/Ton-UCLA1119-rv.pdf.

[4] C. Loutan, and D. Hawkins, "Integration of renewable resources: transmission and operating issues and recommendations for integrating renewable resources on the California ISO-controlled grid," California Independent System Operator, CAISO report, Nov. 2007.

[5] T. Ackermann, *Wind Power in Power Systems*, John Wiley and Sons, 2005.

[6] J. C. Smith,. M. R. Milligan, E. A. DeMeo, and B. Parsons, "Utility wind integration and operating impact state of the art," IEEE Trans. Power Systems., vol. 22, no. 3, pp. 900-908, August 2007.

[7] R. Zavadil, J. King, L. Xiadong, M. Ahlstrom, B. Lee, D. Moon, C. Finley, L. Alnes, L. Jones, F. Hudry, M. Monstream, and S. Lai, J. Smith, "Xcel Energy and the Minnesota Department of Commerce Wind Integration Study-Final Report," EnerNex Corporation and Wind Logics, Inc., Sep. 2004, accessed Nov. 17, 2006. [Online]. Available: http://www.state.mn.us/cgi-bin/portal/mn/jsp/content.do?contentid=536904447&contenttype=EDITORIAL&hpage=true&agency= Commerce.

[8] GE Energy, The Effects of Integrating Wind Power on Transmission System Planning, Reliability, and Operations: Report on Phase 2, Prepared for The New York State Energy Research and Development Authority, City, State, Mar. 2005.

[9] M. Milligan, H. Shiu, B. Kirby, and K. Jackson, "A multi-year analysis of renewable energy impacts in California: Results from the renewable portfolio standards integration cost analysis," WINDPOWER 2006 Conference and Exhibition, Pittsburgh, Pennsylvania, June. 2006, preprint accessed August 2006, available electronically at http://www.osti.gov/bridge.

[10] Electrotek Concepts, We Energies Energy Systems Operation Impacts of Wind Generation Integration Study, prepared for We Energies, Jul. 2003, accessed Nov. 17, 2006. [Online]. Available: http://www.uwig.org/WeEnergiesWindImpacts_FinalReport.pdf.

[11] M. Milligan and K. Porter, "Determining the capacity value of wind: A survey of methods and implementation," WINDPOWER 2005, Denver, CO, May 2005, preprint accessed Aug. 10, 2006. [Online]. Available: www.nrel.gov/docs/fy05osti/38062.pdf.

[12] Y. Wan, Wind Power Plant Behaviors: Analysis of Long-Term Wind Power Data, National Renewable Energy Lab., Golden, CO, Tech. Rep. NREL/TP-500-36651, 2004, accessed Aug. 10, 2006. [Online]. Available: http://www.nrel.gov/docs/fy04osti/36551.pdf.

[13] D. Brooks, E. Lo, R. Zavadil, S. Santoso, and J. Smith, Characterizing the Impacts of Significant Wind Generation Facilities on Bulk Power System Operation Planning, prepared for Utility Wind Integration Group. Arlington, VA, May 2003, accessed Nov. 17, 2006. [Online]. Available: http://www.uwig.org/UWIGOpImpactsFinal7-15-03.pdf.

[14] H. Shiu, M. Milligan, B. Kirby, and K. Jackson, California Renewables Portfolio Standard, Renewable Generation Cost Analysis: Multi-Year Analysis Results and Recommendations, California Wind Energy Collaborative for the California Energy Commission. Sacramento, CA, Jun. 2006, accessed Nov. 17, 2006. [Online]. Available: http://www.energy.ca.gov/2006publications/CEC-500-2006-064/CEC-500-2006-064.pdf.

[15] Growing Wind, Final Report of the NYISO 2010 Wind Generation Study. September 2010. [Online]. Available: http://www.uwig.org/GROWING_WIND_Final_Report_of_the_NYISO _2010_ Wind_Generation _Study.pdf.

[16] R. Gross, P. Heptonstall, D. Anderson, T. Green, M. Leach, and J. Skea, "The Costs and Impacts of Intermittency: An assessment of the evidense on the costs and impacts of intermittent generation on the British electricity network," UK Energy Research Center (UKERC), March 2006.

[17] http://www1.eere.energy.gov/buildings.

[18] https://www.nvenergy.com/home/saveenergy/rebates/coolshare.cfm.

[19] Bagen, and R. Billinton, "Evaluation of different operation strategies in small stand-alone power systems," *IEEE Trans*. *Energy Conversion*, vol.20, pp. 654–660, Sep. 2005.

[20] D. B. Nelson, M.H. Nehrir, and C. Wang, "Unit sizing of stand-alone hybrid wind/PV/fuel cell power generation systems," in *Proc*. 2005 *IEEE Power Engineering Society General Meeting*, pp. 2115-2122.

[21] B. S. Borowy, Z.M. Salameh, "Methodology for optimally sizing the combination of a battery bank and PV array in a wind/PV hybrid system, " *IEEE Trans. Energy Convers.*, vol. 11, no. 2, pp. 367-375, Jun. 1996.

[22] O. C. Onar, M. Uzunoglu, and M. S. Alam, "Modeling, control and simulation for an autonomous wind turbine/photovoltaic/fuel cell/ultra-capacitor hybrid power system," *J. Power Sources,* vol. 185, no. 2, pp. 1273-1283, Dec. 2008.

[23] C. Wang, and M. H. Nehrir, "Power management of a stand-alone wind/photovoltaic/fuel cell energy system," *IEEE Trans. Energy Conversion,* vol. 23, no. 3, pp. 957-967, Sep. 2008.

[24] S. R. Connors, J. G. McGowan, and J. F. Manwell, "Wind/diesel village-scale electric power systems: The performance and economic analysis of a simulated village system," *Solar Wind Technol.,* vol. 7, no. 4, pp. 423-439, 1990.

[25] F. Bonanno, A. Consoli, S. Lombardo, and A. Raciti, "A logistical model for performance evaluations of hybrid generation systems," *IEEE Trans. Industry Applications,* vol. 34, no. 6, pp. 1397-1403, Dec. 1998.

[26] C. Abbey, J. Robinson, and G. Joos, "Integrating renewable energy sources and storage into isolated diesel generator supplied electric power systems, " in *Proc. 13th Conf. Power Electron. Motion Control,* Poznan, Sep. 2008.

[27] E. I. Vrettos, and S. A. Papathanassiou, "Operating policy and optimal sizing of a high penetration RES-BESS system for small isolated grids," *IEEE Trans. Energy Convers.*, vo26. 11, no. 3, pp. 744-756, Sep. 2011.

[28] T. Senjyu, D. Hayashi, A. Yona, N. Urasaki, and T. Fumabashi, "Optimal configuration of power generating systems in isolated island with renewable energy, " *Renewable Energy,* vol. 32, no. 11, pp. 1917-1033, Sep. 2007.

[29] R. Dufo-Lopez, and J. L. Bernal-Agustin, "Multi-objective design of PV-wind-diesel-hydrogen-battery system, " *Renewable Energy,* vol. 33, no. 12, pp. 2559-2572, Dec. 2008.

[30] R. Chedid, and S. Rahman, "Unit sizing and control of hybrid wind-solar power systems," *IEEE Trans. Energy Conversion,* vol. 12, no. 1, pp. 79-85, Mar. 1997.

[31] L. Wang, and C. Singh, "Multicriteria design of hybrid power generation systems based on a modified particle swarm optimization algorithm, " *IEEE Trans. Energy Converion,* vol. 24, no. 1, pp. 163-172, Mar. 2009.

[32] S. Diaf, D. Diaf, M. Belhamel, M. Haddadi, and A. Louche, "A methodology for optimal sizing of autonomous hybrid PV/wind system," *Energy Policy,* vol. 35, pp. 5708-5718, Aug. 2007.

[33] J. P. Barton, and D. G. Infield, "Energy storage and its use with intermittent renewable energy," *IEEE Trans*. *Energy Conversion*, vol.19, no. 2, pp. 441–448, Jun. 2004.

[34] G. Tina, S. Gagliano, and S. Raiti, "Hybrid solar/wind power system probabilistic modeling for long-term performance assessment," *Solar Energy,* vol. 80, pp. 578-588, 2006.

[35] H. Yang, W. Zhou, L. Lu, and Z. Fang, "Optimal sizing method for stand-alone hybrid solar-wind system with LPSL technology by using genetic algorithm," *Solar Energy,* vol. 82, pp. 354-367, 2008.

[36] S. H. Karaki, R. B. Chedid, and R. Ramadan, "Probabilistic performance assessments of autonomous solar-wind energy conversion systems," *IEEE Trans*. *Energy Conversion*, vol.14, no. 3, pp. 766–772, Sep. 1999.

[37] L. N. Kishore, and E. Fernandez, "Reliability well-being assessment of PV-wind hybrid system using Monte Carlo simulation," in *Proc. Int. Conf. Emerging Trends in Electrical and Computer Technology (ICETECT),* Roorkee, India, Mar. 2011.

[38] R. Karki, and R. Billinton, "Reliability/cost implications of PV and wind energy utilization in small isolated power systems," *IEEE Trans*. *Energy Conversion*, vol.16, no. 4, pp. 368–373, Dec. 2001.

[39] A. Burgio, D. Menniti, A. Pinnarelli, and N. Sorrentino, "Reliability studies of a PV-WG hybrid system in presence of multi-micro storage systems," in *Proc. IEEE PowerTech Conf.,* Bucharest, Romania, Jun. 2009.

[40] D. K. Khatod, V. Pant, and J. Sharma, "Analytical approach for well-being assessment of small autonomous power systems with solar and wind energy sources," *IEEE Trans*. *Energy Conversion*, vol.25, no. 2, pp. 535–545, Jun. 2010.

[41] I. P. Gyuk, S. Eckroad, Energy storage for grid connected wind generation applications. U. S. Department of Energy 2004; Washington, DC, EPRI-DOE Handbook Supplement.

[42] B. Parsons, M. Milligan, J. C. Smith, E. DeMeo, B. Oakleaf, K. Wolf , "Grid impacts of wind power variability: Recent assessments from a variety of utilities in the United States," European Wind Energy Conference, Athens, Greece, 2006.

[43] H. Shiu, M. Milligan, B. Kirby, K. Jackson, California Renewables Portfolio Standard, Renewable Generation Cost Analysis: Multi-Year Analysis Results and Recommendations. California Wind Energy Collaborative for the California Energy Commission Sacramento, CA, 2006.

[44] M. Milligan, H. Shiu, B. Kirby, K. Jackson, "A multi-year analysis of renewable energy impacts in California: Results from the renewable portfolio standards integration cost analysis. WINDPOWER Conference and Exhibition, Pittsburgh, Pennsylvania, 2006.

[45] H. Bouillon, P. Fosel, J. Neubarth, W. Winter, Wind report 2004. E. ON Netz, Bayreuth, Germany, 2004.

[46] R. Gross, P. Heptonstall, D. Anderson, T. Green, M. Leach, J. Skea, "The Costs and Impacts of Intermittency: An assessment of the evidense on the costs and impacts of intermittent generation on the British electricity network," UK Energy Research Center (UKERC) 2006.

[47] P. Poonpun, W. Jewell, “Analysis of the cost per Kilowatt hour to store electricity,” IEEE Trans Energy Convs., 23(2): 529-534, 2008.

[48] S. Y. Wang, J. L. Yu, “Optimal sizing of the CAES system in a power system with high wind penetration,” Int Journal Electr Power Energy Syst., 37:117-125, 2012.

[49] R. Loisel, “Power system flexibility with electricity storage technologies: A technical-economic assessment of a large-scale storage facility“ Int. Journal Electr. Power Energy Syst., 42:542-552, 2012.

[50] H. Daneshi, A. K. Srivastava, “Security-constrained unit commitment with wind generation and compressed air energy storage,” IET Gener. Transm. Distrib., 6:167-175, 2012.

[51] J. Eyer, G. Corey, “Energy storage for the electricity grid: benefits and market potential assessment guide,” Sandia National Laboratories, SAND2010-0815, 2010.

[52] M. O. Buygi, H.M. Shanechi, G. Balzer, M.Shahidehpour, “Transmission Planning Approaches in Restructured Power Systems, ” in Proc. 2003 IEEE Power Tech Conf., vol.2, pp. 23-26, Bologna , June 2003.

[53] P. Maghouli, S. H. Hosseini, M. Oloomi, and M. Shahidehpour, “A Multi-Objective Framework for Transmission Expansion Planning in Deregulated Enviroments,” IEEE Trans. Power Syst., vol. 24, no. 2, pp. 1051-1061, May 2009.

[54] B. K. Marcus, Hedge Fund for Dummies, McGraw-Hill/Irwin, 2003.

[55] J. Choi, T. Tran, A. EL-Keib, R. Thomas, H. Oh, and R. Billinton, “A Method for Transmission System Expansion Planning Considering Probabilistic Reliability Criteria,” IEEE Trans. Power Syst., vol. 20, no. 3, pp. 1606–1615, Aug. 2005.

[56] H. Salazar, L. Chen-Ching; R.F. Chu, “Decision Analysis of Merchant Transmission Investment by Perpetual Options Theory,” IEEE Trans. Power Syst., vol.22, no.3, pp.1194-1201, Aug. 2007.

[57] http://www.windpoweringamerica.gov/wind_installed_capacity.asp.

[58] G. A. Orfanos, I. I. Skoteinos, P. S. Georgilakis, and N. D. Hatziargyriou, “Transmission Expansion Planning in Deregulated Electricity Markets for Increased Wind Power Penetration, ” in Proc. 2010 7th International Conf. on the European Energy Market (EEM) , pp. 1-7, Madrid, June 2010.

[59] I. da Silva, R. Romero, and C. A. Murari, “Transmission Network Expansion Planning with Security Constraints,” in Proc. Inst. Elect. Eng.,Gen., Transm., Distrib., vol. 152, no. 6, pp. 828–836, Nov. 2005.

[60] S. Blumsack, “Network Topologies and Transmission Investment under Electric Industry Restructuring,” Ph.D. dissertation, Department of Engineering and Public Policy., Carnegie Mellon University, Pittsburgh, 2006. [Online]. Available: http://www.andrew.cmu.edu/~sblumsac.

[61] U.S. Department of Energy, Transmission Bottleneck Project Report, March 2003.

[62] E. L. da Silva, H. A. Gil, and J. M. Areiza, “Transmission network expansion planning under an improved genetic algorithm,” IEEE Trans. Power Systems, vol. 15, no. 3, pp. 1168-1175, Aug. 2000.

[63] H. Zhang, V. Vittal, G. T. Heydt, and J. Quintero, ”A mixed-integer linear programming approach for multi-stage security-constrained transmission expansion planning,” IEEE Trans. Power Systems, vol. 27, no. 2, pp. 1125-1133, May 2012.

[64] D. J. Molina, J. Contreras, and H. Rudnick,”A principal-agent approach to transmission expansion—Part I: regulatory framework,” IEEE Trans. Power Systems, vol. 28, no. 1, pp. 256-263, Feb. 2013.

[65] G. B. Shrestha and P. A. J. Fonseka, “Congestion-driven transmission expansion in competitive power markets,” IEEE Trans. Power Syst., vol. 19, no. 3, pp. 1658–1665, Aug. 2004.

[66] M. Oloomi, G. Balzer,H.M. Shanechi, and M. Shahidehpour, "Market based transmission expansion planning," IEEE Trans. Power Syst., vol. 19, no. 4, pp. 2060–2067, Nov. 2004.
[67] P. Maghouli, S. H. Hosseini, M. O. Buygi, and M. Shahidehpour, "A scenario-based multi-objective model for multi-stage transmission expansion planning," IEEE Trans. Power Systems, vol. 26, no. 1, pp. 470-478, Feb. 2011.
[68] M. Moeini-Aghtaie, A. Abbaspour, M. Fotuhi-Firuzabad "Incorporating Large-Scale Distant Wind Farms in Probabilistic Transmission Expansion Planning—Part I: Theory and Algorithm " IEEE Trans. Power Syst., vol. 27, no. 3, pp. 1585-1593, Aug 2012.
[69] S. Lopez, A. Aguilera, and G. Blanco, "Transmission expansion planning under uncertainty: an approach based on real option and game theory against nature," IEEE Latin America Trans., vol. 11, no. 1, pp. 566-571, Feb. 2013.
[70] Y. Wang, H. Cheng, C. Wang, Z. Hu, L. Yao, Z. Ma, and Z. Zhu, "Pareto optimally-based multi-objective transmission planning considering transmission congestion," Electric Power Systems Research, vol. 78, no. 9, pp. 1619-1626, Sep. 2008.
[71] M. Shivaie, M. S. Sepasian, and M. K. Sheikh-El-Eslami, "Multi-objective transmission expansion planning based on reliability and market considering phase shifter transformers by fuzzy-genetic algorithm," Int. Trans. Electrical Energy Systems, DOI: 10.1002/etep.1672, 2012.
[72] H. Yu, C. Y. Chung, K. P. Wong and J. H. Zhang "A Chance Constrained Transmission Network Expansion Planning Method With Consideration of Load and Wind Farm Uncertainties" IEEE Trans. Power Syst., vol. 24, no. 3, pp. 1568-1578, Aug. 2009.
[73] G. Latorre, R. D. Cruz, and J. M. Areiza, "Classification of Publications and Models on Transmission Expansion Planning," presented at IEEE PES Transmission and Distribution Conf., Brazil, Mar. 2002.
[74] T. De la Torre, J. W. Feltes, T. G. S. Roman, and H. M. Merril, "Deregulation, privatization, and competition: transmission planning under uncertainty," IEEE Trans. PWRS, vol. 14, no. 2, pp. 460-465,May 1999.
[75] M. R. Patel, Wind and Solar Power Systems, Boca Raton, FL: CRC Press, 1999.
[76] J. Hetzer, D. C. Yu, and K. Bhattarai, "An economic dispatch model incorporating wind power," IEEE Trans. Energy Conversion, vol. 23, no. 2, pp. 603-611, Jun. 2008.
[77] S. Roy, "Market constrained optimal planning for wind energy conversion systems over multiple installation sites," IEEE Trans. Energy Conversion, vol. 17, no. 1, pp. 124-129, Mar. 2002.
[78] J. Wang, M. Shahidehpour, and Z. Li, "Security-constrained unit commitment with volatile wind power generation," IEEE Trans. Power Systems, vol. 23, no. 3, pp. 1319-1327, Aug. 2008.
[79] F. Hu, Z. Yan, Y. MI, and S. Chen, "Unit commitment based on modified unit decommitment method," presented at IEEE PES General Meeting, June 2004.
[80] E. Rosenblueth, "Point estimation for probability moments," Proc. Nat.Acad. Sci. United States Amer., vol. 72, no. 10, pp. 3812–3814, Oct.1975.
[81] C. Su, and C. Lu, "Two-point estimate method for quantifying transfer capability uncertainty," IEEE Trans. Power Systems, vol. 20, no. 2, pp. 573-579, May 2005.
[82] G. Verbic, and C. A. Canizares, "Probabilistic optimal power flow in electricity markets based on two-point estimate method," IEEE Trans. Power Systems, vol. 21, no. 4, pp. 1883-1893, Nov. 2006.
[83] K. Zou, A. P. Agalgaonkar, K. M. Muttaqi, and S. Perera, " Distribution system planning with incorporating DG reactive capability and system uncertainties," IEEE Trans. Sustainable Energy., vol. 3, no.1, pp. 112-123, Jan. 2012.
[84] J. C. Bezdek, Pattern Recognition with Fuzzy Objective Function Algorithms, New York: Plenum Press, 1981.

[85] http://mesonet.agron.iastate.edu/agclimate/info.phtml
[86] D. J. Ketchen, and C. L. Shook, "The application of cluster analysis in strategic management research: an analysis and critique," Strategic Management Journal, vol. 17, pp. 441-458, 1996.
[87] Y. M. Atwa, E. F. El-Saadany, M. M. A. Salama, R. Seethapathy, M. Assam, and S. Conti, "Adequacy evaluation of distribution system including wind/solar DG during different modes of operation," IEEE Trans. Power Systems, vol. 26, no. 4, pp. 1945-1952, Nov. 2011.
[88] V. A. Graham, and K. G. T. Hollands, "A method to generate synthetic hourly solar radiation globally," Solar Energy, vol. 44, pp. 333-341, 1990.
[89] http://www.ecodirect.com/Solar-Power-Inverter-Comparison-s/247.htm
[90] http://www.greenworldinvestor.com/topics/solar-renewable-energy-greeninvest/solar-inverters/
[91] T. Weise. (2009, June 26). Global Optimization Algorithms - Theory and Application -. (2nd ed.) [Online]. Available: http://www.it-weise.de/projects/book.pdf.
[92] Z. Xu, Z. Y. Dong, and K. P. Wong, "Transmission planning in a deregulated environment," IEE Proc.-Gener. Transm. Distrib., vol. 153, no. 3, May 2006.
[93] T. Mosher, "Economic valuation of energy storage coupled with photovoltaic: current technologies and future projections," M.Sc. dissertation, Dept. Aeronautics and Astronautics, Massachusetts Institute of Technology, Jun. 2010.
[94] A. Schellenberg, W. Rosehart, and J. Aguado, "Cumulant-based probabilistic optimal power flow (p-opf) with gaussian and gamma distributions," IEEE Trans. Power Systems, vol. 20, no. 2, pp. 773-781. May 2005.
[95] G. J. Hahn and S. S. Shapiro, Statistical Models in Engineering, New York: Wiley, 1967.
[96] M. Madrigal, K. Ponnambalam, and V. H. Quintana, "Probabilistic optimal power flow," in Proc. 1998 IEEE Canadian Conf. on Electrical and Computer Engineering, pp. 385–388, May 1998.
[97] W. D. Tian, D. Sutanto, Y. B. Lee, and H. R. Outhred, "Cumulant based probabilistic power system simulation using Laguerre polynomials," IEEE Trans. Energy Conversion, vol. 4, no. 4, pp. 567–574, Dec. 1989.
[98] http://transmission.bpa.gov/business/operations/wind/
[99] http://www.nrel.gov/eis/pdfs/uwig_spring_2011_speckman.pdf
[100] Alternative sectoral load shapes for NEMS, August 2001
[101] G. Barbose, N. Darghouth, R. Wiser, and J. Seel, Tracking the sun IV: An historical summary of the installed cost of photovoltaics in the United States, Lawrence Berkeley National Laboratory, Sep. 2011.
[102] R. Wiser, and M. Bolinger, 2010 wind technologies market report, U.S. Department of Energy, June 2011.
[103] www.eosenergystorage.com/technology
[104] http://www.stats.ox.ac.uk/~doucet/samsi_course.html
[105] R. Karki, P. Hu. And R. Billinton, "A simplified wind power generation model for reliability evaluation," IEEE Trans. Energy Conversion, vol. 21, no. 2, pp. 533-540, Jun. 2006.
[106] L. Martin, L. F. Zarzalejo, J. Polo, A. Navarro, R. Marchante, and M. Cony, "Prediction of global solar irradiance based on time series analysis: Application to solar thermal power plants energy production planning," Solar Energy, vol. 84, no. 10, pp. 1772-1781, Oct. 2010.
[107] R. Karki, D. Dhungana and R. Billinton, "An Appropriate Wind Model for Wind Integrated Power Systems Reliability Evaluation Considering Wind Speed Correlations," Appl. Sci., vol. 3, pp. 107-121, Feb. 2013.

[108] A. B. Rodrigues, and M. G. Da Silva, "Probabilistic assessment of available transfer capability based on Monte Carlo method with sequential simulation," IEEE Trans. Power Systems, vol. 22, no. 1, pp. 484-492, Feb. 2007.
[109] R. A. Gonzalez-Fernandez, and A. M. Leite da Silva, "Reliability assessment of time-dependent systems via sequential cross-entropy Monte Carlo simulation," IEEE Trans. Power Systems, vol. 26, no. 4, pp. 2381-2389, Nov. 2011.
[110] N. R. Godha, S. R. Deshmukh, and R. V. Dagade, "Time sequential Monte Carlo simulation for evaluation of reliability indices of power distribution system," 2012 IEEE Symposium on Computers & Informatics (ISCI 2012), Feb, 2012.
[111] J.S. Al-Sumait, A. K. Al-Othman, and J. K. Sykulski, "Application of pattern search method to power system valve-point economic load dispatch," Electric Power and Energy Systems, vol. 29, pp. 720-730, Jun. 2007.
[112] R. M. Lewis, and V. Torczon, "A globally convergent augmented Lagrangian pattern search algorithm for optimization with general constraints and simple bounds," Society for Industrial and Applied Mathematics (SIAM), vol. 12, no. 4, pp. 1075-1089, 2002.
[113] R. T. Marler and J. S. Arora, "Survey of multi-objective optimization methods for engineering," Structural and Multidisciplinary Optimization, vol. 26, no. 6, pp. 369-395, April 2004.
[114] Available: http://transmission.bpa.gov/business/operations/wind/
[115] H. Moghimi, A. Ahmadi, J. Aghaei, A. Rabiee, "Stochastic techno-economic operation of power systems in the presence of distributed energy resources," Int. Jour. Electr. Power Energy Syst., Vol. 45, pp: 477-488, 2013.
[116] W. C. Briceno Vicente, R. Caire, N. Hadjsaid, "Probabilistic load flow for voltage assessment in radial systems with wind power," Int. Jour. Electr. Power Energy Syst., Vol. 41, pp: 27-33, 2012.
[117] Y. Gao, "Adequacy assessment of composite generation and transmission systems incorporating wind energy conversion systems," A Ph.D. thesis submitted to the Department of Electrical Engineering, University of Saskatchewan 2010.
[118] T. Das, J. D. McCalley, "Compressed air energy storage," Iowa State University, Ames, Iowa, 2012.
[119] S. M. Schoenung, W. V. Hassenzahl, "Long vs. short-term energy storage technologies analysis: A life-cycle cost study," Sandia National Laboratories, SAND2003-2783, Aug. 2003.
[120] M. Kintner-Meyer, M. Elizondo, F. Tuffner, "Energy storage for power systems applications: A regional assessment for the Northwest Power Pool (NWPP)," A report prepared for the U.S. DOE, April 2010.
[121] T. Wu, Z. Alaywan, A. D. Papalexopoulos, "Locational marginal price calculations using the distribute-slack power-flow formulation," IEEE Trans. Power Syst., Vol. 20, No. 2, pp: 1188-1190, 2005.
[122] X. Liu and J. Zhong, "Point estimate method for probabilistic optimal power flow with wind generation," Int. Conf. on Electrical Engineering (ICEE), Algeria, 2009.
[123] M. A. Hassan, M. A. Abido, "Optimal design of microgrids in autonomous and grid-connected modes using particle swarm optimization," IEEE Trans. Power Electr., Vol. 26, No. 3, pp: 755-769, 2011.
[124] A report prepared by the Reliability Test System Task Force of the Application of Probability Methods Subcommittee. IEEE reliability test system. IEEE Trans Power Apparatus and Syst., PAS-Vol. 98, No. 6, pp: 2047-2054, 1979.
[125] Available: http://transmission.bpa.gov/business/operations/wind.
[126] Available: www.usbr.gov/pn/agrimet/webaghrread.html.

[127] J. Pan, Y. Teklu, S. Rahman and K. Jun, "Review of usage-based transmission cost allocation method under open access," IEEE Trans. Power Systems, vol. 15, no. 4, pp. 1218-1224, Nov. 2000.
[128] H. Markowitz, Portfolio Selection, Wiley, New York, 1959.
[129] M. Liu, and F. F. Wu, "Portfolio optimization in electricity markets," Electric Power Systems Research, vo. 77, pp. 1000-1009, 2007.
[130] F. F. Wu, F. L. Zheng, and F.S. Wen, "Transmission investment and expansion planning in a restructured electricity market," Energy, vol. 31, no. 6-7, pp. 954-966, May-Jun. 2006.
[131] R. Billinton, and R. N. Allan, "Reliability evaluation of power systems, New York and London: Plenum," 1994.
[132] P. K. Shukla, and K. Deb, "On finding multiple pareto-optimal solutions using classical and evolutionary generating methods," Eur. J. Oper. Res., vol. 181, pp. 1630-1652, Sep. 2007.
[133] K. Deb, A. Pratap, A. Agarwal, and T. Meyarivan, "A fast and elitist multi-objective genetic algorithm: NSGA II," IEEE Trans. Evol. Comput., vol. 6, no. 2, pp. 182-197, Apr. 2002.
[134] J. M. Morales, and J. Perez-Ruiz, "Point estimate schemes to solve the probabilistic power flow," IEEE Trans. Power Systems, vol. 22, no. 4, pp. 1594-1601, Nov. 2007.
[135] H. P. Hong, "An efficient point estimate method for probabilistic analysis," Reliab. Eng. Syst. Saf., vol. 59, pp. 261-267, 1998.
[136] IEEE committee report, "A reliability test system, "IEEE Trans. Power Apparatus and Systems, vol. 4, no. 3, pp. 1238-1244, 1989.
[137] R. D. Zimmerman, C. E. Murillo-Sanchez, and R. J. Thomas, "Matpower: Steady-State Operations, Planning and Analysis Tools for Power Systems Research and Education," IEEE Trans. Power Systems,, vol. 26, no. 1, pp. 12, Feb. 2011.
[138] A. Arabali, M. Ghofrani, M. Etezadi-Amoli, and Y. Baghzouz, "Ramping requirements and operation cost in a power system with dispersed wind generation," in *Proc. IEEE PES Transmission and Distribution Conference and Exposition (T&D)*, May 2012.
[139] A. Arabali, M. Ghofrani, M. Etezadi-Amoli, M. S. Fadali, Y. Baghzouz, "Genetic Algorithm Based Optimization Approach for Energy Management," *IEEE Transactions on Power Delivery*, Vol. 28, No. 1, Page(s): 162 – 170, Jan. 2013.
[140] A. Arabali, M. Ghofrani, M. Etezadi-Amoli, M. S. Fadali, "Stochastic Performance Assessment and Sizing for a Hybrid Power System of Solar/Wind/Energy Storage," *IEEE Transactions on Sustainable Energy*, (Accepted).
[141] A. Arabali, M. Ghofrani, M. Etezadi-Amoli, "Cost Analysis of a Power System Using Probabilistic Optimal Power Flow with Energy Storage Integration and Wind Generation," *International Journal of Electrical Power & Energy Systems (IJEPES)*, Elsevier, Vol. 53, No. , Page(s): 832-841, Dec. 2013.
[142] A. Arabali, M. Ghofrani, M. Etezadi-Amoli, and M. Sami Fadali, "A Multi-Objective Transmission Expansion Planning Framework in Deregulated Power Systems with Wind Generation," *IEEE Transactions on Power Systems*.